Analysis and Traction Control of a Rocker-Bogie Planetary Rover

by

Hervé Hacot

Submitted to the
Department of Mechanical Engineering
in partial fulfillment of the requirements for the degree of

Master of Science in Mechanical Engineering

at the

Massachusetts Institute of Technology

June, 1998

© 1998 Massachusetts Institute of Technology

Signature of Author _____
Department of Mechanical Engineering
May 8, 1998

Certified By _____
Steven Dubowsky
Thesis Supervisor

Accepted By _____
Ain A. Sonin
Chairman, Departmental Graduate Committee

Analysis and Traction Control of a Rocker-Bogie Planetary Rover

by

Hervé Hacot

Abstract

Robotic rovers have become important tools in planetary exploration. Future missions require improved rover performance. This thesis presents an analysis of a six-wheeled prototype rover. Its design is based on the rocker-bogie configuration.

A procedure is presented which can rapidly compute the configuration of the rover as a function of its environment. Also, a quasi-static force analysis of the system is detailed. It considers realistic physical constraints such as wheel slip and actuator saturation. A computer simulation with a graphic interface is developed to evaluate performance and enhance the understanding of the system.

The analysis leads to the design of a fuzzy logic controller that increases rover traction and mobility. Analytical and experimental studies are performed to validate the analysis and control scheme.

Thesis Supervisor: Dr. Steven Dubowsky
Professor of Mechanical Engineering

Acknowledgment

I would like to thank Professor Dubowsky for giving me the opportunity to work in this research group and for his guidance and technical assistance over the past two years. The support and sponsorship of NASA and JPL is also recognized and acknowledged.

I would also like to thank my past and present project colleagues and friends Shane Farritor, David Bevly and Robert Burn for their considerable help on my research. Also, thanks to all the other members of the research group for making this experience so rich and enjoyable. It is a wonderful experience to be in a place where people from all around the world can gather and learn from each other. Thanks also to all the people who read my thesis and transformed it into proper English.

I would like to thank my whole family for their support as well: my brother and sister, for encouraging me to go to MIT, and most of all my parents, for their constant care and support.

Finally, thanks to Vicky for all her help, attention, patience and love.

Table of Contents

List of Figures

1. Introduction

1.1. Motivations

Since the Viking mission in 1976, Mars exploration had been set aside. However, interest in the red planet has been greatly heightened by a recent analysis of the Antarctic ice field SNC meteorite "Allen Hills 84001". The chemistry, mineralogy and texture of this rock indicate biological origin and the possible existence of past primitive life on Mars. This is why NASA has started an ambitious planetary exploration program.

To minimize the cost of planetary exploration, robots are preferred to humans who require significant resources and supplies. Specifically, rovers which have high mobility and can transport scientific equipment are ideal (Weisbin *et al.*, 1997) and thus are important assets for future scientific exploration of planetary surfaces. Such vehicles will enable wide area imaging and identification of science sites, spectroscopically-based chemical analysis of surface terrain, collection of loose soil and extracted rock samples and other useful tasks. This science data collection is fundamental to understanding the formative processes of Martian geology, a possible history of life, and the possible suitability of the Martian environment to future habitation.

On July 4th 1997, the Sojourner rover landed successfully on Mars and started exploring the surface (Mars Pathfinder, 1997). Even though its range of motion was limited by the field of view of the lander, Sojourner was able to send back a significant amount of useful information about Martian climate and geology. More ambitious missions

are planned for the future. After the Mars Global Surveyor mission, which will map the surface of the planet through a satellite in 1998, rovers might be used widely in the 2001, 2003 and 2005 missions. The '01 and '03 missions will carry long-range rovers that will traverse tens of kilometers, visiting numerous sites, over many months. Such rovers will be equipped with manipulators to extract many soil and rock samples, analyzing some *in situ* and caching the most promising materials for the '05 sample and retrieval return mission, which will enable far more detailed earth-based analysis of morphology, chemistry and comparative mineralogy.

1.2. Purpose of this Research and Literature Review

The Martian environment (see Figure 1-1) is difficult to traverse and is challenging for future rovers. It is important for an exploration rover not to become trapped or get hung up during its mission. To design and control these rovers, analytical models of how they interact with their environments are essential. Models are also needed for rover action planning (Farritor *et al.*, 1998). The purpose of this research is to develop an analytical model of a rocker-bogie based rover (Hayati *et al.*, 1997). Specifically, the Lightweight Survivable Rover (Schencker *et al.*, 1997), a future candidate for exploration missions, is studied. This research also presents a controller, based on the physics of the system, that improves the traction of the vehicle. Experimental results corroborate the theory.

Figure 1-1: Mars Landscape (Viking Lander, 1976).

Simple mobility analysis of rocker-bogie vehicles has been developed and used for design evaluation (Linderman *et al.* 1992; Chottiner, 1992). In the available published works, the rocker-bogie configuration is modeled as a planar system, which is not sufficient to determine how the rover can perform in its environment. The posture of the rover must indeed be computed in real time. Detailed models of the full 3-D mechanics of rocker-bogie rovers have not been developed. Further models, which include the manipulator's influence, are also required to effectively plan and control the actions of these rovers. It is indeed important for a planner to be able to predict if a rover can successfully negotiate a given terrain obstacles, such as a ditch, without being trapped, and the effects of the interactions between the manipulator ad the ground.

Soil-tire interaction models are important for a complete and detailed analysis of rovers. A lot of research has been conducted in this area, and several different models have been defined (Ben Amar *et al.* 1995; Bekker, 1969). They are, however, complex and require a dynamic simulation of the system. This introduces other difficult issues such as non holonomic constraints.

Improving the performance of a four-wheel rover has also been explored (Sreenivasan, 1994). In this work, actuator redundancy and the position of the center of mass of a vehicle (the Gofor) are exploited to improve traction. The method relies on real-time measurements of wheel/ground contact forces, which are difficult to obtain in practice. Traction can also be improved by monitoring the skidding of the rover wheels on the ground (Van der Burg, 1997).

In future planetary exploration missions, rovers will be somewhat autonomous and will have to predict how they will perform on any given terrain. This is why analytical models of such rovers are required. This research presents a model that considers the 3-D structure of the system, and the computation of useful evaluation measures. The model

characterizes the interactions between the wheels and thus leads to the design of a traction controller.

1.3. Outline of the Thesis

This thesis is divided into six chapters. This chapter serves as an introduction and overview of the work.

Chapter 2 introduces the rover kinematics. It also presents an overview of the analysis structure and an efficient method of solving the inverse kinematics of the rover.

Chapter 3 presents the rover force analysis. A model of soil-tire interaction is developed. The redundancy in actuators of the rover makes the problem more difficult to solve. A methodology that computes the optimum solution to the problem is presented.

Chapter 4 characterizes the influence of the different rover parameters on the system. A set of heuristic rules is deduced from the understanding of the physics of the system and implemented using a fuzzy logic controller. Simulation results show the behavior of the controller.

Chapter 5 describes the design of the experimental rover and of its environment. Experiments were conducted that validate the rover analysis. Two rover control systems are also compared.

Chapter 6 outlines general conclusions regarding the analysis of the system and traction control, and presents suggestions for further work.

The appendices to this thesis give detailed information on the analysis and its implementation. Appendix A presents kinematic relations of the rover. Appendix B details equations of the rover's force analysis. Appendix C presents a general defuzzification procedure. Appendix D details the laboratory rover design.

2. Rover Kinematic Analysis

2.1. Introduction

This chapter describes the kinematics of the rover, which is the first step of the analysis. Knowing the pose and attitude of the rover in its environment is important for the force analysis of the rover and is necessary for the computation of useful evaluation parameters such as stability. Section 2.2 presents the design of the rover studied. Section 2.3 is an outline of the structure of the system analysis and simulation. This structure must be defined to stress the importance of the inverse kinematics procedure. Section 2.4 defines the kinematic parameters of the system and presents a method that solves the inverse kinematics.

2.2. Rover Design

2.2.1. Design Requirements Overview

Launching equipment into space is very expensive. Therefore, space and weight constraints are extremely important to the system design. It is also important to maximize the science instrumentation payload while minimizing the physical rover load (Shirley *et al*, 1997). Future missions will require the rover to travel long distances. Therefore, safety, stability and power consumption are key parameters. Additionally, the rover will need to be partially autonomous and to manipulate soil samples.

2.2.2. Rocker Bogie Design

As the Sojourner rover, the LSR-1 is representative of a class of NASA prototype planetary rovers based on a rocker-bogie mobility design (Bickler, 1992). This design has six independently driven wheels mounted on an articulated frame (see Figure 2-1). The frame has two rocker arms connected to a main body. Each rocker has a rear wheel connected to one end and a secondary rocker, called a bogie, connected to the other. At each end of the bogie is a drive wheel and the bogie is connected to the rocker with a free pivoting joint. The rockers are connected to the main body with a differential so that the pitch angle of the body is the average of the pitch angles of the rockers. A more detailed description of the design is given in (Bickler, 1992).

With this design, while traversing uneven terrain, each wheel tends to remain in contact with the ground. Additionally, the weight of the rover is well distributed over the six wheels. This allows each wheel to develop good ground traction resulting in a highly mobile rover.
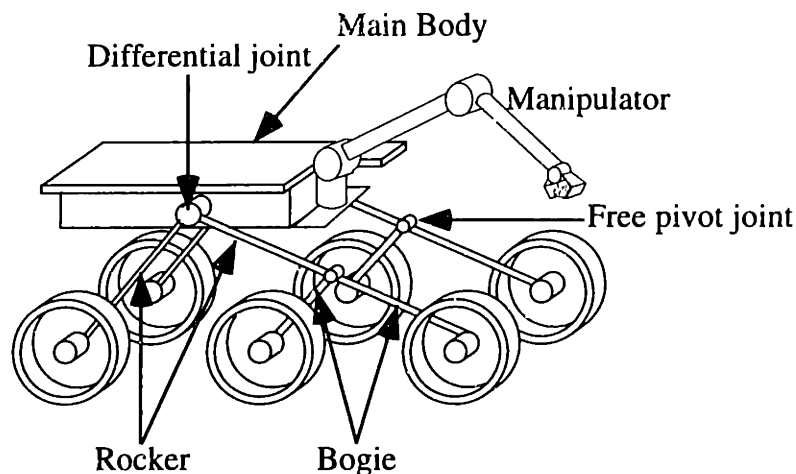
Figure 2-1 : Rocker-Bogie Design.

2.2.3. LSR-1 Features

The LSR-1 is a prototype, 7-kilogram rover with six 20-centimeter-diameter wheels. It is 97cm long, 70cm wide, and has 29cm of ground clearance. In comparison, Sojourner is an 11kg microrover with 13cm diameter wheels, 63cm long, 45cm wide, and has 15cm of ground clearance (Schencker *et al.*, 1997). Compared with Sojourner, LSR-1 is designed to operate over larger obstacles (~0.4m), broader thermal latitudes (equatorial to near polar regions), longer distances (multiple kilometers), and extended duration (multiple months).

The LSR-1 is also equipped with a 0.7m long 3-dof manipulator (Schenker *et al.*, 1997-2). The manipulator's mass is 1 kg (approximately 15% of the total rover mass) and its range of operation is large. This is later shown to have a significant influence on the mechanics of the system. The LSR-1 rover is designed to be volume and mass efficient. Volume is saved with the compact structure and with the wheels that collapse to as little as 25% of operational field volume (Sword *et al.*, 1997) (see Figure 2-2) during its transport to Mars.

Figure 2-2 : LSR-1 Volume Efficient Deployable Rigid Wheels. (Schencker *et al.*, 1997)

Mass is saved by removing any steering actuators. Therefore, LSR-1 is a skid steering vehicle. In comparison, four wheels of the Sojourner rover can steer by turning in

place the front and back wheels. Figure 2-3 shows the Sojourner and LSR-1 prototypes side by side. The LSR-1 weighs 4kg less than Sojourner.
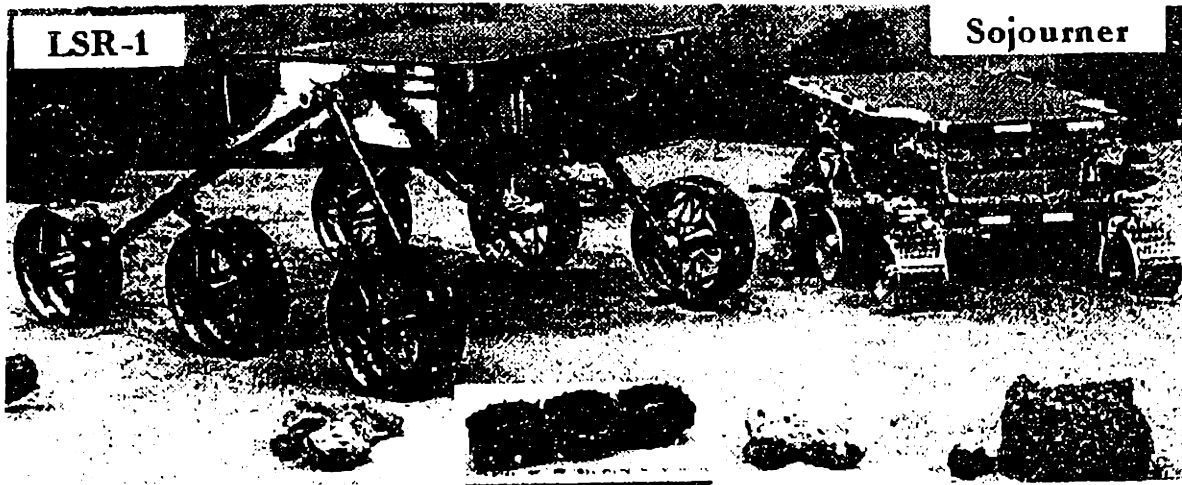
Figure 2-3 : LSR-1 and Sojourner Rovers (Schencker *et al.*, 1997)

The LSR-1 is designed to be lightweight and able to travel kilometers on the Mars surface. It is hence a serious candidate for future exploration missions and a detailed physics-based model of this rover is presented in this research.

2.3. System Analysis Structure

This section describes the organization of the rover analysis (see Figure 2-4). It is used as a tool for action planning methodology, which requires the repeated execution of the simulation (the simulation is estimated to be called about 30,000 times to converge to an acceptable action plan) (Farritor *et al.*, 1998). Therefore, it is important to keep the model as computationally simple as possible while maintaining an acceptable level of fidelity for future on-board implementation.

Several assumptions can simplify the rover analysis. A key to this is to recognize that the practical constraints of space systems, such as weight and power, require rovers to travel at slow speeds (approximately 3 cm/s for the LSR-1, or a wheel angular velocity of

1.5 rpm). Therefore, dynamic effects are very small and a quasi-static model is used here to describe its behavior.

A rover's ability to negotiate a given terrain is a function of the profile of the ground and the surface characteristics. Rovers have sensors such as stereo cameras and laser based systems capable of producing maps of the terrain around the rover (Matthies *et al.*, 1997). Estimates of soil characteristics are much more complex. On-line adaptive or identification methods, as well as pre-established estimates may be used. Some identification algorithms have been developed for simpler systems (Le *et al.*, 1997). This area remains an open research topic and is not addressed here: the ground characteristics are considered as input to the simulation.

Another important assumption used in this analysis relates to the rocker-bogie design. As seen in Section 2.2, the rover design is such that the rover wheels tend to remain in contact with the ground. Moreover, since the vehicle speed is very small, the wheels are not expected to bounce. Therefore, the model considers that the six wheels are always in contact with the ground.

The action plan is another input and is part of the action planning methodology. It consists of a list of actions that the rover is required to execute. Such actions can be, for example, "Move Forward 1 cm". They are commands to the rover and define the next position of the vehicle. The distances considered by these actions are small enough to be physically relevant. The action module methodology is detailed in (Farritor, 1998). The actions are read and the new desired rover position is computed. This position is the input for the inverse kinematics algorithm (see Section 2.4). This procedure determines the geometry of the wheel/ground contact. A quasi-static analysis is then performed (see Figure 2-4). It determines whether the rover will slip, what the actuator characteristics are, what is the stability of the vehicle, and other useful parameters for planning. Obviously,

the attitude of the rover is critical to this analysis. This justifies the development of the inverse kinematics procedure. The inverse kinematics and force analysis are performed at each step of the action plan and must therefore be very computationally efficient.
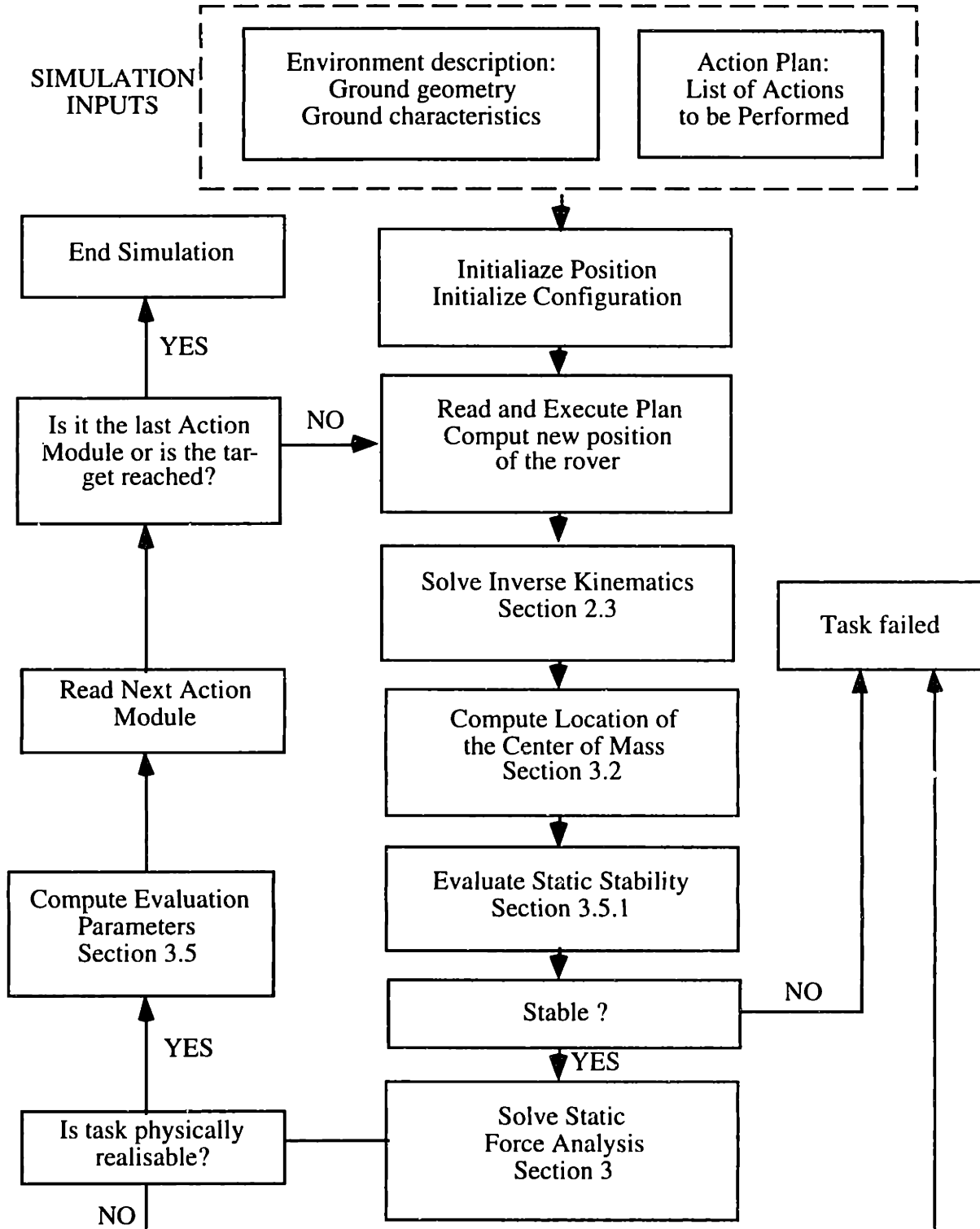
Figure 2-4 : Analysis Structure.

The structure and the main assumptions that simplify the analysis have been presented in this section. The importance of the inverse kinematics has also been stressed. This procedure is detailed in the following section.

2.4. Inverse Kinematics

2.4.1. Frames definition

It is essential to define the different frames that are used in the analysis. The reference frame is referred hereafter to as the ground frame or R_{ground} (x_{ground}, y_{ground}, z_{ground}). Let R' (x',y',z') be defined as the rotated frame along z_{ground} by an angle Ψ (yaw angle). The vector x' is then the heading direction of the rover. R'' (x'',y'',z'') is obtained from R' by a rotation Θ (roll angle) around x'. The origin of this frame is taken to be in the middle of the rover body. The vector y'' represents the transversal direction of the rover. R_{rover} is obtained from R'' by a rotation Φ (pitch angle) around y''. Figure 2-5 summarizes these definitions. The angles (Ψ, Θ, Φ) are in other words the Euler angles of the system.
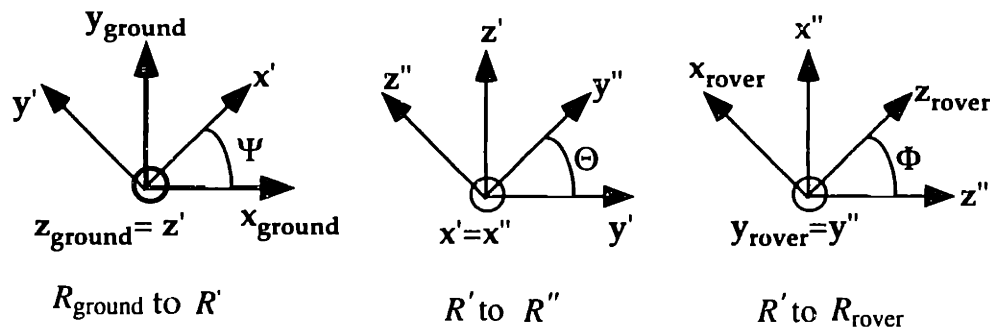
Figure 2-5: Frame Definitions.

2.4.2. Ground representation

3-D scanned points
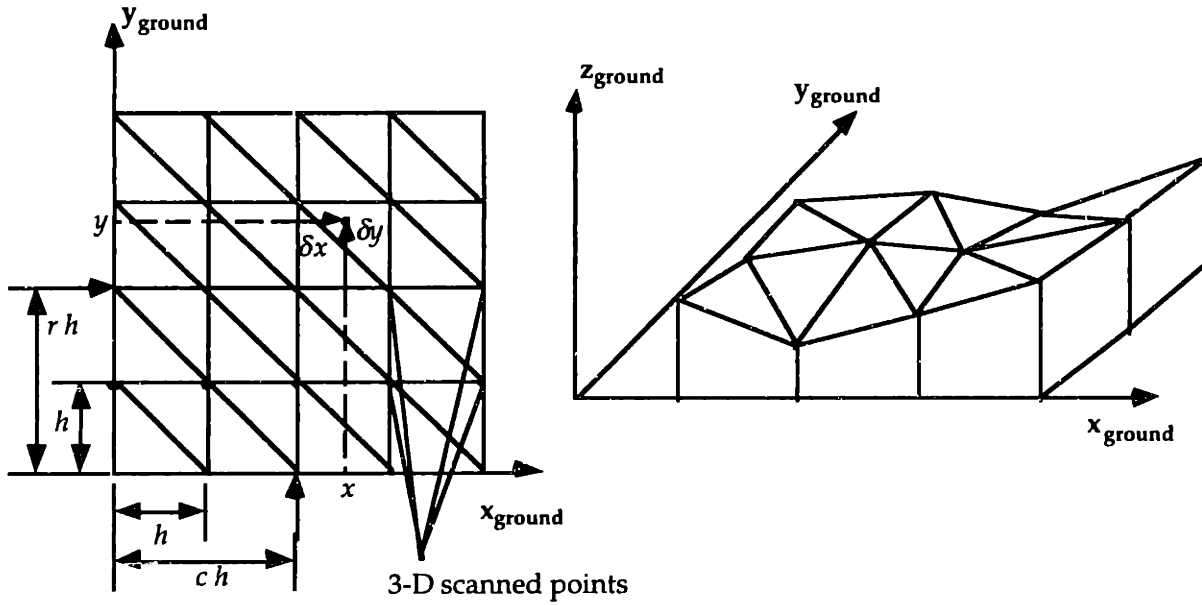
Figure 2-6: Ground Representation.

As seen in Section 2.3, the ground is input to the simulation. It is represented by a matrix of point altitudes. These points are equally spaced by h in the x_{ground} and y_{ground} direction (see Figure 2-6). This representation is relevant to rover missions, since the mapping of the environment of the rover is likely be done by laser triangulation techniques (Krotkov *et al.*, 1994). In the analysis, h is defined as one quarter of the wheel diameter, *i.e.* 5 cm. The points are joined to each other by planes see Figure 2-6.

It is then possible to write a function that computes the altitude of the ground at any point. This function is thereafter called $z_{ground}(x, y)$.

The following steps are taken to solve for z_{ground} given a point (x,y). First, r and c are calculated. They are defined as the row and column respectively of the lower left point of the square in which the point (x,y) is located (see Figure 2-6). Their expressions are given by the equations (2-1) and (2-2).

$$r = \text{floor}\left(\frac{y}{h}\right)$$

(2 - 1)

$$c = \text{floor}\left(\frac{x}{h}\right)$$

(2 - 2)

where floor(x) is the greatest integer less than or equal to x.

Two cases must be taken into account: the desired point could be either in the lower left plane or in the upper right plane as seen in Figure 2-7. The variables δx and δy are defined by δx=x-c h and δy=y - r h.
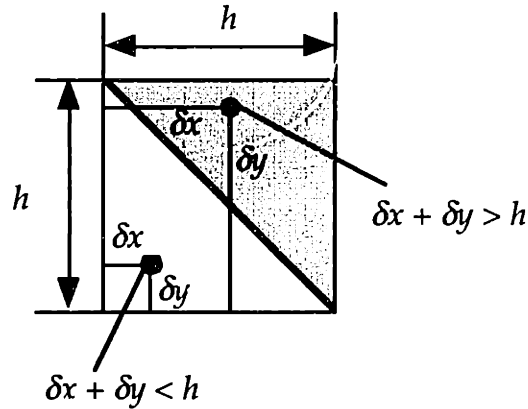
Figure 2-7: Ground Altitude Determination.

If $\delta x + \delta y \leq h$, then :

$$z_{\text{ground}} = M(r,c) - \frac{\left[h \cdot \delta x \cdot (M(r+1,c) - M(r,c)) + \delta y \cdot h \cdot (M(r,c+1) - M(r,c))\right]}{h^2}$$

(2 - 3)

If $dx + dy > h$, then :

$$z_{\text{ground}} = M(r+1,c+1) - \frac{h \cdot (h - \delta x) \cdot (M(r+1,c+1) - M(r,c+1))}{h^2}$$
$$- \frac{(h - \delta y) \cdot h \cdot (M(r+1,c+1) - M(r+1,c))}{h^2}$$

(2 - 4)

where M is the matrix of the ground altitude points.

These formulae enable rapid calculation of the altitude of any point on the ground and are widely used in the inverse kinematics procedure.

2.4.3. Kinematic parameters
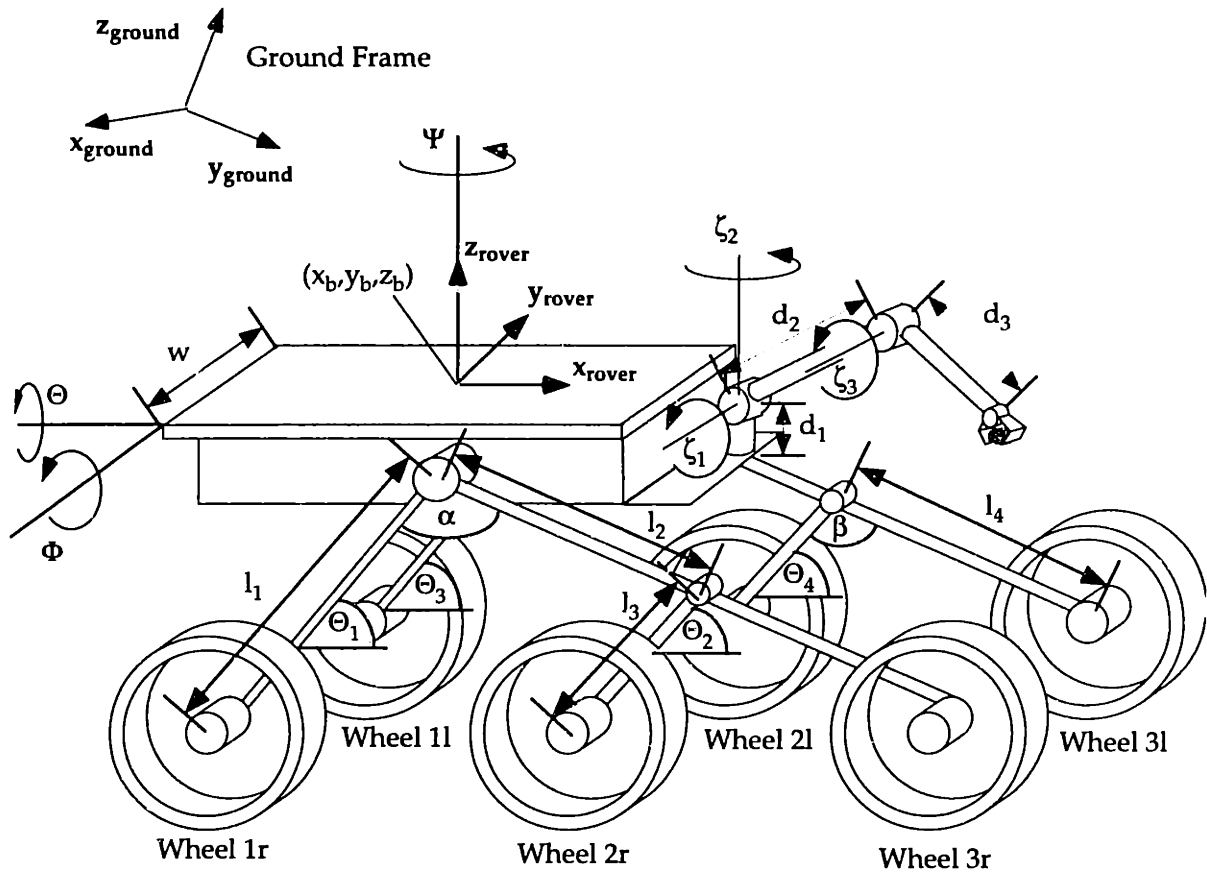
Figure 2-8: LSR-1 Kinematic Parameters.

The configuration and the position of the rover alone can be fully defined by ten parameters (see Figure 2-8):

• The position of the center of the body in R_{ground} is defined by (x_b, y_b, z_b).

• The rover's orientation is defined by (ψ, Θ, ϕ), using the Euler notation given in Section 2.4.1, for the yaw, roll and pitch of the rover respectively.

• The configuration of the rocker-bogie mechanism is defined by the angles $(\Theta_1, \Theta_2, \Theta_3, \Theta_4)$ measured in the plane (x_{rover}, z_{rover}).

The manipulator kinematics are also taken into account. It has a torso-shoulder-elbow (roll/pitch/pitch) configuration with additional end-arm pitch degree of freedom and

clamshell tool in the end effector. The inverse kinematics of this type of manipulator is a classical problem and can be found in (Bonitz, 1997). It is not detailed here.

At this point, it is necessary to outline the inverse kinematics procedure. All the wheels are assumed to be in contact with the ground. Loop closure equations can be written as functions of the variables and parameters presented above. Since there are six contact points with the ground, six independent equations can be written.

These closure loop equations give the altitude of the rover wheels as functions of the kinematic variables. The problem is to find the set of variables that satisfies the constraints that all the wheels are in contact with the ground. Therefore, it is necessary to be able to measure the distance between the wheel height that is determined by the rover kinematics and the ground. This is done by developing a function, called z_{center} that computes the altitude of a wheel center, given its position (x_{center}, y_{center}) and its orientation (Θ and Ψ) and given the additional constraint that the wheel is touching the ground.

The difference between the altitude computed with z_{center} and the altitude computed from the rover kinematic relations define an error, that is used for iterative numerical methods. The next section describes this function.

2.4.4. Determination of the altitude of the center of a wheel

As it was previously discussed, it is necessary to model the wheel-ground geometric interface. In other words, the goal is to define a function that determines the altitude z of the center of a wheel given its coordinates (x,y), orientation (Θ,Ψ) and the additional constraint that the wheel touches the ground (see Figure 2-9).
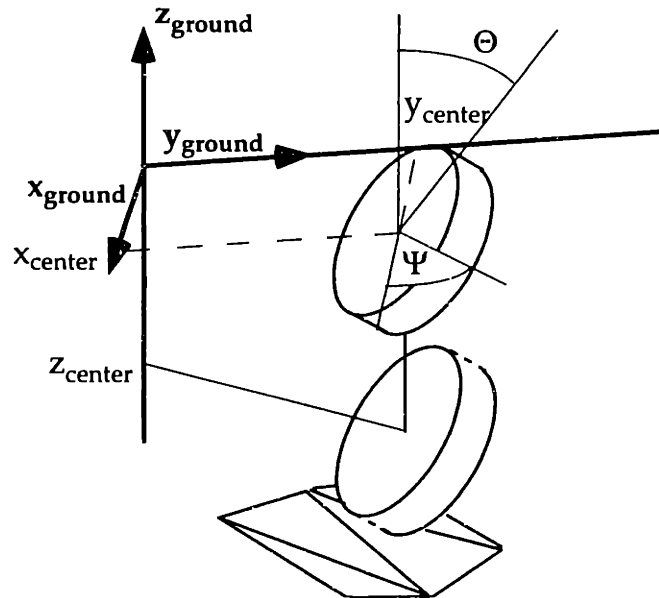
Figure 2-9: Determination of the Altitude of a Wheel.

The wheel is represented geometrically as a rigid cylinder. This can however account for the compliance of the wheels by using a wheel effective radius (see Figure 2-10). Different geometric contact models have been implemented and tested and are represented in Figure 2-11. This figure represents the side view of the wheel (i.e. rotated by the roll Θ). The first model is more accurate but presents drawbacks. The wheel can have different contact points, and a search algorithm is necessary to find the most suitable contact point, since the different wheel contact points can lead to different wheel altitudes. The second model, however, is extremely simple. It models the ground as a plane under the wheel. Therefore, there is a unique contact point, and the position of the wheel is computed very easi'y. This method has been chosen for its simplicity and computational speed.
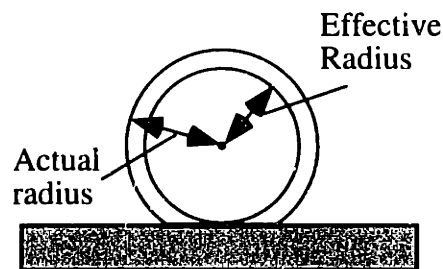
Figure 2-10: Wheel Effective Radius

Different wheel positions   The wheel position is unique
are possible

Model 1: piece wise terrain   Model 2: Averaged ground
Multiple Contact Points   One contact point
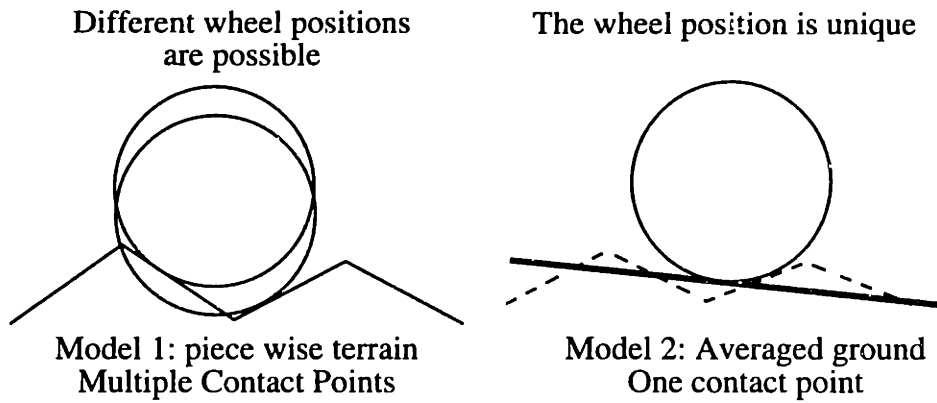
Figure 2-11: Ground-Wheel Contact Representations.

The model presented above considers only disks (2-D) and not cylinders (3-D). Hence, the wheel cylinder is modeled as three equally spaced circles. The ground is represented as a plane in the vicinity of the wheel. The altitude of the center is taken as the maximum of the three altitudes of each constituent circle (see Figure 2-12).
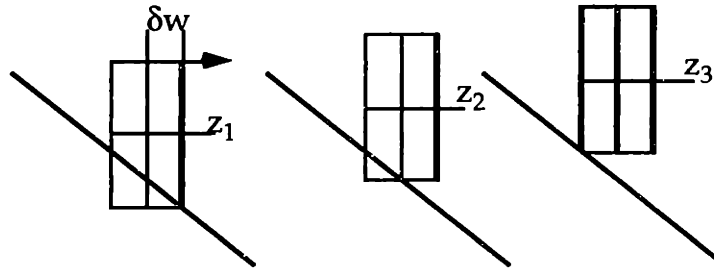
Figure 2-12: Three Cases for Wheel Altitude Computation.

Equation (2-5) determines the wheel altitude, given the wheel configuration and the ground profile (see Figure 2-13).

$$z_{center} = z_{ground}(x, y) + rad \cdot \cos(\alpha_g) \cdot \cos(\Theta) + \delta w \cdot \sin(\Theta)$$

$$(2 - 5)$$

Here, α_g is given by the ground geometry and δw is half the width of the wheel, and x and y can be deduced from x_{center} and y_{center} and Θ and Ψ (see Figure 2-13).

$$(2 - 6)$$

$$y = y_{center} + \left(\delta w \cdot \cos(\Theta) + \frac{r}{\cos(\alpha_g)} \sin(\Theta) \right) \cdot \cos(\Psi)$$

$$(2 - 7)$$

$$x = x_{center} + \left(\delta w \cdot \cos(\Theta) + \frac{r}{\cos(\alpha_g)} \sin(\Theta) \right) \cdot \sin(\Psi)$$
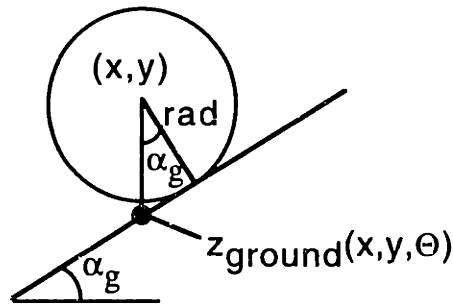
Figure 2-13: Wheel Center Altitude Determination.

In conclusion, this section has presented and defined a function (see Equation (2-5)) that is critical to the inverse kinematics problem. It computes the altitude that a wheel would have if it was touching the ground, given its configuration and position, x and y, in the ground frame.

2.4.5. Problem Statement

Using the ground/tire interaction model presented in Section 2.4.4, it is possible to state the inverse kinematics problem. Section 2.4.3 showed that ten variables need to be computed to fully represent the rover attitude. From three of these ten, it is possible to calculate the remaining seven parameters, given by seven kinematic equations. In this analysis, the three variables that are considered as input parameters are the position (x_{2r}, y_{2r}) in the ground frame of the right middle wheel and the heading angle Ψ of the rover. The angle Ψ can be measured using "sun sensors" (Kaliardos, 1993). The seven equations are presented below (Equations (2-8) through (2-14)).

Because of the differential mechanism in the rover body, ϕ, Θ_1 and Θ_3 are linked by the following relation:

$$\phi = \frac{\Theta_1 + \Theta_3}{2} - \gamma \qquad (2 - 8)$$

where γ is the angle Θ_1 when the rover is on a horizontal ground. The six closure loop equations are given by the equations (2-9) through (2-14).

$$z_{2r} = z_{center}(x_{2r}, y_{2r}, \Theta)$$ (2 - 9)

$$z_{2r} - z_{center}(x_{3r}, y_{3r}, \Theta) = \cos(\Theta) \cdot (l_3 \cdot \sin(\Theta_2) - l_4 \cdot \sin(\Theta_2 + \beta))$$ (2 - 10)

$$z_{2r} - z_{center}(x_{1r}, y_{1r}, \Theta) = \cos(\Theta) \cdot (l_3 \cdot \sin(\Theta_2) + l_2 \cdot \sin(\Theta_1 + \alpha) - l_1 \cdot \sin(\Theta_1))$$ (2 - 11)

$$z_{2r} - z_{center}(x_{1l}, y_{1l}, \Theta) = \cos(\Theta) \cdot (l_3 \cdot \sin(\Theta_2) + l_2 \cdot \sin(\Theta_1 + \alpha) - l_1 \cdot \sin(\Theta_3)) + w \cdot \sin(\Theta)$$ (2 - 12)

$$z_{2r} - z_{center}(x_{2l}, y_{2l}, \Theta) = \cos(\Theta) \cdot (l_3 \cdot \sin(\Theta_2) + l_2 \cdot \sin(\Theta_1 + \alpha) - l_2 \cdot \sin(\Theta_3 + \alpha) - l_3 \cdot \sin(\Theta_4) + w \cdot \sin(\Theta)$$ (2 - 13)

$$z_{2r} - z_{center}(x_{3r}, y_{3r}, \Theta) = \cos(\Theta) \cdot (l_3 \cdot \sin(\Theta_2) + l_2 \cdot \sin(\Theta_1 + \alpha) - l_2 \cdot \sin(\Theta_3 + \alpha) + l_4 \cdot \sin(\Theta_4 + \beta) + w \cdot \sin(\Theta)$$ (2 - 14)

where the subscripts r and l refer to right and left respectively. The subscripts 1,2 and 3 refer to the rear, middle and front wheels respectively. The quantities x_{1l}, y_{1l}, x_{2l}, y_{2l}, x_{3l}, y_{3l}, x_{1r}, y_{1r}, x_{3r}, y_{3r} are functions of x_{2r}, y_{2r}, Θ, Ψ and the rocker-bogie angles. They represent the center locations of their respective wheels (see Figure 2-8). Their expressions are detailed in Appendix A.

These equations relate the difference between the altitude that the wheel has on a given rover configuration and the altitude it would have if it touched the ground with its center defined by the kinematic relations. The goal is to reduce that difference to zero. This system of equations is highly non-linear. Some numerical methods (steepest descent, Newton's method) have been used in an attempt to solve the problem. However, convergence of such algorithms is not ensured.

Newton's method is based in the following principle : the equations are written as $F(x)=0$, where $x=[z_{2r}, \Theta_1, \Theta_2, \Theta_3, \Theta_4, \Theta]$.

The Jacobian of **F** is represented by **J**. Newton's method gives:

$$x^{k+1} = x^k - J^{-1} \cdot F(\overset{k}{x})$$

(2 - 15)

where x^k is the estimated root at the kth iteration.

Here, J is the source of convergence problems. Newton's method can work very effectively if J is continuous. The function F is not continuously differentiable, because of the function z_{center} that is function of the ground changes. Therefore, convergence is not ensured and oscillations are frequent (Arora, 1989).

The steepest descent method has also been investigated. In this case, the goal is to find x that minimizes $g(x) = \|F(x)\|^2$. The iterative scheme is :

$$x^{k+1} = x^k + \alpha^k \cdot \nabla\left(g\left(x^k\right)\right)$$

(2 - 16)

Again, this method tends to oscillate, for the same reasons as the Newton's method.

This section has presented the rover's kinematic relations. It has been shown that the conventional numerical methods often fail to converge. The following section presents a simple and efficient method that solves the problem.

2.4.6. Solving Method

To find a solution to the inverse kinematics problem, some approximations need to be made. These reasonable assumptions not only make the problem solvable, but they also lead to a computationally fast and simple solution method.

The rover is first translated to a new desired position in its previous configuration. The new wheel positions are used to calculate an estimate Θ_{est} of Θ. This estimate is calculated by taking the average of the altitude of the ground on each side and dividing it by the width of the rover (see Figure 2-14 and Equation (2-17)).

$$\Theta_{est} = \frac{z_{right} - z_{left}}{width}$$

(2 - 17)
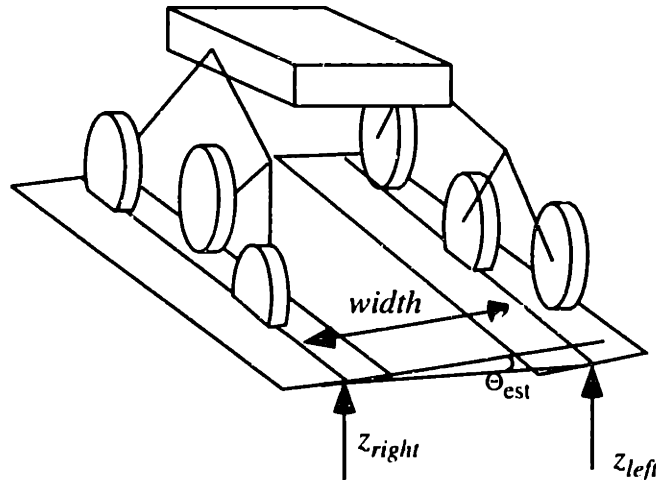
Figure 2-14: Roll Estimation.

This estimate is the starting point of future calculations. The variable z_{2r} can be deduced from (2-9): Ψ, x_{2r} and y_{2r} are input variables and Θ is known; hence $z_{center}(x_{2r}, y_{2r}, \Theta)$ is known. Finding Θ_2 is then much easier. Equation (2-10) is now dependent on one variable. The bisection method is then used to find its solution. It is very easy to implement, and convergence is ensured, because no conditions must be verified on the differentiability of the function. It only needs to be continuous (which is the case).

This approach is actually equivalent to keeping the roll of the body and the middle wheel position fixed while changing the angle Θ_2 until the front wheel touches the ground. The same method is then be applied to Θ_1, with equation (2-11). This is equivalent to holding the joint of the rocker-bogie fixed, and to changing Θ_1 until the rear wheel is in contact with the ground. This solves the problem for the right side.

The same procedure is repeated for the left side. The starting value for the left side is again the position of the middle wheel. This outputs the angles Θ_1, Θ_2, Θ_3 and Θ_4. Of course, the value of Θ_{est} has to be modified. This correction is done according to Figure 2-15. Both planes are attached together using Equation (2-18).

$$z_{2l} - z_{2r} = (h_r - h_l) \cdot \cos(\Theta) + width \cdot \sin(\Theta)$$

(2 - 18)
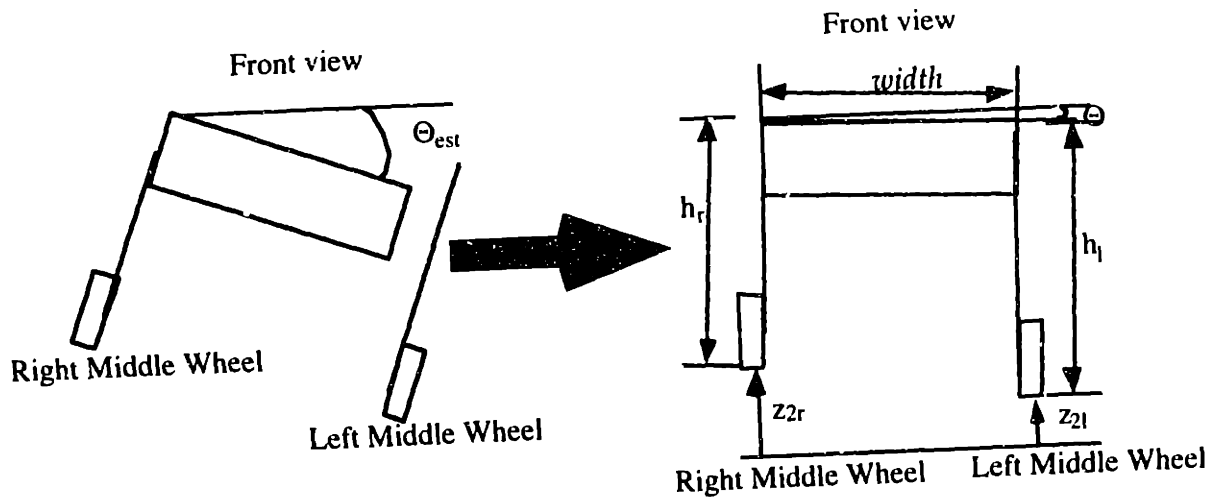
Figure 2-15: Roll Angle Correction.

As long as the ground's characteristic length is larger than the rover's, these approximations appear to be good enough for the model. After the approximated roll angle is changed, the errors are less than 2% of the diameter of the wheel. This amounts to less than 0.1 degree error in angles. This is of the same order of magnitude as unmodelled phenomena such as wheel compliance and poor ground characterization. Not only is this solution computationally simple and efficient, it also proves to be very accurate.

2.5. Conclusions

This chapter presented the LSR-1 design and kinematic characteristics. The structure of the simulation has also been outlined. It explains and stresses the importance of the inverse kinematics in the analysis. Different reference frames have been defined and the inverse kinematics procedure has been developed. Under some simplifying assumptions, the rover's attitude can be computed quickly and convergence has been proven. The knowledge of the kinematic parameters and variables is the first step to the development of the force analysis.

3. Rover Force analysis and Simulation

3.1. Introduction

This chapter presents the force analysis of the rover. The 3-D balance is delineated in Section 3.2. Ground-tire interaction models are used to introduce additional equations. Section 3.3 presents a planar analysis of the rover. Section 3.4 details a solution method to the problem. Useful evaluation parameters are defined and computed in Section 3.5. The graphic interface has been developed and is presented in Section 3.6.

3.2. Force Analysis

3.2.1. Main Assumptions

The force analysis determines if the rover is physically able to perform a task. An easy way to evaluate this is to determine if the rover can stay in static equilibrium in its current position. This evaluation method is consistent with the fact that the rover is going to move at slow speeds: a quasi-static approximation is appropriate.

Moreover, under this hypothesis, if the different evaluation positions of the rover are closely distributed in space and time, the torque distribution on the wheels that verifies the rover's balance can be approximated as the actual commanded torques and can be used to calculate power consumption.

3.2.2. Rover center of mass and input force computation

The position of the center of mass affects the load distribution on the wheels and the stability of the vehicle. It is therefore critical to compute its location. From this, the input force to the system can be deduced.

3.2.2.1. Rover Masses Distribution
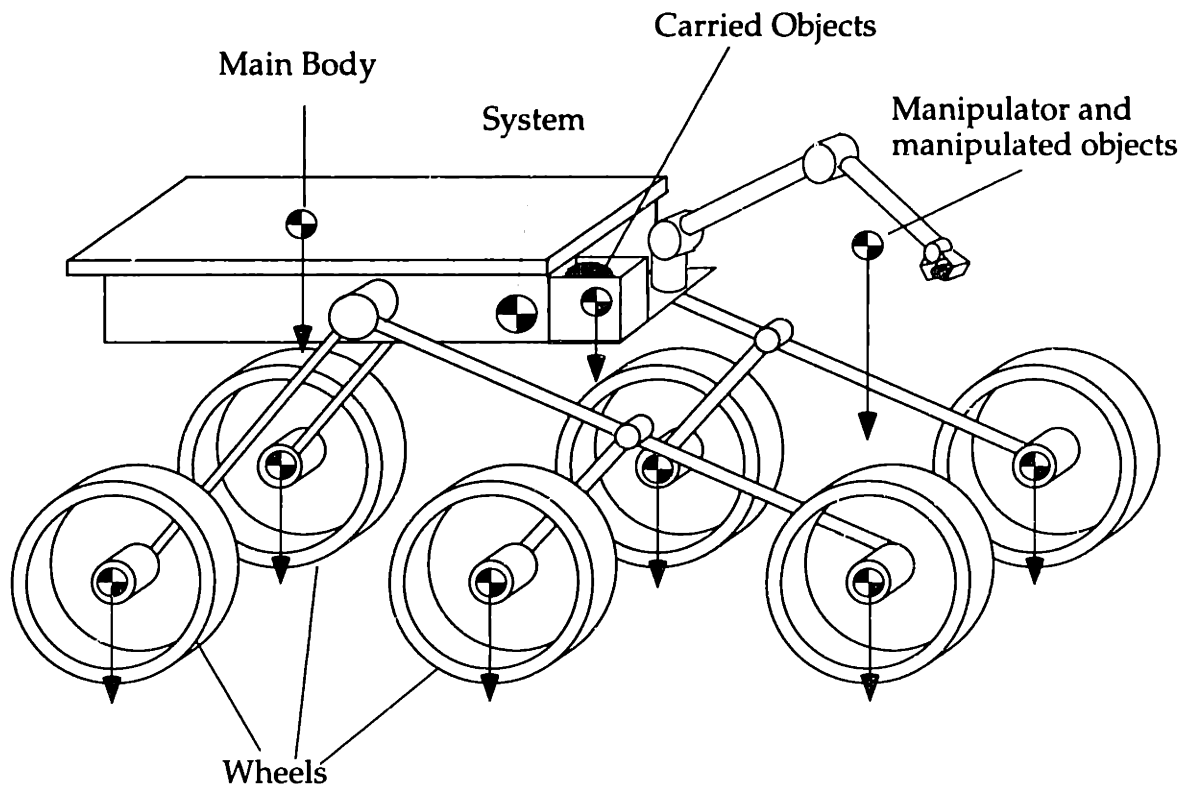
Figure 3-1: Rover Mass Distribution.

The rover mass distribution is shown in Figure 3-1. Contribution to the system mass can be summarized as follows:

- The main body, which will contain the science experimental equipment, the computer and power supplies.

- The wheels. The motors' masses are not negligible. This is why the LSR-1 design does not include any steering wheels. Extra actuators are not desirable.

- The manipulator represents approximately 15% of the mass of the rover and whose range of motion is large enough to affect the center of mass position (Schenker *et al.*, 1997-3). The position of the center of mass of this subsystem is computed with the knowledge of the kinematics of the arm.

- Additional masses are rock samples gripped by the arm and those loaded or carried into the rover. Their influence must be taken into account too.

The locations of all these elements are fully determined by the kinematics of the rover. Moreover, the masses of the rover's parts are known, and it is assumed that rover sensors can estimate the masses of the rocks quite well. Volume estimates can lead to such mass estimations. All these systems and sensor readings are taken into account for the computation of the center of mass position. While simple, this task is important since it affects the rover's stability and balance equations.

3.2.2.2. Input Forces to the System

Since the rover's force analysis is performed under the quasi-static assumption, the input forces can be expressed as a wrench that will be located at the center of the body. This input wrench vector is composed of six components computed in ($\mathbf{x}$", $\mathbf{y}$", $\mathbf{z}$") : [F_{xi}, F_{yi}, F_{zi}, M_{xi}, M_{yi}, M_{zi}]^T.

The quantities F_{xi}, F_{yi} and F_{zi} are the components of the sum of all the externally applied forces in $\mathbf{x}$", $\mathbf{y}$" and $\mathbf{z}$" respectively. M_{xi}, M_{yi} and M_{zi} are the components respectively in $\mathbf{x}$", $\mathbf{y}$" and $\mathbf{z}$" of the moment created by the sum of the externally applied forces on the center of the body. These external forces can be arbitrary forces or moments along the direction of motion of the system. Forces resulting from the manipulator's interaction with its environment can be represented too. In the following sections, the lumped input wrench vector will be referred to as $\mathbf{F_i}$.

3.2.3. Transversal Forces Computation

With the input force F_i to the system considered to be known, the three-dimensional analysis can be developed.

The rover mechanics are quite complex. Since there are six contact points with the ground, the system is statically indeterminate. Modeling it as a solid results in 36 unknowns (six per wheel), that have to be computed with only six equilibrium equations! (see Figure 3-2). The problem can then not be uniquely solved. Some simplifications help to reduce the number of unknowns. The moments created by the ground are small with respect to the moment that are induced by the rover transversal forces and can ignored, leaving only the friction forces.
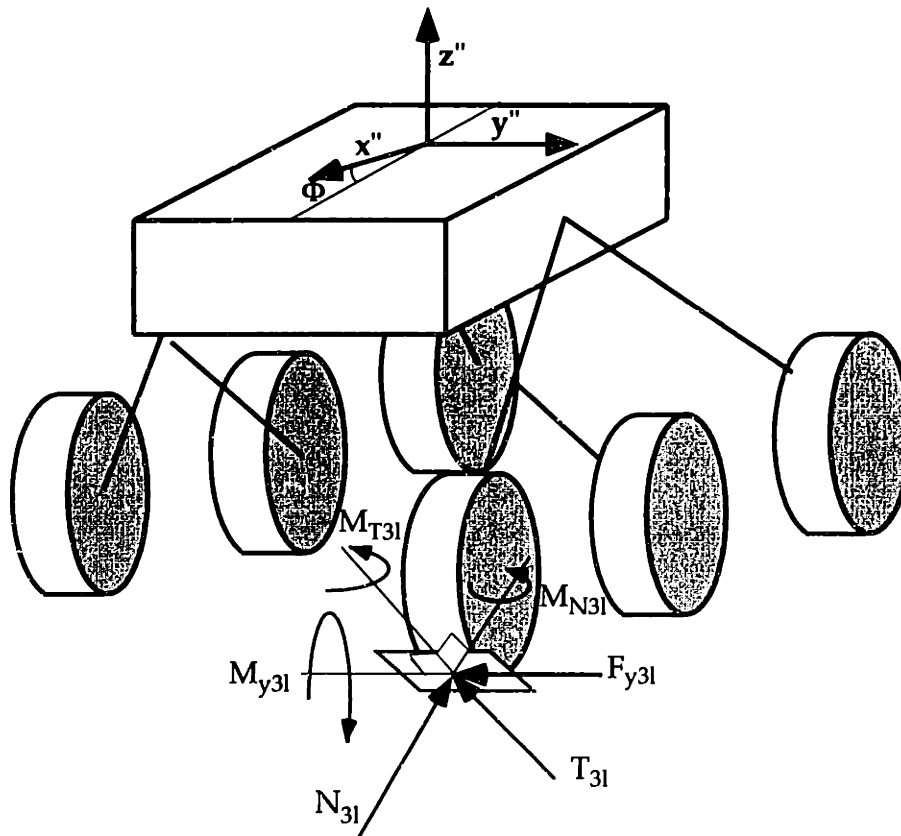
Figure 3-2: Force Analysis Unknowns (Represented on one wheel only).

Even with these simplifications, the system remains statically indeterminate, with 18 unknowns (three per wheel) for six balance equations. The most common way to eliminate the extra unknowns is to make some elements of the structure compliant (Beer *et al.*, 1981). Then, additional equations can be written.

In the case of the rover, the most compliant elements of the structure are the tires, since the rocker-bogie structure is intended to be very rigid. The following model is used to represent the wheel/terrain interactions.

First, the $\ldots$ngitudinal forces (T_{ir} or T_{il}) are controlled by the wheel torques, where i refers to the wheel number. The normal forces (N_{ir} or N_{il}) are defined by the system and are not friction forces. But the transverse forces (F_{yir} or F_{yil}) can only be computed using a model of soil-tire interaction, more specifically the compliance of the wheels.
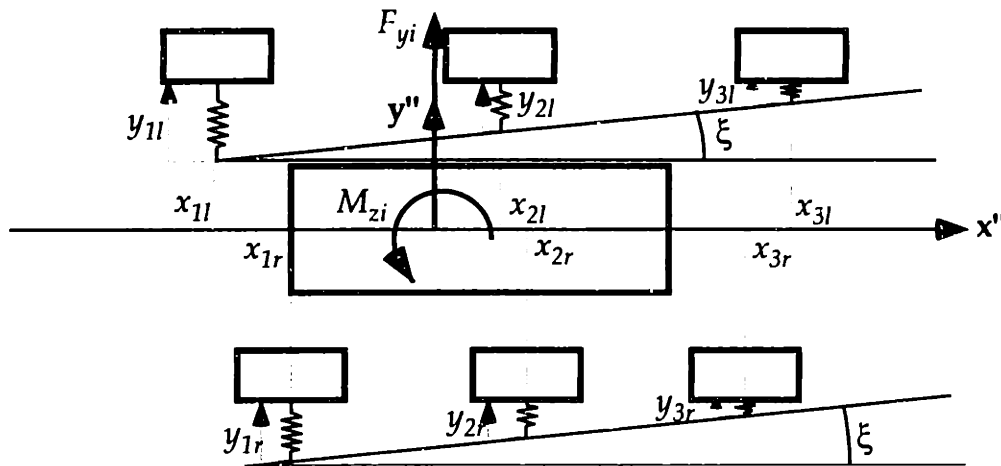
Figure 3-3: System Compliance.

Naturally, the transverse forces need to equilibrate the transverse input force F_{yi}.(see Figure 3-3). They are also modeled to create no net moment on the body. This assumption is plausible. Indeed, when the rover is sitting exactly perpendicular to a slope and that no external forces other than gravity are exerted, it will not turn in place.

The compliance of the wheels is represented by a spring of stiffness k and is assumed to be the same for all the wheels. Therefore, the problem is to find the relations between the relative displacements y_i of the wheels. The equations are:

$$k \cdot \left(y_{1r} + y_{2r} + y_{3r} + y_{1l} + y_{2l} + y_{3l} \right) + F_{yi} = 0 \qquad \text{(3-1)}$$

$$\sum_{i=1}^{i=3} \left(x_{ir} \cdot y_{ir} + x_{il} \cdot y_{il} \right) = 0 \qquad \text{(3-2)}$$

where x_i is given by the kinematics of the rover. Equation (3-1) is the balance of forces in the y" direction, and Equation (3-2) is the moment balance equation along z".

Since the rest of the body is relatively more rigid than the tires, all the displacements y_{ir} or y_{il} are related to each other. This problem is similar to the balance of a beam on three compliant points. The displacement of the springs are linearly coupled because the beam is rigid (under small angle approximation). Here, the rover is taken as a rigid element too. Therefore, the displacements y_{ir} and y_{il} are linearly coupled, as shown in Figure 3-3, inducing Equations (3-3) through (3-6):

$$y_{2r} = y_{1r} + \xi \cdot (x_{2r} - x_{1r}) \qquad \text{(3-3)}$$

$$y_{3r} = y_{1r} + \xi \cdot (x_{3r} - x_{1r}) \qquad \text{(3-4)}$$

$$y_{2l} = y_{1l} + \xi \cdot (x_{2l} - x_{1l}) \qquad \text{(3-5)}$$

$$y_{3l} = y_{1l} + \xi \cdot (x_{3l} - x_{1l}) \qquad \text{(3-6)}$$

The parameter ξ is the slope of the line joining all the relative displacements on the same side, see Figure 3-3. There are six equations and seven unknowns: another constraint is added.

$$y_{1l} = y_{1r} \qquad \text{(3-7)}$$

This constraint means that both rear wheels have the same contribution to the force balance. If the rover is such that all the wheels are at the same relative positions (i.e. $x_{1r}=x_{1l}$, $x_{2r}=x_{2l}$, $x_{3r}=x_{3l}$), then by symmetry, the forces will be the same on each pair of wheels. Equation (3-7) verifies this.

It is then possible to solve for ξ and y_{1r}. Their expressions are given in Equations (3-8) and (3-9).

$$y_{1r} = \frac{F_{yi} \cdot \sum_i (x_i \cdot \Delta x_i)}{k \cdot \left(\sum_i \sum_j (x_i \Delta x_j) - 6 \cdot \sum_i (x_i \cdot \Delta x_i) \right)} \qquad (3\text{-}8)$$

$$\xi = -\frac{F_{yi} \cdot \sum_i (x_i)}{k \cdot \left(\sum_i \sum_j (x_i \Delta x_j) - 6 \cdot \sum_i (x_i \cdot \Delta x_i) \right)} \qquad (3\text{-}9)$$

where x_i represents any x_{ir} or x_{il}, and $\Delta x_i = (x_i - x_l)$.

This model gives the values of the transverse forces acting on the wheels and reduces the hyperstaticity of the system. The remaining unknowns are the normal forces N_{ir} and N_{il} and longitudinal forces T_{ir} and T_{il}. They can be deduced using free body diagrams as is described below.

3.2.4. Main body balance

The rest of the analysis is conducted using free-body diagrams (see Figure 3-4). The main body is separated from the rest of the rover. By writing the balance equations for the body, it is possible to calculate the forces that are applied to each side of the rover. This section describes the main body balance.

The body's balance is written in the R'' frame, defined in section 2.4.1. The unknowns of the static equilibrium of the rover are F_{zr}, F_{zl}, F_{yr}, F_{yl}, F_{xr}, F_{xl}, and M_{zr}, M_{zl}, M_{yr}, M_{yl}, M_{xr}, M_{xl}. Here, the subscripts x, y, and z refer to the x'', y'' and z'' directions respectively. The equilibrium equations are scalar and the sign convention used is that the unknowns are positive in the directions shown in Figure 3-4.
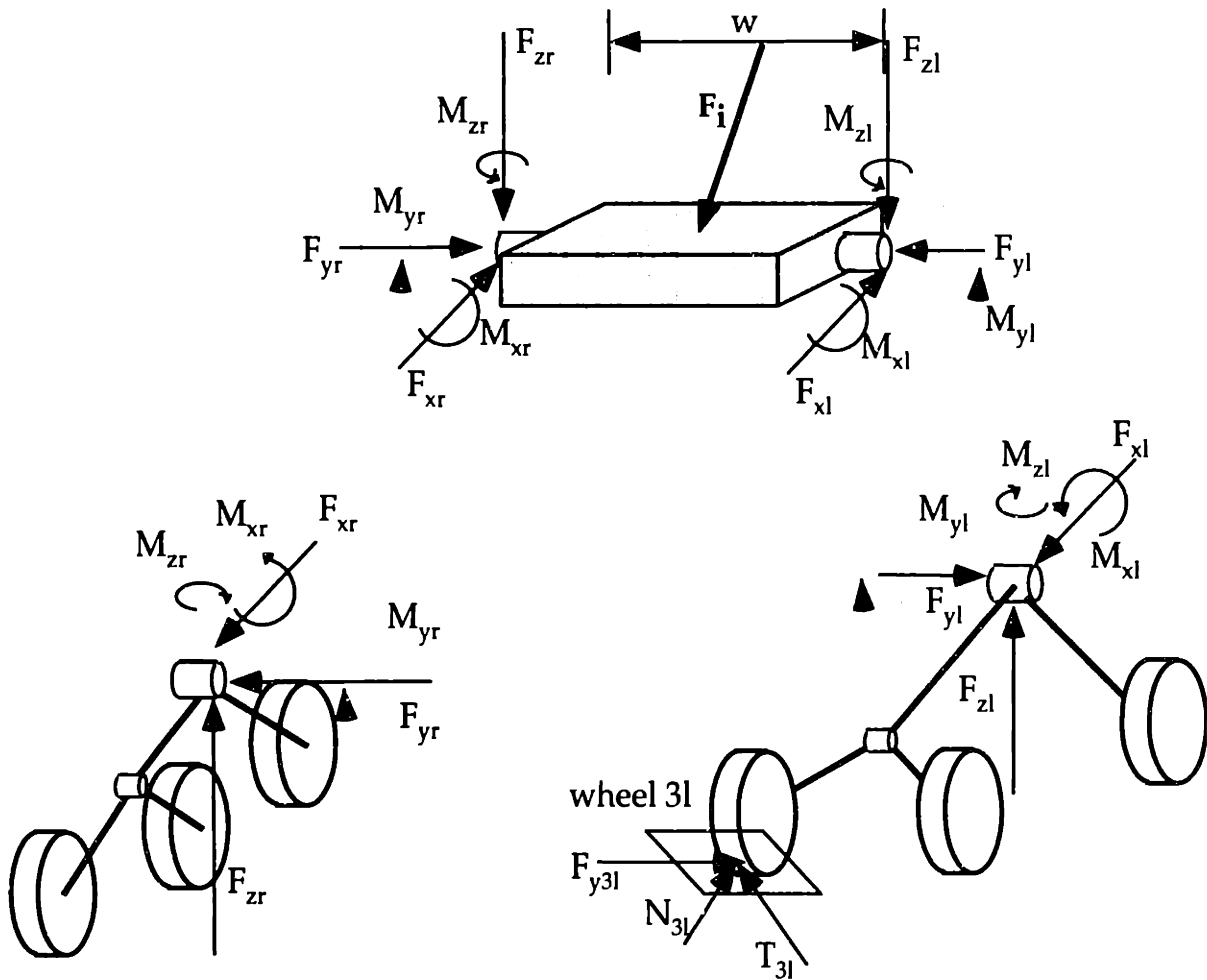
Figure 3-4: Rover Balance.

The input $\mathbf{F_i}$ is a vector of three forces and three moments which are applied at the center of the body (more precisely, in the middle of the two body-rocker joints). They are positive in the directions defined by R''. The influence of the transverse forces are also taken as inputs to the static body balance. These forces induce forces in the **y"** direction that exactly compensate for $\mathbf{F_{yi}}$, (therefore F_{yr} and F_{yl} are known) and moments in the **x"** and **z"** directions. The sum of the moments in the **z"** direction is zero because of the model used in the previous section. The moments in the **x"** direction should be affected by the longitudinal and normal forces on the wheels as well, but in the model, the width of the rocker-bogie mechanism is zero. Consequently, these moments are only functions of the transverse forces and are input to the body balance equations.

Using the directions of the forces defined in Figure 3-4 and using the components of the vectors **u**, **v** and **w** (defined in Figure 3-5) along the z'' axis (referred to as u_{zr}, v_{zr} and w_{zr} for the right side and u_{zl}, v_{zl} and w_{zl} on the left side), F_{yr}, F_{yl}, M_{xr}, M_{xl}, M_{zr} and M_{zl} can be deduced, since they are functions of the transverse forces only, and are given by:

$$F_{yr} = F_{y1r} + F_{y2r} + F_{y3r} \tag{3-10}$$

$$F_{yl} = -(F_{y1l} + F_{y2l} + F_{y3l}) \tag{3-11}$$

$$M_{zr} + M_{zl} = 0 \tag{3-12}$$

$$M_{xr} = -\left(F_{y1r} \cdot u_{zr} + F_{y2r} \cdot v_{2r} + F_{y3r} \cdot w_{3r}\right) \tag{3-13}$$

$$M_{xl} = -\left(F_{y1l} \cdot u_{zl} + F_{y2l} \cdot v_{2l} + F_{y3l} \cdot w_{3l}\right) \tag{3-14}$$
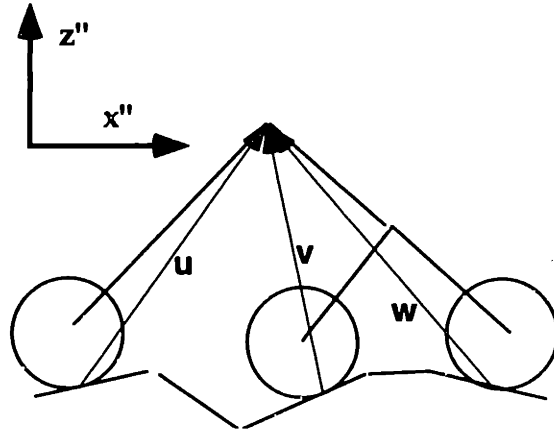
Figure 3-5: Transverse Forces Influence.

The remaining unknowns to the body balance are then : F_{zr}, F_{zl}, F_{xr}, F_{xl}, M_{yr} and M_{yl}. The quantities F_{zl} and F_{zr} are the forces in the z'' direction acting from the rocker to the body. F_{xr} and F_{xl} are in the x'' direction. The balance equations of the system are:

$$F_{xr} + F_{xl} = F_{xi} \tag{3-15}$$

$$F_{xr} \cdot \frac{w}{2} - F_{xl} \cdot \frac{w}{2} = M_{zi} + M_{zr} + M_{zl} \tag{3-16}$$

$$M_{yr} + M_{yl} = M_{yi} \tag{3-17}$$

$$F_{zr} + F_{zl} = F_{zi} \tag{3-18}$$

$$F_{zl} \cdot \frac{w}{2} - F_{zr} \cdot \frac{w}{2} = M_{xi} - M_{xr} - M_{xl} \qquad \text{(3-19)}$$

There are only five equations to solve for the six unknowns (the force equation in y" does not provide any new information and is not considered here). An additional equation is needed to solve for the moments in the y" direction. Here, it is assumed ᴜᵤat both sides have the same contribution to that balance, hence the additional equation:

$$M_{yr} = M_{yl} \qquad \text{(3-20)}$$

The forces acting on the body can then be calculated and expressed as functions of the input forces and of F_{yr}, F_{yl}, M_{xr}, M_{xl}, M_{zr} and M_{zl}, that are defined by the transverse forces only. Their expressions are :

$$F_{xl} = \frac{F_{xi}}{2} - \frac{M_{zi}}{w} \qquad \text{(3-21)}$$

$$F_{xr} = \frac{F_{xi}}{2} + \frac{M_{zi}}{w} \qquad \text{(3-22)}$$

$$M_{yr} = \frac{M_{yi}}{2} \qquad \text{(3-23)}$$

$$M_{yl} = \frac{M_{yi}}{2} \qquad \text{(3-24)}$$

$$F_{zl} = \frac{F_{zi}}{2} + \frac{M_{xi} - M_{xr} - M_{xl}}{w} \qquad \text{(3-25)}$$

$$F_{zr} = \frac{F_{zi}}{2} - \frac{M_{xi} - M_{xr} - M_{xl}}{w} \qquad \text{(3-26)}$$

These results can be checked intuitively. For example, if the center of mass is shifted to the right side of the body then M_{xi} increases and, from (3-25), F_{zr} becomes more negative. Also, if the roll of the body is positive, more weight should be transferred to the right side. What happens then is that the transversal forces F_{yi} become more positive. Therefore, M_{xr} and M_{xl} become more negative (from (3-13) and (3-14)) and so does F_{zr} from (3-26). Such rapid tests suggest that the equations are correct.

From these solutions, the forces that will be applied to each rover side can be deduced. The rocker-bogie mechanism is modeled as a two-dimension system. The following sections present the force analysis of the rocker-bogie, address the issue of actuator redundancy, and present a method to find an optimum wheel torque distribution.

3.3. Planar Analysis of the Rocker-Bogie

This section presents the planar quasi-static force analysis of the rocker-bogie mechanism. Some planar analysis has been developed for mobility evaluation of the rocker-bogie design in (Linderman *et al.*, 1992). This analysis is a general tool to accommodate any sort of input of rocker-bogie configuration. It can then be used to study the effect of the kinematic parameters on the load distribution.

The model is shown in Figure 3-6. In this model, there are six unknowns (T_i, N_i, i=1,2,3) and four independent static equilibrium equations. There are indeed two equilibrium equations for the forces in the **x"** and **z"** directions, and two moment equations on the rocker-bogie pivot joint. The moment equation must be zero at that point for both the rocker and the bogie, hence two equations.

The inputs to the system are F_x^i, F_z^i and M_y^i. They are related to the parameters calculated in the previous section (F_{xr}, F_{zr}, etc.) based on the free body diagram in Figure 3-4. The geometry of the ground, and therefore the directions of the traction and normal forces are known. The direction of these forces are defined by the inverse kinematics procedure that locally considers the ground as a plane under each wheel (see Chapter 2). To perform the force analysis, the positions of the wheel contact points with respect to the rocker-bogie joint are required. The vectors **u**, **v** and **w** connect the wheel/ground contact points to the rocker-bogie joint (see Figure 3-6). Vector **z** connects the rocker/body joint to the rocker/bogie joint. Their components along **x"** and **z"** are written with x and z

subscripts respectively. The expression of these vectors as function of the kinematics of the rover can be found in Appendix B.
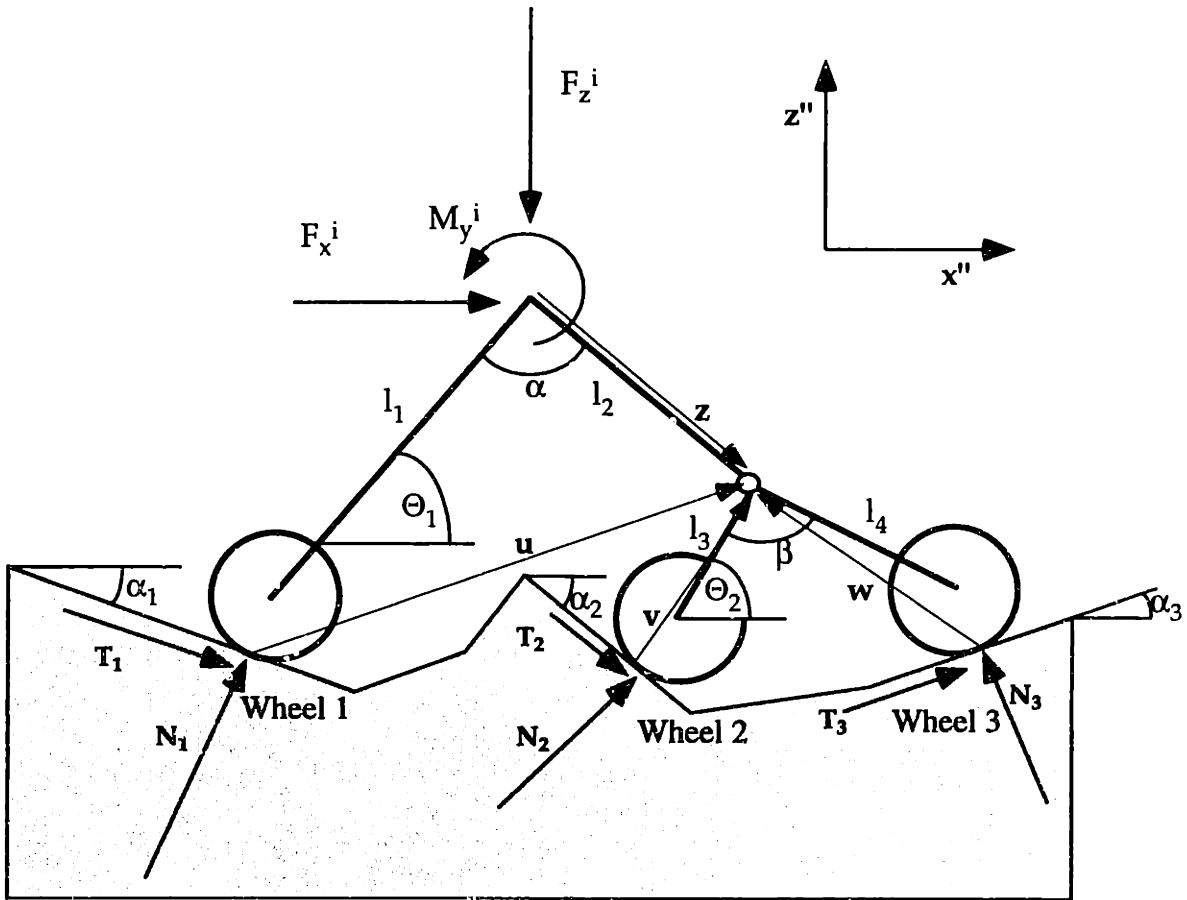
Figure 3-6: Rover Planar Analysis.

The static equilibrium equations are:

$$T_1 \cdot c_1 + T_2 \cdot c_2 + T_3 \cdot c_3 - N_1 \cdot s_1 - N_2 \cdot s_2 - N_3 \cdot s_3 + F_x^i = 0 \tag{3-27}$$

$$T_1 \cdot s_1 + T_2 \cdot s_2 + T_3 \cdot s_3 + N_1 \cdot c_1 + N_2 \cdot c_2 + N_3 \cdot c_3 - F_z^i = 0 \tag{3-28}$$

$$T_1 \cdot c_1 \cdot u_y - T_1 \cdot s_1 \cdot u_x - N_1 \cdot s_1 \cdot u_y - N_1 \cdot c_1 \cdot u_x + M_y^i + F_x^i \cdot z_y + F_z^i \cdot z_x = 0 \tag{3-29}$$

$$T_2 \cdot c_2 \cdot v_y - T_2 \cdot s_2 \cdot v_x - N_2 \cdot s_2 \cdot v_y - N_2 \cdot c_2 \cdot v_x$$
$$+ T_3 \cdot c_3 \cdot w_y - T_3 \cdot s_3 \cdot w_x - N_3 \cdot s_3 \cdot w_y - N_3 \cdot c_3 \cdot w_x = 0 \tag{3-30}$$

where $c_i = \cos(\alpha_i)$ and $s_i = \sin(\alpha_i)$, $i=1,2,3$. These equations can also be expressed in matrix form (see Equation (3-31)).

$$\mathbf{A} \cdot \begin{bmatrix} T_1 & T_2 & T_3 N_1 & N_2 & N_3 \end{bmatrix}^T = \begin{bmatrix} -F_x^i & F_z^i & -M_y^i - F_x^i \cdot z_y - F_z^i \cdot z_x & 0 \end{bmatrix}^T \qquad (3\text{-}31)$$

where **A** is a 4x6 matrix (four equations, six unknowns). Hence the system of equations is underdetermined and its null space is at least of dimension two. A more detailed study of this matrix can be found in Appendix B.

This system cannot be uniquely solved. However, it is very important to note that some of the unknowns can be controlled or constrained. Equilibrium of a wheel is given by Equation (3-32) (assuming that the wheel is not slipping).

$$\tau_i = rad \cdot T_i \qquad (3\text{-}32)$$

where *rad* is the radius of the wheel, T_i the traction force and τ_i is the torque applied to the wheel by the motor. It is equivalent to consider the traction forces or the wheel torques, since they are related by the constant *rad*.

Since there are two infinities of solutions, two traction forces can be arbitrarily chosen. The rear and middle wheel traction forces are considered as command inputs. The other forces, including the third traction force and the other normal forces are uniquely determined by these inputs. For example, if the rover is standing on a flat terrain, two traction forces can be applie .1 the wheels 1 and 2. To obtain equilibrium, the thi·d force must be equal to the opposite of the sum of the other two. This intuitively verifies the double infinity of solutions.

The problem can then be restated by using the traction forces T_1 and T_2 as parameters and inputs to the system :

$$\mathbf{B} \cdot \begin{bmatrix} T_3 & N_1 & N_2 & N_3 \end{bmatrix}^T = \mathbf{C} \cdot T_1 + \mathbf{D} \cdot T_2 + \mathbf{E} \qquad (3\text{-}33)$$

where **B** is 4x4, and **C**, **D** and **E** are 4x1 vectors.

If **B** is invertible, T_3, N_1, N_2 and N_3 are linear functions of T_1 and T_2.

$$
\begin{bmatrix} T_3 \\ N_1 \\ N_2 \\ N_3 \end{bmatrix} = \begin{bmatrix} c'_1 \\ c'_2 \\ c'_3 \\ c'_4 \end{bmatrix} \cdot T_1 + \begin{bmatrix} d'_1 \\ d'_2 \\ d'_3 \\ d'_4 \end{bmatrix} \cdot T_2 + \begin{bmatrix} e'_1 \\ e'_2 \\ e'_3 \\ e'_4 \end{bmatrix}
$$
(3-34)

Properties of **B** and the expressions of the solutions are described in Appendix B.

Any couple (T_1, T_2) defines a solution to the equilibrium equations. However, the solution must satisfy the physical constraints such as motor saturation, wheel slip and that the normal forces must be positive.

Firstly, constraints on the sign of the normal forces must be verified:

1) $N_i \geq 0 \quad \forall i$ (3-35)

Clearly, the normal forces must be positive. The condition $N_i < 0$ implies that the ground would have to pull down on the wheel to maintain equilibrium.

Secondly, the motors cannot create an infinite torque. Physical limitations of the system have to be taken into account.

2) $|rad \cdot T_i| \leq \tau_{sat} \ , \ \forall i$ (3-36)

Thirdly, a limitation on the traction force due to wheel slip must be verified. The maximum traction force is limited by the product of the coefficient of friction and the normal force on the wheel.

3) $|T_i| \leq \mu \cdot N_i \ , \ \forall i$ (3-37)

These three constraints must be satisfied at all times and for all the wheels. Finding a couple (T_1, T_2) that satisfies these three constraints is challenging.

A common way of finding a solution to such over determined problems is the pseudo-inverse method. An advantage of this method is that it is very simple to implement and it is computationally efficient. The pseudo inverse of a matrix **A** is defined as $\mathbf{A}^\# = \mathbf{A}^T$

$(A\ A^T)^{-1}$. The solution to $A\ x = b$ given by this method is: $x = A^{\#}\ b$. The method minimizes $\|x\|^2$ (Doty, 1993).

In the case of the rover, however, some of the unknowns cannot be directly actuated (the normal forces). Hence the optimum solution found with the pseudo-inverse would have little relation to the power consumption. Also, there is no guarantee that the physical constraints are verified. Another method must be used that fully considers the physics of the system. It is described in the following section.

3.4. Force Analysis Solution
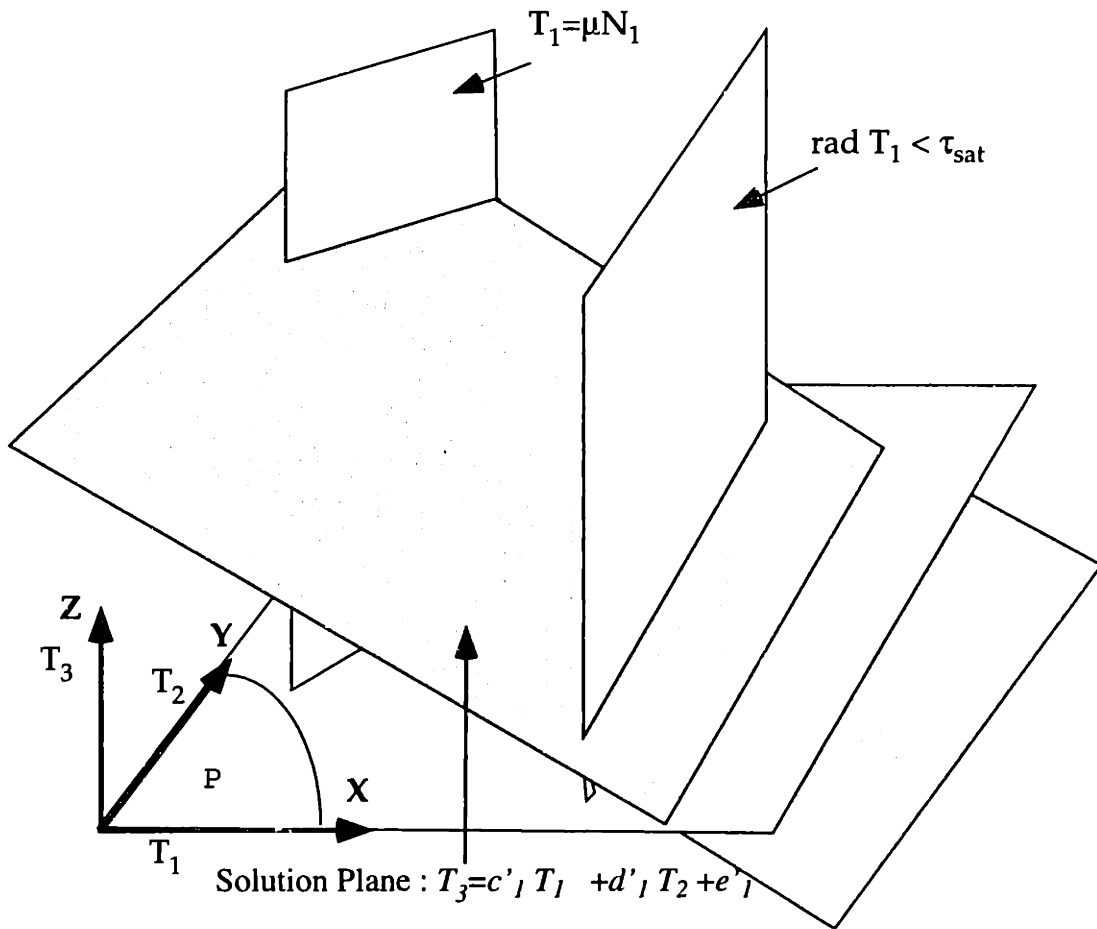
3.4.1. Solution Space

Figure 3-7: 3-D Solution Space.

To solve for the underdetermined force analysis while verifying all the physical constraints, a good representation of the problem is necessary. The previous section describes how to express T_3, N_1, N_2 and N_3 as linear functions of T_1 and T_2. A 3-D visualization of the solution space is shown in Figure 3-7. Here, the plane defined by $T_3=c'_1 T_1 +d'_1 T_2 +e'_1$ is represented. This plane is the solution space which contains the two infinities of solutions. Other planes are drawn that represent the physical constraints of the system. These constraint planes are represented by such equation as $rad\ T_i = \tau_{sat}$ or $T_i = \mu\ N_i$ (see Table 3-1).

It is easier to view the orthogonal projection of the solution plane onto the (X,Y) plane. The plane (X,Y) will be referred to as P (see Figure 3-8).

The constraints are also projected into P. They are functions of T_1 and T_2 only, therefore they become lines in P (see Equation 3-34). There are nine constraints (three per wheel). Since some of these constraints are represented using absolute values, they are broken into two constraint equations (one if the term inside the absolute value is negative, and the other if the term inside the absolute value is negative). Six of the nine constraints are represented with absolute values, leading to 12 equations. In total, 15 equations must be computed. They are represented on Table 3-1.

Table 3-1: Physical Constraints

1	$rad \cdot T_1 \le \tau_{sat}$	2	$rad \cdot T_1 \ge -\tau_{sat}$
3	$rad \cdot T_2 \le \tau_{sat}$	4	$rad \cdot T_2 \ge -\tau_{sat}$
5	$rad \cdot T_3 \le \tau_{sat}$	6	$rad \cdot T_3 \ge -\tau_{sat}$
7	$T_1 \le \mu \cdot N_1$	8	$T_1 \ge -\mu \cdot N_1$
9	$T_2 \le \mu \cdot N_2$	10	$T_2 \ge -\mu \cdot N_2$
11	$T_3 \le \mu \cdot N_3$	12	$T_3 \ge -\mu \cdot N_3$
13	$N_1 \ge 0$	14	$N_2 \ge 0$
15	$N_3 \ge 0$		
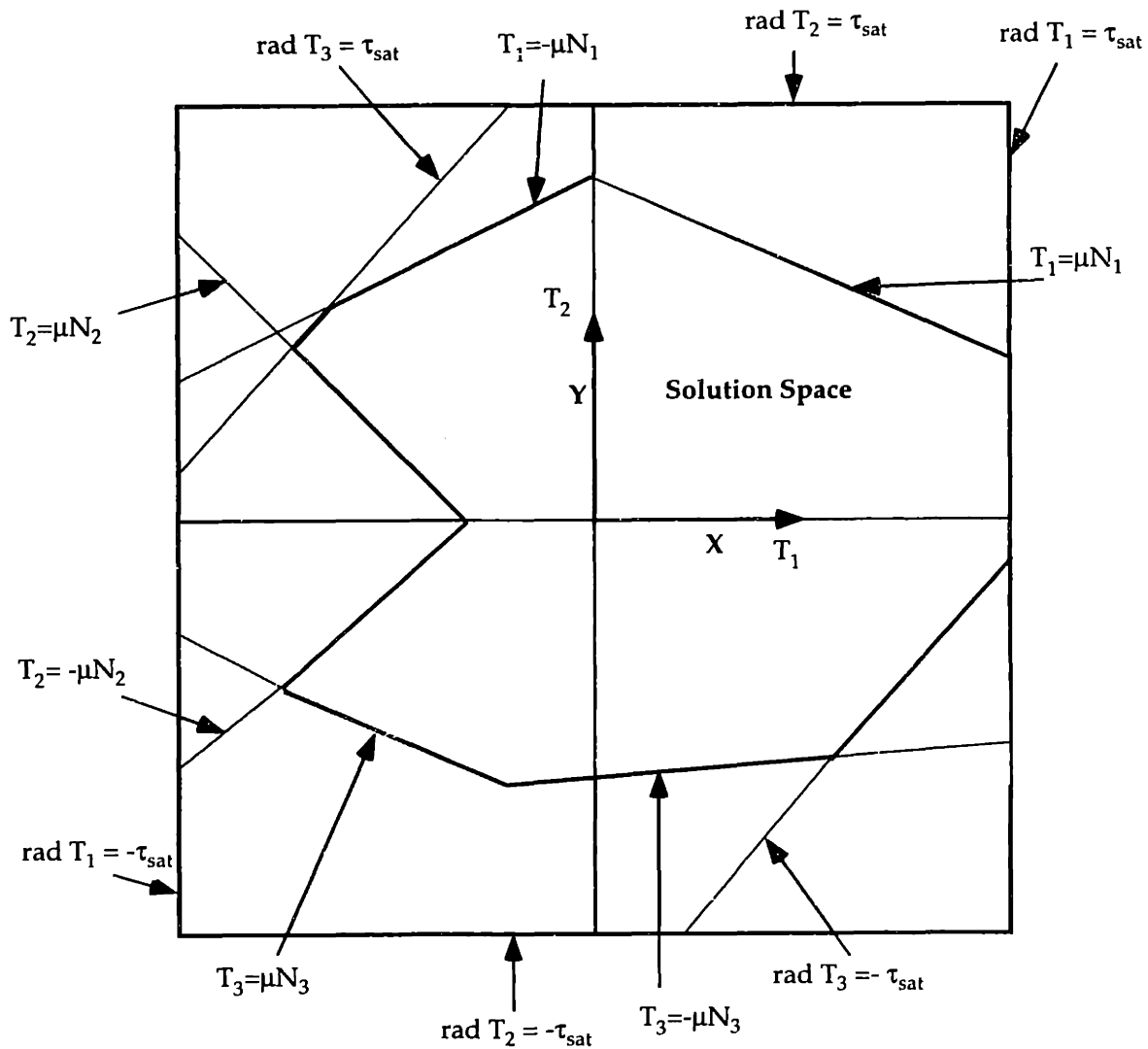
Figure 3-8: 2-D Visualization of the Solution Space.

This fully defines the solution space. The following method uses this representation to find a suitable solution to the underdetermined system of equations.

3.4.2. Solution Search for the Statics of the Rover

The solution space contains either zero or an infinity of solutions. It is then necessary to define criteria to choose the best solution. Since power consumption is critical in planetary exploration missions, the minimization of this variable is chosen as the criteria in finding a solution.

For systems actuated by DC motors using pulse-width-modulated amplifiers (as in this case), the power consumed can be estimated by the power dissipation in the motors' resistances (Dubowsky *et al.*, 1995). Therefore, power consumption in the wheels is a function of the square of the motor current (see Equation 3-38).

$$P = \sum_k R \cdot i_k^2 \qquad (3\text{-}38)$$

where R is the motor resistance and i_k the current through the motor k. The motor current i_k is defined by Equation (3-39).

$$i_k = \frac{\tau_{motor,k}}{k_{motor}} \qquad (3\text{-}39)$$

where $\tau_{motor,k}$ is the torque applied by the motor and k_{motor} is the motor constant. The quantity $\tau_{motor,k}$ is related to the output motor torque by the gear ratio r (see Equation (3-40)).

$$\tau_{motor,k} = \frac{\tau_k}{r} \qquad (3\text{-}40)$$

where r is the gear ratio of motor k. The power consumption can be deduced from (3-38), (3-39) and (3-40) and is given by:

$$P = \frac{R}{r \cdot k_{motor}^2} \sum_k \cdot \tau_k^2 = \frac{R \cdot rad^2}{r \cdot k_{motor}^2} \sum_k \cdot T_k^2 \qquad (3\text{-}41)$$

In other words P can be written as a second order function of T_1 and T_2. The function P is an elliptic paraboloid. Since P is a second order polynomial, it has a unique global extremum. Moreover since P is always greater than or equal to zero, that extremum is a minimum (if it were a maximum, then the branches of the paraboloid would tend to negative infinity): P is monotonically increasing away from the minimum point.

The solution that minimizes power consumption can now be found. To do this, the system of equations (3-42) must be solved.

$$\min(P) \Rightarrow \begin{cases} \dfrac{\partial P}{\partial T_1} = 0 \\ \dfrac{\partial P}{\partial T_2} = 0 \end{cases} \qquad \text{(3-42)}$$

Since P is second order, Equation (3-42) is a linear system of equations which is solved numerically. only. If the computed minimum value does not violate any constraint, it is the solution. If it does, the optimum lies on one of the violated constraints (because P is monotonous). The following steps are used to compute the optimum:

1) The constraints that are violated by the minimum are set aside. They are defined as the active constraints (see Figure 3-9).

2) If only one of these constraints is violated, the solution is taken as the closest point to the minimum that lies along the line equation of the constraint. The equation specific to that geometric problem can be found in (Anton, 1984). This is not necessarily the optimum solution but it can be found rapidly. The algorithm ends.

3) If more than one constraint is active, it is not possible to use the step 2) method the closest point to the minimum on any active constraint is not guaranteed to satisfy all the conditions. Therefore, the easiest and fastest way to find a solution is to look at the intersection of the constraints lines. The algorithm calculates the intersection of the active constraints with all the other constraints (the intersections between non-active constraints are not interesting since the optimum should lie on an active constraint).

The active intersections set A is defined as the set of the intersections that do not violate any constraint. If A is void, there are no solutions. If not, the solution is taken as the active intersection that has the minimum power. This configuration is presented in Figure 3-9.
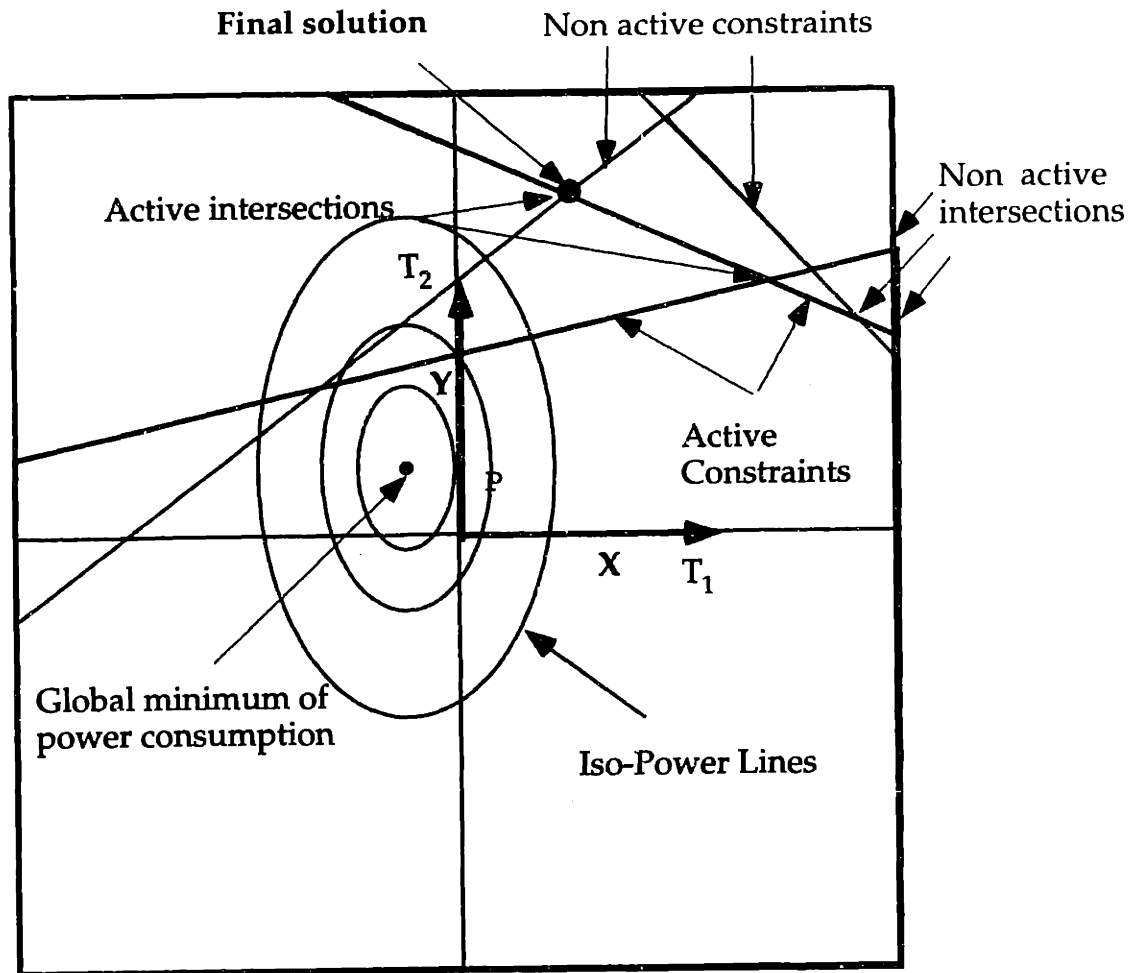
Figure 3-9: Force Analysis Solution Search Method.

Of course, this solution does not always provide the optimum solution, because the constraints intersections are not always the optimum. But it is sufficient to determine if a suitable solution can be found.

3.5. Calculation of Important Parameters

It is necessary to define and compute some measures that give an indication of how well the rover is performing. The factors considered here are: static stability, power consumption, actuator saturation, wheel slip and distance traveled. The definitions and computation of these measures are presented below. For reasons of robustness, they are represented as non-dimensional ratios. Some errors in the model or ground representation are likely to alter the real value of that ratio.

3.5.1. Stability Margin

There are different ways to determine the stability of a vehicle. If dynamics is important one measure of stability is the energy required to tip over the vehicle (Ghasempoor *et al.*, 1995; Messuri *et al.*, 1985).

However, in the case of the LSR, dynamics are negligible. Consequently, stability margin is defined as a function of the location of the center of mass with respect to the wheels' contact points. A means to evaluate this stability is to project the center of mass on the horizontal plane of the wheel footprint polygon projection (see Figure 3-10).

The distance from the center of mass to the border of the stability polygon defines the system stability. Therefore, the stability margin can be defined as:

$$S = \frac{d_{min}}{d^0_{min}}$$

(3-43)

where d_{min} is the minimum distance between the center of mass and the stability polygon, and d^0_{min} is the nominal minimum distance evaluated when the rover is at its most stable position, *i.e.* on an horizontal surface (see Figure 3-10).

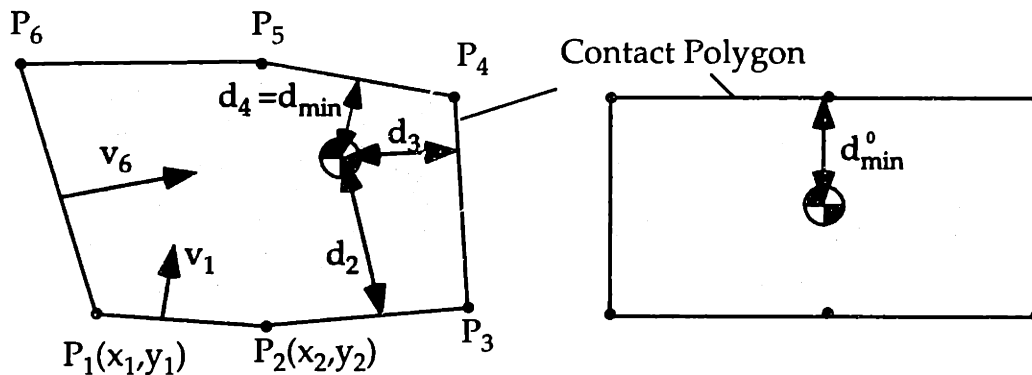**Figure 3-10: Stability Margin Definition.**

Let $P_i(x_i, y_i)$ be the coordinates of the ith contact point between the wheel and the ground in R_{ground}. The origin of R_{ground} is translated to the center of mass of the system.

Here, the stability polygon's vertices are ordered from 1 to 6 (the sides are $[P_iP_{i+1}]$). Let $\mathbf{v}_i$ be the normalized vector orthogonal to $\mathbf{P_iP_{i+1}}$ pointing towards the center of the polygon. Let d_i be the distance between $[P_iP_{i+1}]$ and the center of mass. The quantity d_i is deduced with the following formulae :

$$\mathbf{v}_i = \begin{bmatrix} -(y_{i+1} - y_i) \\ x_{i+1} - x_i \end{bmatrix} \cdot \frac{1}{\sqrt{(y_{i+1} - y_i)^2 + (x_{i+1} - x_i)^2}} \qquad (3\text{-}44)$$

$$d_i = \mathbf{P_iO} \bullet \mathbf{v}_i = \frac{x_i \cdot (y_{i+1} - y_i) - y_i \cdot (x_{i+1} - x_i)}{\sqrt{(y_{i+1} - y_i)^2 + (x_{i+1} - x_i)^2}} \qquad (3\text{-}45)$$

If $\exists\ i/d_i<0$, then the center of mass is out of the stability polygon. $d_{min}=0$. Else, $d_{min}=\min(d_i),= i=1...6$.

This method gives a good representation of the stability of the vehicle. However, it does not consider top heaviness: using this method, if the center of mass has the same projection on the contact polygon, its altitude does not affect the stability. In reality, it does, because a small perturbation on the rover would destabilize the rover more easily if the center of mass is high (see Figure 3-11).
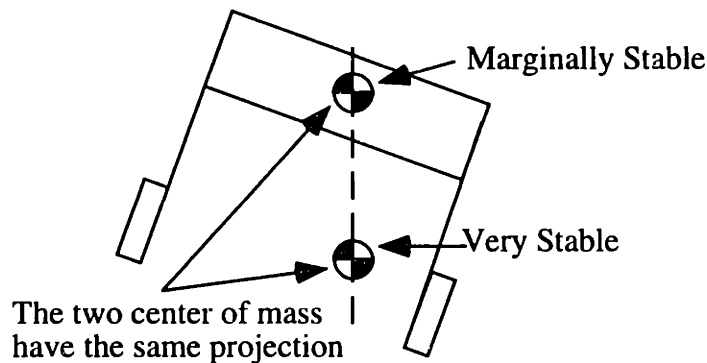
Figure 3-11: Top Heaviness.

Another method considers top heaviness in a more accurate way (Papadopoulos *et al.*, 1996).

Let L_i be the line joining the wheel contact points P_i and P_{i+1}. Let η_i be the angle between the vertical direction and the line that is orthogonal to L_i and contains the center of mass of the system (see Figure 3-12). The stability margin S is then defined as:

$$S = \min_i \left(\frac{\eta_i}{\eta_i^{nom}} \right) \tag{3-46}$$

where η_i^{nom} is the angle measured when η_i the rover is standing on a horizontal surface.
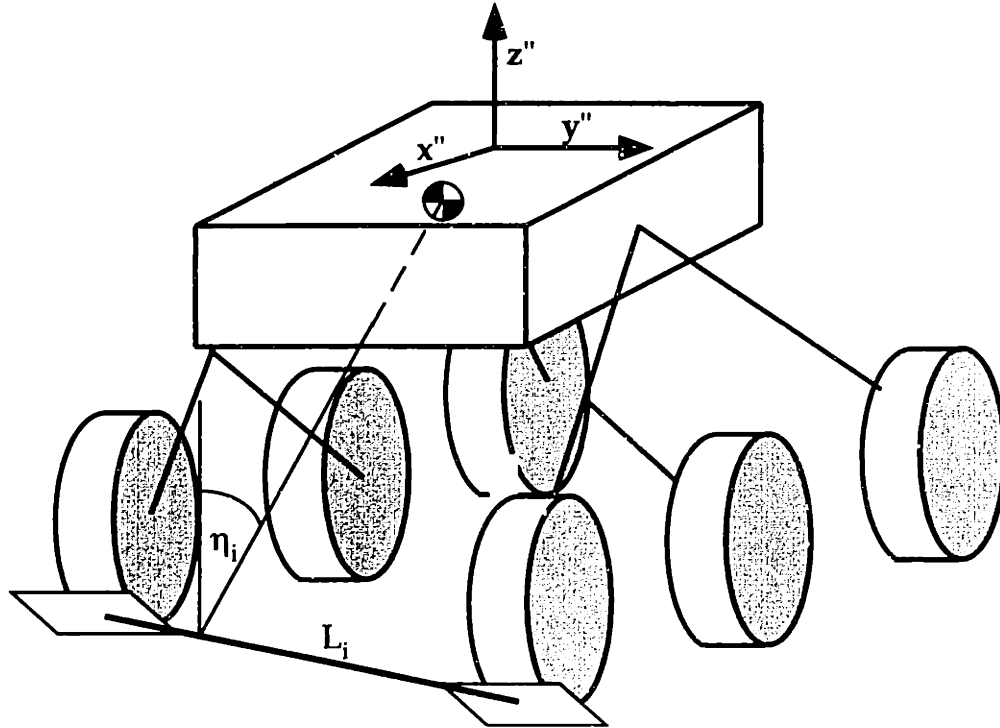
Figure 3-12: Stability Margin that considers Top-Heaviness.

3.5.2. Actuator characteristics

It is important to determine how the wheel torques are close to saturation (τ_{sat}). The torque saturation ratio measure is important in determining if the rover can move over obstacles. The torque saturation ratio is defined by Equation (3-47).

$$\tau_{ratio,i} = \frac{|\tau_i|}{\tau_{sat}} \tag{3-47}$$

3.5.3. Slip ratio

The slip ratio determines how close a wheel is from slipping. The ith wheel slip ratio S_i is defined as :

$$S_i = \frac{T_i / N_i}{\mu_i} \qquad \text{(3-48)}$$

where μ_i is the local coefficient of friction under wheel i. The slip ratio can be seen as the ratio between the coefficient of friction at which the wheel would slip and the actual coefficient of friction.

3.5.4. Power and Distance

The distance traveled by the rover across the terrain is also calculated. Power consumption is a crucial element. Its computation is detailed in Section 3.4.2.

It is felt that these measures are useful evaluation tools. Different designs can be implemented in the simulation and the influence of the kinematic parameters can be investigated.

3.6. Graphical Simulation

A graphical representation of the system is also beneficial to enhance the understanding of the system and to verify the veracity of the model.

The simulation includes a graphical interface. It originated from Mechanical System Visualizer (MSV), a 3-D graphical software (Torres, 1993). The original version has been upgraded to meet the requirements of the simulation (Cassenti, 1997). Specifically, it was upgraded to enable the representation of a meshed surface for the terrain, and to create a user interface window. The rover is displayed as it moves and interacts with its environment.

Figure 3-13 shows a typical instance of the graphical interface.
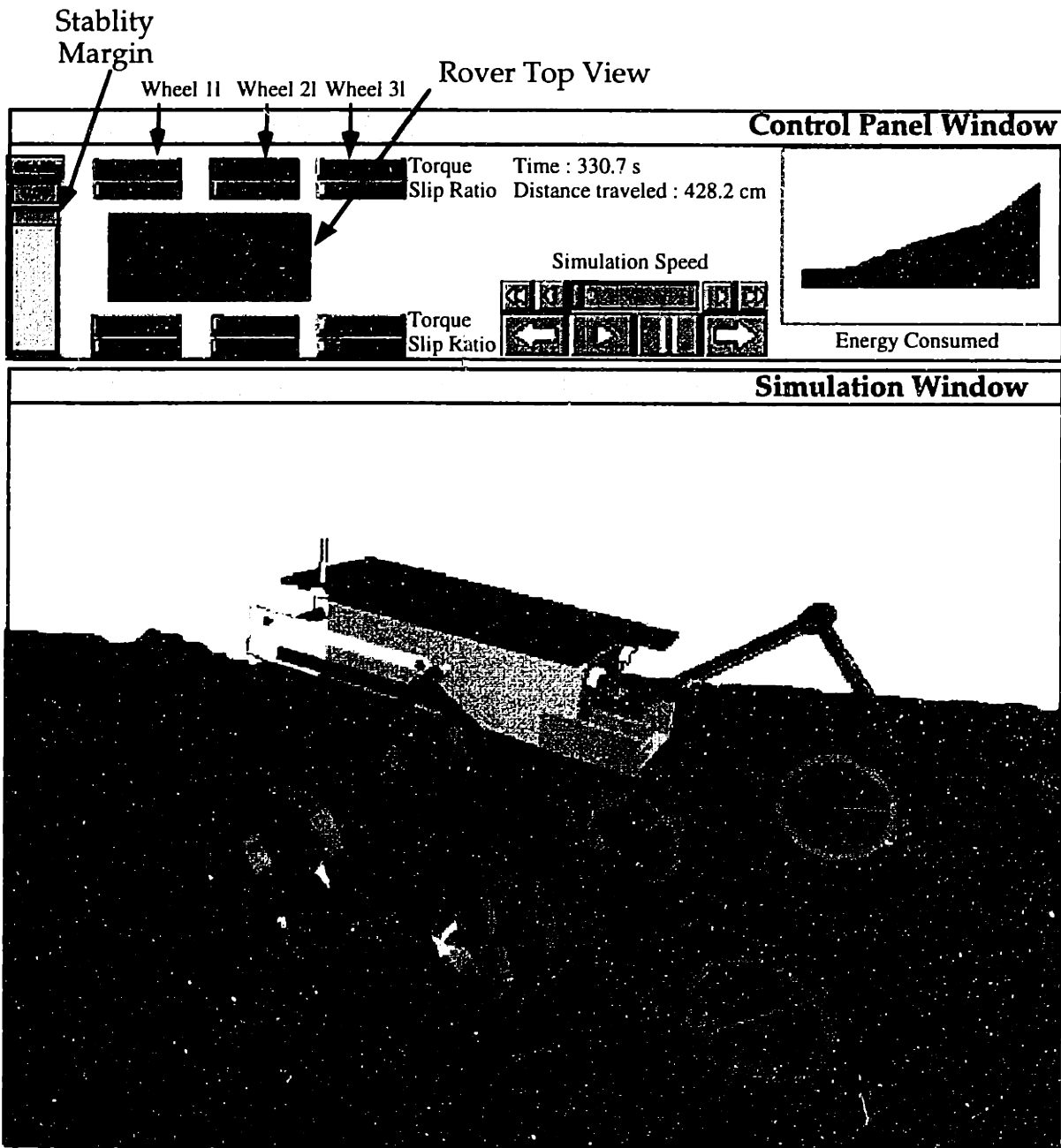

Figure 3-13: Graphical Simulation.

Additional features are included. First, it is possible to display the ground reaction forces. This makes it possible to check the load is distribution on the wheels.

Other features are displayed in another "Control Panel" window. This window displays the measures defined in Section 3.5, and updates them as the rover moves. This

was created using a C-code library, called the Forms library, a graphical user interface toolkit for Silicon Graphics Workstations (Overmars, 1995). More details on how the simulation and the graphics work can be found in (Hacot, 1998).

Stability margin is displayed on the left corner of the "Control Panel" window. Also, a rover top view is displayed and torque saturation and slip ratios are shown for each wheel. Finally, energy consumption is represented in a graph that is updated in real time.

There are also buttons that allow a user interface with the simulation. These buttons allow the user to stop, pause, step forward or backwards, at any desired speed. These capabilities proved useful in evaluating rover performance.

3.7. Conclusion

This chapter has presented the rover force analysis and simulation. The analysis is performed using a quasi-static model. The input force to the system can be arbitrarily chosen and can reflect the manipulator's interactions with the ground. The analysis shows that the actuator redundancy can be used to affect the load distribution on the wheel. A method has been developed that finds a solution to the under-determined system of equations for static equilibrium. A graphical interface has been developed that enhances the understanding of the physics of the system and displays different useful evaluation parameters. The analysis is not specific to a single configuration of the rocker-bogie mechanism. The kinematic parameters can be varied and their influence to the mechanics of the system can be studied.

4. Rover Traction Control

4.1. Introduction

The purpose of this chapter is to analyze the rover static equations with the aim of developing an active traction control algorithm. A planar simulation of the rocker-bogie mechanism is written in Section 4.2. The results are analyzed and heuristics are deduced in Section 4.3. A traction controller based on the heuristics is designed and implemented in Section 4.4.

4.2. Rover Planar Simulation

4.2.1. Motivation

In Chapter 3, a 3-D force analysis of the rover was presented. The main feature of the mechanism is its actuator and kinematic redundancy. This leads to coupling between wheel normal forces. This can be intuitively verified: for example, the middle wheel can lift up the front wheel if it is moving faster than the rear wheel.

Redundancy in contact force allocation is also addressed in (Venkataraman *et al.*, 1997). The normal force distribution can also be affected by the position of the center of mass of the system (Sreenivasan et al., 1997).

Normal force interaction must be controlled properly in order to avoid a loss of wheel contact which could reduce stability. Control of normal forces can also help reduce

wheel slip. It is widely known that a slipping wheel "digs in" easily on soft soil; this can induce rover positioning errors, if they are based on the wheel rotations.

It is thus useful to develop a planar hence simple simulation of the system to characterize the system redundancy and how it can be used to improve normal forces interaction.

4.2.2. Planar Simulation

In Chapter 3, the system was required to be in equilibrium, so the wheel torques had to verify balance equations that were dictated by the external forces. Specifically, the rover was required to maintain contact with the ground. Here, the approach is different. The wheel torques are treated as input to the system. The goal is to see how the system reacts to this input. Thus wheel contact loss is allowed.

The inputs to the simulation are (see Figure 3-6): α_1, α_2, α_3, τ_1, τ_2, τ_3, M_y^i and F_z^i. The unknowns that have to be determined are the normal forces on the wheels (N_1, N_2, N_3) and the rover body force F_x^i. The quasi static hypothesis is again used. In other words, it is assumed that the rover mass is big enough and that F_x^i is small enough so that the rover acceleration is small. The four balance equations lead to the following system :

$$\mathbf{M} \cdot \begin{bmatrix} F_x^i \\ N_1 \\ N_2 \\ N_3 \end{bmatrix} = \mathbf{X} \tag{4-1}$$

where $\mathbf{M}$ is a 4x4 square matrix (see Equation (4-3)) and $\mathbf{X}$ is a 4x1 vector function of the input (traction forces) and of the kinematics of the mechanism (see Equation (4-4)). Note that the vector $\mathbf{X}$ is a function of the traction forces, not the wheel torques. However, these traction forces can be deduced from the wheel torques, as described below.

The expressions for **M** and **X** are:

$$\mathbf{M} = \begin{bmatrix} 1 & -s_1 & -s_2 & -s_3 \\ 0 & c_1 & c_2 & c_3 \\ z_y & -s_1 \cdot u_y - c_1 \cdot u_x & 0 & 0 \\ 0 & 0 & -s_2 \cdot v_y - c_2 \cdot v_x & -s_3 \cdot w_y - c_3 \cdot w_x \end{bmatrix}$$

(4-2)

$$\mathbf{X} = \begin{bmatrix} -T_1 \cdot c_1 - T_2 \cdot c_2 - T_3 \cdot c_3 \\ -T_1 \cdot s_1 - T_2 \cdot s_2 - T_3 \cdot s_3 \\ F_z^i \cdot z_x - M_y^i - (T_1 \cdot c_1 \cdot u_y - T_1 \cdot s_1 \cdot u_x) \\ -\left(T_2 \cdot c_2 \cdot v_y - T_2 \cdot s_2 \cdot v_x + T_3 \cdot c_3 \cdot w_y - T_3 \cdot s_3 \cdot w_x\right) \end{bmatrix}$$

(4-3)

where $c_i = \cos(\alpha_i)$ and $s_i = \sin(\alpha_i)$.

The system is solvable by simply inverting **M**, either analytically or numerically. However, the values of T_i must still be deduced from τ_i.

An iterative method is used to compute the traction and normal forces of the system given the rover kinematics and environment characteristics. Figure 4-1 shows the algorithm structure.

The initial values of the traction forces are given by Equation 3-32. This equation assumes that the wheels are not slipping. Given these initial values, Equation 4-1 is solved and wheel slip or loss of contact can be verified. If the ith wheel loses contact (i.e. if the normal force N_i is negative), T_i and N_i are set automatically to zero for the rest of the algorithm. This adds an extra constraint to the system. However, the system is still solvable. If wheel slip is detected (i.e. $|T_i| > \mu\,N_i$), the value of T_i is incrementally decreased in the absolute sense, and the system is solved again. This algorithm is iterated until a solution without wheel slip is found.

Note that it is not possible to directly assign $|T_i| = \mu\,N_i$, as the equations of equilibrium would no longer be verified. Thus T_i must be gradually decreased until $|T_i| = \mu\,N_i$ is satisfied by the system of equations.
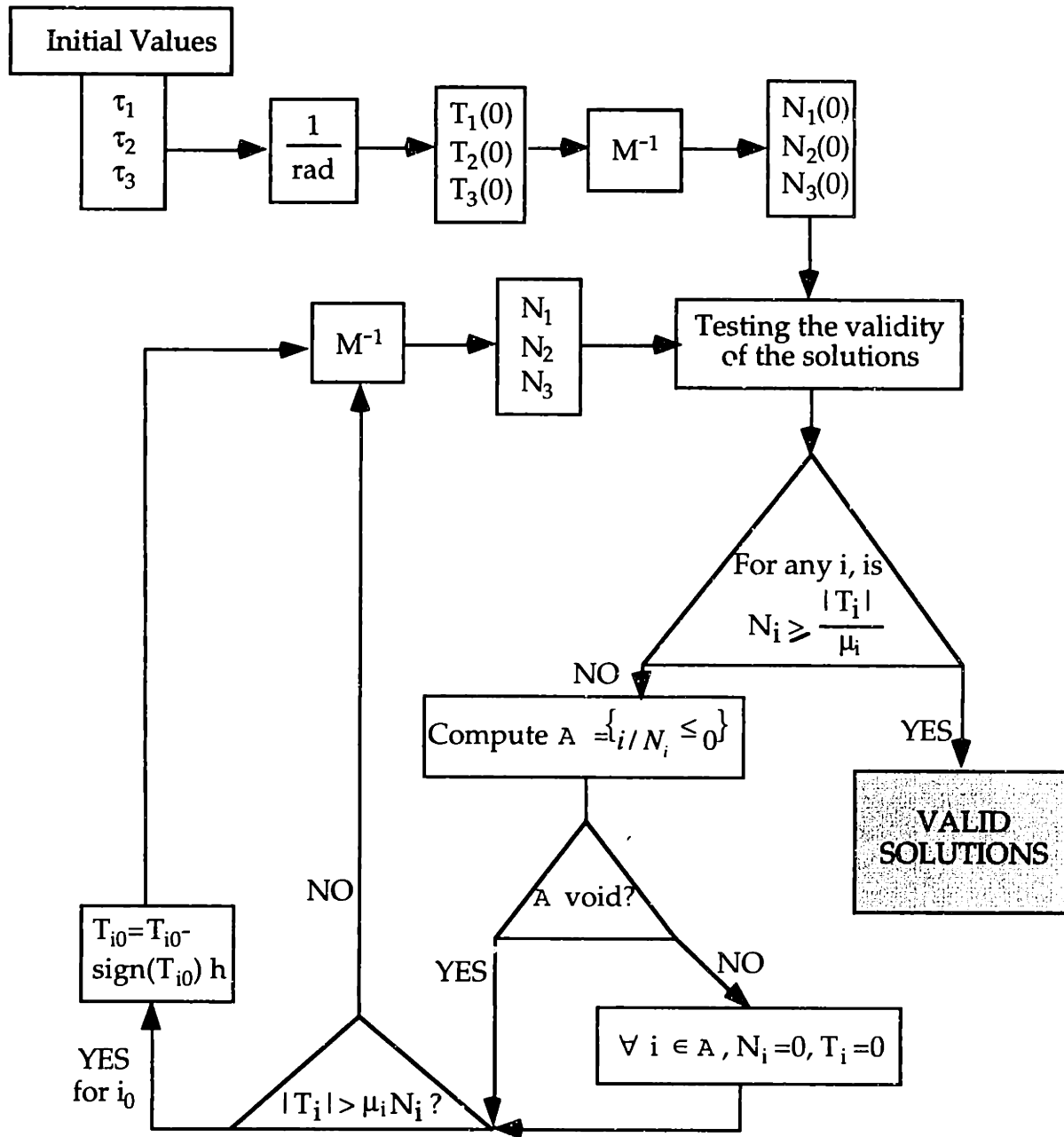
Figure 4-1: Planar Simulation Structure.

The algorithm determines whether wheels lose contact or slip. Some rules are used to calculate the wheel velocities. The system is assumed to be in quasi-static equilibrium. This means that the accelerations and moments of the different elements are almost zero. Here, the rover acceleration is deduced from F_x^i. The acceleration of the links of the rover are assumed to be small enough so that the values of the normal forces are correct. The

body velocity v_{rover} can be deduced from the acceleration of the rover. If a wheel is not slipping its angular velocity ω_i is :

$$\omega_i = \frac{v_{rover}}{rad} \qquad (4\text{-}4)$$

where *rad* is the radius of the wheel. The value of ω_i should be relatively small.

If the wheel is slipping or has lost contact, its angular acceleration is given by:

$$\dot{\omega}_i = \frac{\tau_i - T_i \cdot rad}{I_i} \qquad (4\text{-}5)$$

where I_i is the inertia of the ith wheel. Note that T_i is zero when contact is lost. Here the wheel angular velocity should increase rapidly.

Although this model is a very simplified version of reality (especially for wheel velocity computation), it is accurate enough to gain insight in the mechanics of the rover. Simulation results for different rover and terrain configurations are presented in the following section.

4.3. Simulation Results

This section presents the results of the planar simulation. Different representative tasks are presented: the rover rolling on a flat ground; the rover with its middle wheel on a step; the rover on uneven terrain. The results presented are the variations of the three normal forces as functions of each wheel input torque. A wheel torque is varied while the other two are put to zero. Since the system of equations determining the state of the vehicle is linear, each influence is additive. Therefore, each wheel is powered separately to isolate their influence. Wheel 1 is the rear wheel, wheel 2 is the middle wheel and wheel 3 is the front wheel (see Figure 3-6).

4.3.1. Flat Ground Results

In this case, the rover is on a flat ground. The simulation results are shown in Figure 4-2.
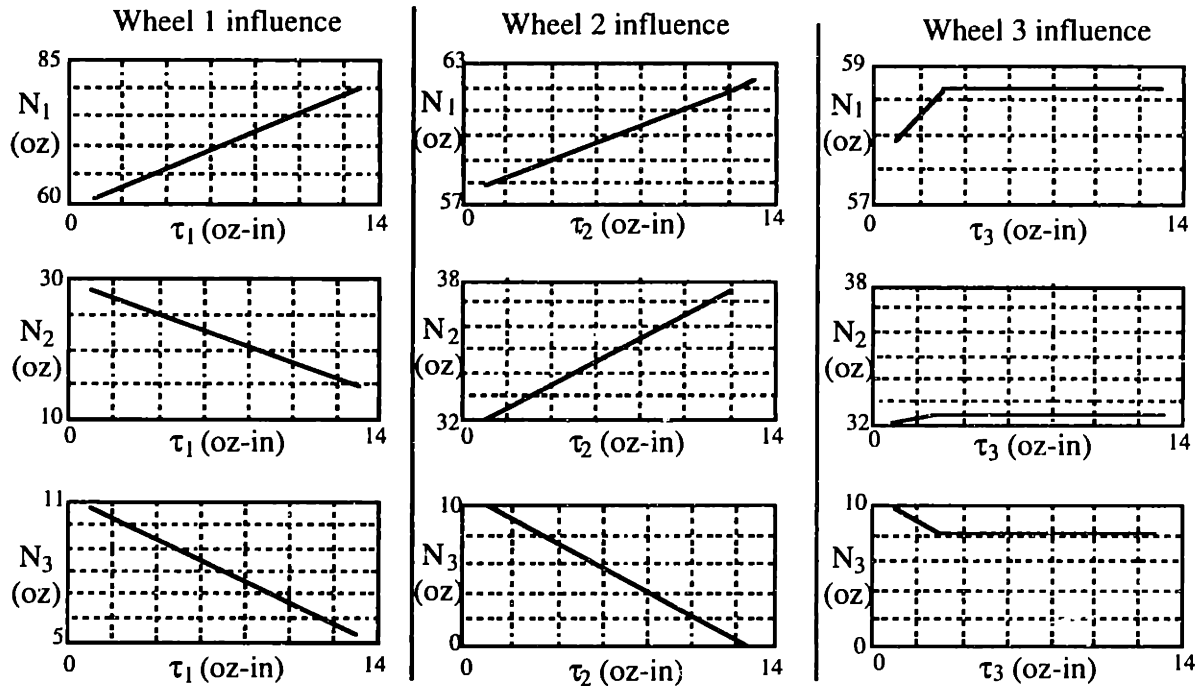

Figure 4-2: Simulation Results - Flat Ground.

It can be seen that the rear wheel (wheel 1) has a tendency to increase its normal force and to lift up the other wheels (i.e. decrease their normal force). The middle wheel tends to lift up the front one, and the front wheel has the same effect.

It is interesting to look at the wheel normal forces distribution. In this case, the rear wheel is supporting most of the load (about 60%), the middle has about 30% of the load and the front wheel only 10%. This is due to the geometry of the system and the relative position of the center of mass. In this case, the center of mass is located on the body/rocker joint. If it is translated forward, the front two wheels get more load, and the rear wheel, less. When the center of mass is above the middle wheel, the front and rear wheel share the same amount of load. If the center of mass is on the vertical of the rocker-

bogie joint, the rear normal force is zero: the rocker is on the verge of rotating around the free pivot joint. The initial normal force on the wheel (at $T_r=0$) affects the magnitude of the influence of the wheel. For example, the front wheel has almost no effect on the other two. The plateau that can be noticed on the plots of the influence of the front wheel is caused by wheel slip.

4.3.2. Middle Wheel on a Step

In this case, the middle wheel is on the a step and the front wheel is below the middle wheel, at the same altitude as the rear wheel (see Figure 4-3). The results are plotted on Figure 4-4.
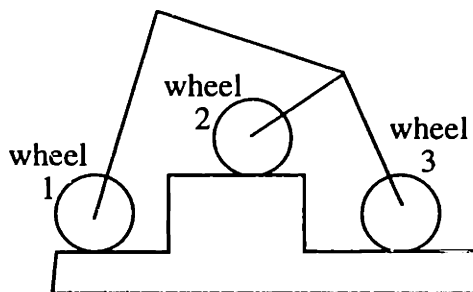

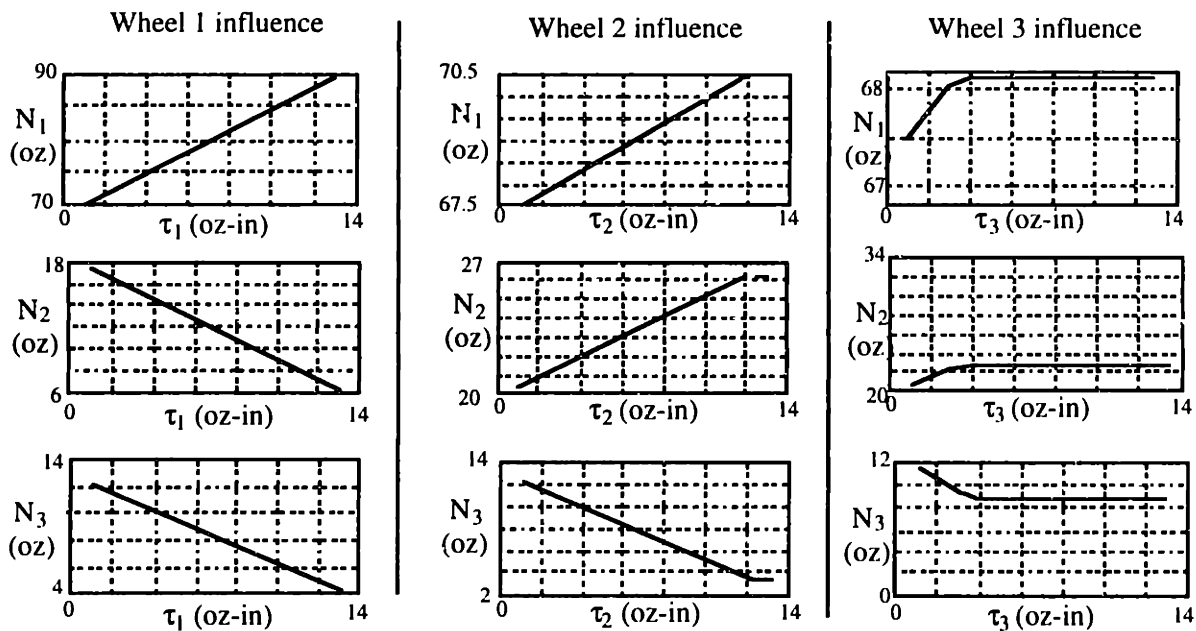**Figure 4-3: Middle Wheel on a Step - Rover Geometry.**

Figure 4-4: Simulation Results - Middle Wheel on a Step.

The rear wheel has a higher normal force than in the first case. The influence of the torques on the normal forces is the same as before, although their relative magnitude is changed.

4.3.3. Front Wheel on a 70 degree slope

In this case, the relative altitudes of the wheel centers are equal. The ground angle under the wheels is zero except for the front wheel, which is at 70 degree (see Figure 4-5). The results are shown in Figure 4-6.
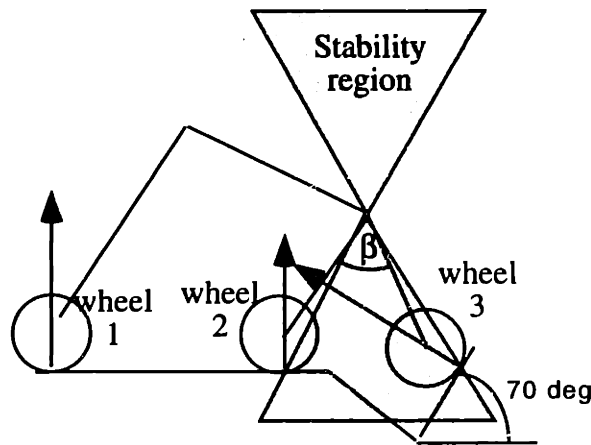
Figure 4-5: Stability Region Definition.

The stability region of Figure 4-5 is defined as the area between the lines joining the rocker-bogie joint and the contact points of the bogie wheels. It is important to note that the normal forces do not intersect in the stability region in this case. If the normal forces do not intersect in this stability region, they both have the same contribution to the moment balance about the bogie joint. Therefore, the system cannot be in equilibrium by itself. If no torque were applied, the front wheel would roll down and the middle wheel would likely lose contact. In the simulation, a constant torque τ_2 of 30 oz-in is added to all the torque distributions to enable N_2 and N_3 to be positive. Here, the action of the front wheel is opposite to the previous results. The influence of the rear wheel on the middle wheel normal force is also accentuated.
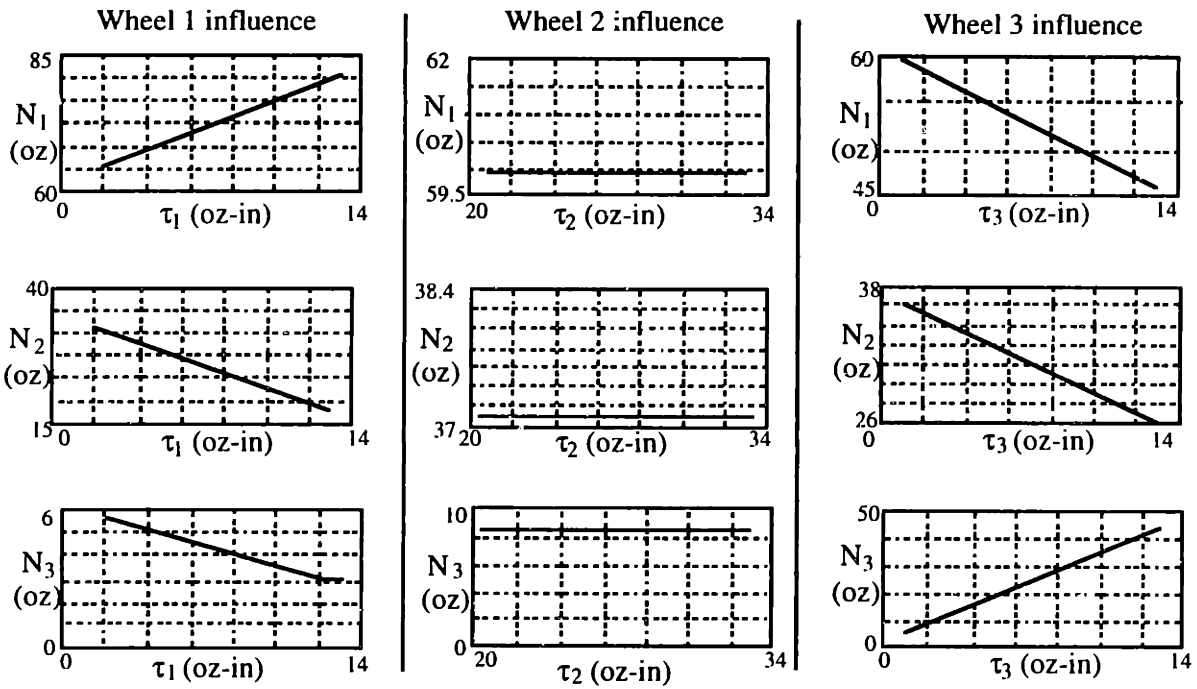
Figure 4-6: Simulation Results - Uneven Terrain

4.3.4. Heuristics

From the results of the previous sections, it is possible to develop some trends.

•Increasing the traction force on the rear wheel tends to cause the rear wheel normal force to increase and to decrease the other two normal forces.

•Increasing the traction force on the middle wheel tends to decrease the front wheel normal force and to increase the other two normal forces.

•Increasing the traction force on the front wheel tends to decrease the front wheel normal force and to increase the other two normal forces.

These trends are physically intuitive. If the rear wheel traction force increases, then the moment in y" increases too. Therefore, to balance this, N_1 must increase.

There are, however, cases when these heuristics are not valid:

• If the rover is in the configuration of Figure 4-7, N_1 is below the bogie joint. In this case, the influence of T_1 to N_1 is opposite to the one that is depicted in the previous examples.
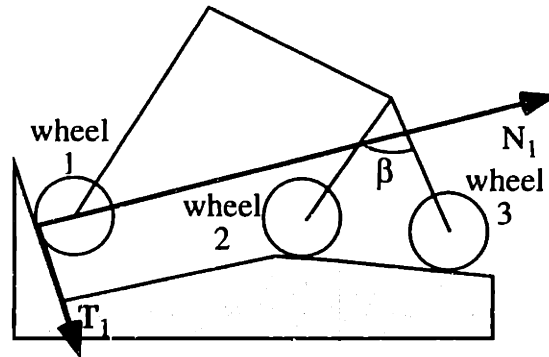
Figure 4-7: An Exception to the Heuristics.

•If the rover is in the configuration of Figure 4-4, the same thing is happening. This was described in Section 4.3.3. Often, when the normal forces do not intersect in the stability region, it has been observed on an experimental rover that one of the wheels loses contact. This stability region is increased with β. Increasing β also tends to lower the rover and decrease its ground clearance, while making it more stable.

This analysis shows some trends which influence normal forces distribution. It also shows the influence of the angle β on the response of the system, and the importance of ground geometry for torque distribution. These observations lead to the design of an active traction controller, based on fuzzy logic.

4.4. Active Traction Control Design

After the analysis of the previous section, a fuzzy logic based controller is the natural choice of traction control. Fuzzy logic can exploit the heuristics developed in Section 4.3.4 in a systematic manner.

4.4.1.Fuzzy Logic Control Theory

A fuzzy-logic controller is depicted by Figure 4-8. The fuzzification process consists of evaluating sensor input and determine the probability of different system states. For example, in the case of a room temperature control, a temperature above 35 C is given a very high value to the state "very hot" and a very small value to the state "cold". Functions are used to evaluate this likeliness of these sensor informations. They are referred to as Measurement Probability Distribution Functions (MPDF).

From these "fuzzy" measurements, fuzzy approximate reasoning is used to infer the output contributed by each rule (fuzzy output). This fuzzy approximation is obtained by using Command Probability Distribution Functions (CPDF). Then the fuzzy outputs determined by each rule are aggregated and go through a defuzzification process to form the output. More details on the fuzzy control theory are in (Ross, 1995).
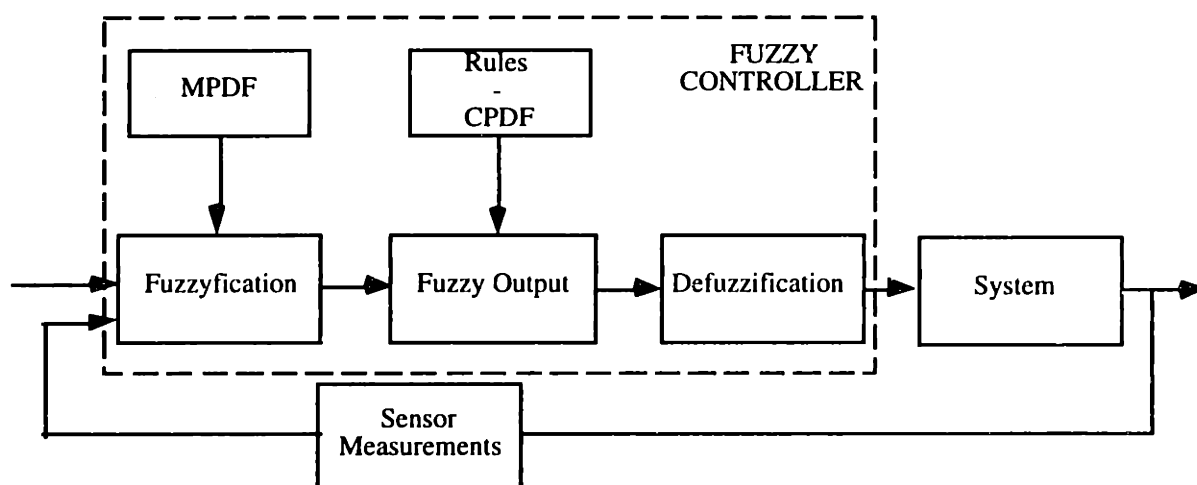

Figure 4-8: Fuzzy Logic Control Overview.

4.4.2.Fuzzy Logic Controller Design

The controller goal is to track a desired wheel angular velocity (so that the rover is moving in the desired direction) while minimizing wheel slip. A desired angular velocity (ω_d) of the wheels is the input of the system.

Sensor measurements and the control law determine by how much the commanded torques should change. They do not induce the command itself, just a change, as an integral controller. If a wheel is rotating too fast, this means it is probably slipping. Therefore, its commanded torque must be reduced (in the absolute sense) and the other wheels must be commanded such that they increase its normal force.

MPDFs are defined to evaluate the probability of different states of the rover wheels such as: wheel slipping backwards (SB), wheel rotating too slowly (SL), wheel at the correct angular velocity (ZR), wheel rotating too fast (FA), and wheel slipping forward (SF). In the same way, CPDFs are defined for the command change: very negative (NB), negative (N), negative small (NS), zero (Z), positive small (PS), positive (P), very positive (PB). The MPDFs and CPDFs are shown in Figure 4-9 and Figure 4-10 respectively.
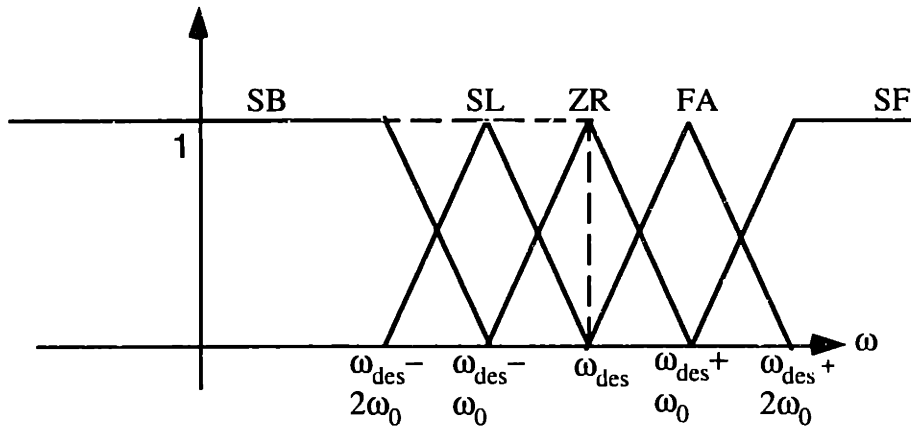

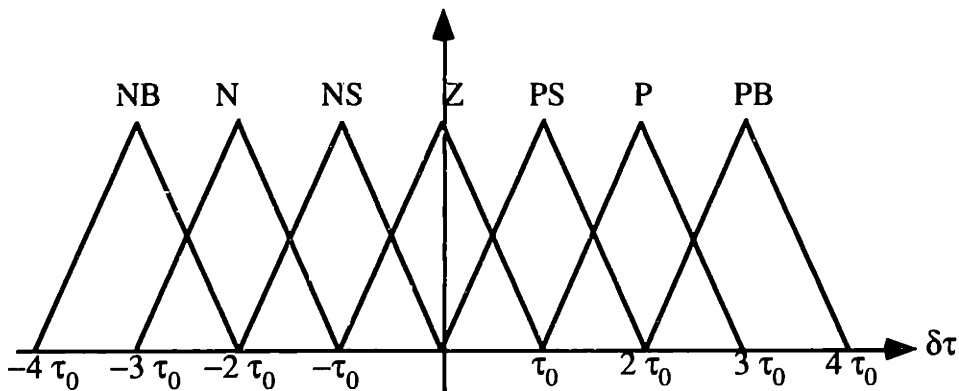**Figure 4-9: Measurement Probability Distribution Functions.**

Figure 4-10: Command Probability Distribution Functions.

Let SB_i be defined as $SB(\omega_i)$. SL_i, ZR_i, FA_i and SF_i, the other measurements, are defined in the same way. From these measurements and from the rules, the fuzzy set of outputs can be deduced. The following example illustrates the technique:

Let the kth condition be: if wheel i is slipping backwards (SB_i) and wheel j is slipping forward (SF_j) then the torque on wheel i is increased a lot (PB).

This is mathematically interpreted as : $PB_{i,k} = min(SB_i, SF_j)$.

The value PB_i, which sets the probability by which the torque change by a positive big number is then defined by:

$$PB_i = \max_k(PB_{i,k}) \qquad\qquad (4\text{-}6)$$

The same process is used for all rules and all the CPDFs.

The fuzzy set of commands for the ith wheel is then represented as in Figure 4-11. A defuzzification procedure deduces the output from that set. It is presented in Appendix C.
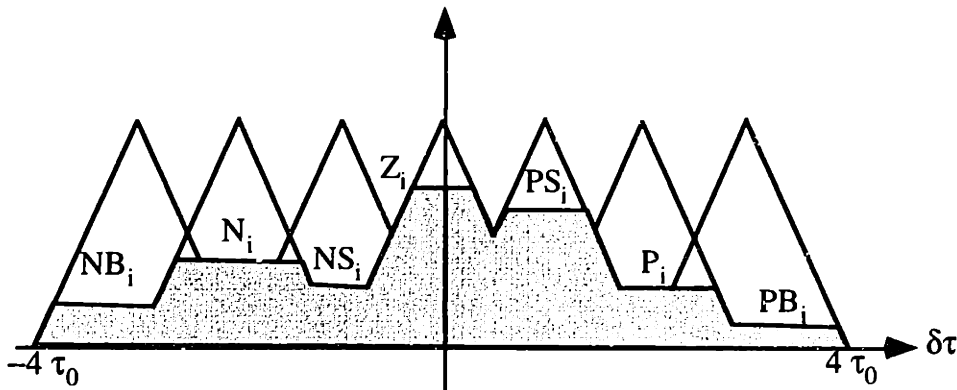

Figure 4-11: Fuzzy Set of Commands.

The set of rules that command the fuzzy logic controller is represented in Table 4-1 and Table 4-2. For simplification, the influence of the two front wheels on the rear wheel normal force is neglected. The interaction between the rear and the other wheels is taken

into account as well as the interaction of the middle and front wheels. This set of rules is only a function of the heuristics developed previously. It has been shown that in some cases the ground geometry can affect the wheel normal forces differently. These rules do not consider those special cases. The rules deduced are the following:

Table 4-1: Set of Rules.

	$SB(\omega_3)$			$NG(\omega_3)$			$ZR(\omega_3)$			$PS(\omega_3)$			$SF(\omega_3)$		
SB_2	NS	PB	PB	NS	PB	P	NS	P	Z	NS	P	NS	N	P	NB
NG_2	NS	PS	PB	-	P	PS	-	S	Z	-	P	NS	-	PS	NB
ZR_2	NS	NS	PB	-	Z	P	-	Z	Z	-	Z	NS	-	NB	N
PS_2	NS	N	PB	-	NS	PS	-	NS	Z	-	NS	Z	-	NB	N
SF_2	NS	NB	P	NS	NB	P	NS	NB	PS	NS	NB	Z	NS	NB	N

Table 4-2: Set of Rules - Rear Wheel.

SB_1			NG_1			ZR_1			PS_1			SF_1		
PB	-	-	P	-	-	Z	-	-	N	-	-	NB	-	-

These tables should be read as follows (for the kth rule):

	$MPDF_i$		
$MPDF_j$	$CPDF_{1,k}$	$CPDF_{2,k}$	$CPDF_{3,k}$

These rules follow the heuristics defined in Section 4.3.4.

The measurement fuzzy values are computed. Defuzzification determines the change in the wheel torques (see Appendix C).

It is important to note that the response of the controller is greatly affected by the choice of τ_0. Increasing τ_0 makes the controller react faster but with much more chatter (see Figure 4-13). The parameter ω_0 also has a big influence on the rover performance. The smaller it is, the more reactive the system is, but the higher its bandwidth.

A representative simulation result is shown below. The rover is simulated while climbing a step with a slope of 20 degrees. The front wheel is on a 3 inch high step, the middle wheel is on the slope and the rear wheel is on a flat ground (see Figure 4-12).
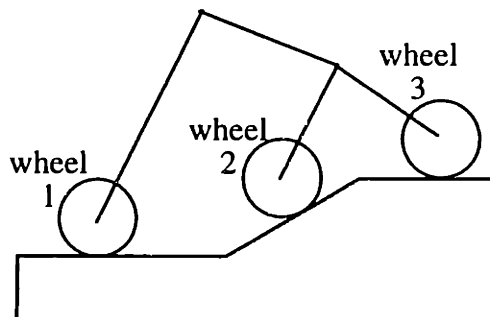

Figure 4-12: Step Climbing Simulation

The front wheel has no load initially. It can be seen, however, that the controller attempts to increase the load on the front wheel, thus reduce wheel slip. The front wheel stops slipping after less than 4 seconds. The rear wheel, by pushing the rover forward, increases its own normal force. Pushing the rover forward, in that geometry, increases the front wheel normal force. The time until the front wheel starts having a positive normal force can be decreased by increasing τ_0. However, when τ_0 is too high, there is some chatter. Figure 4-13 is a representative example of this phenomenon. This chatter is also caused by the fact that the wheel changes fuzzy states between slipping and non slipping, which stresses the importance of ω_0.

It can be seen that the wheel angular velocities do not exactly converge to the desired angular velocities. This is because the goal of the controller is not only to track that angular velocity. What is important is that the wheels turn in the right direction and that they do not slip.
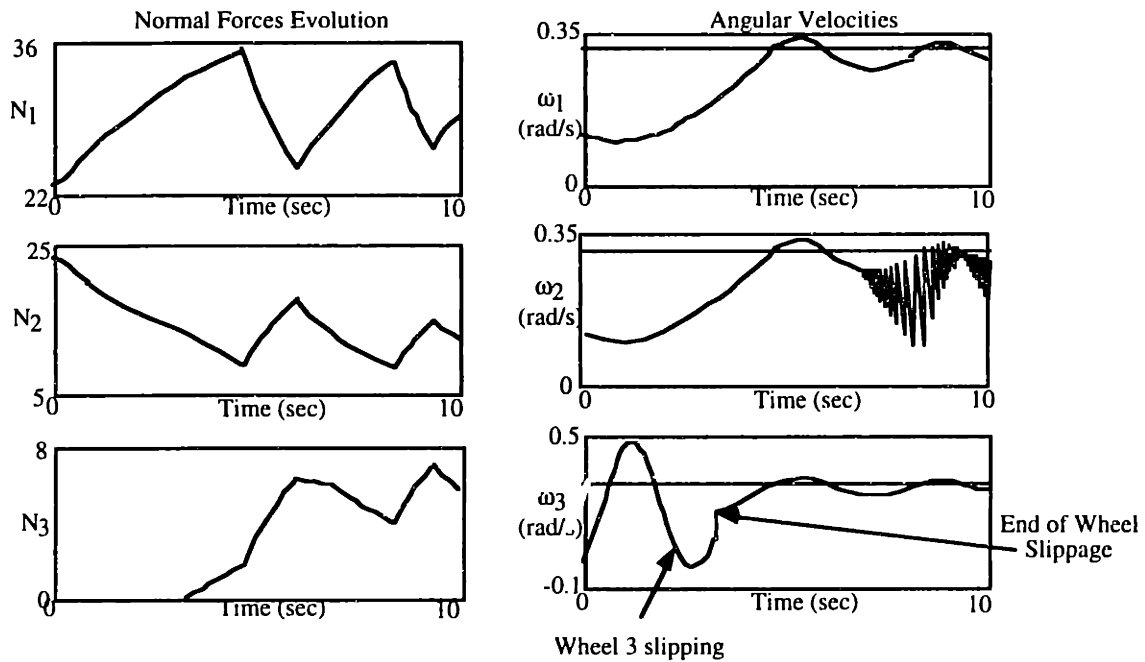
Figure 4-13: Active Traction Control: Simulation Results.

4.5. Conclusions

This chapter has presented planar simulation studies of the relationship between normal force distribution and wheel input torque. A set of heuristic rules was developed based upon the understanding of the physics of the rover. This set of rules is based on the ground geometry which is most commonly encountered. A fuzzy logic controller has been designed to improve traction. Simulation results show that the normal forces can be affected by the wheel torques and an example shows the distribution of the load on the wheels. These results are not enough though because the model is relatively simple. An experimental system is required for validation.

5. Experimental System

5.1. Introduction

This chapter presents some design concepts and experimental results of the MIT Field and Space Robotics Laboratory Mars Rover (MIT/FSRL Rover). Section 5.2 presents the design of the rover, of its environment dubbed "Mars" and proposed future enhancements. Section 5.3 details experiments that have been conducted with the rover. Experiments show that the analytical model results approximate those of the real system. Tests that compare the active traction controller to a PI wheel angular velocity controller are performed and presented.

5.2. Rover Description

5.2.1. Rover design overview

The MIT/FSRL rover is a rocker-bogie type rover. It is a kinematic scale model of the LSR-1 rover (see Figure 5-1 and Figure 5-2). Its footprint is about 14" long by 13" wide and it has a 6" ground clearance.

The rover development project is still underway. Appendix D presents the rover's proposed future evolutions. The experiments described below are conducted with the MOD 1.1 rover. MOD 2 includes the design and construction of a manipulator that is mounted on the rover. The ultimate goal of this project is to construct a self-contained rover (MOD 3). The design of this rover is detailed in (Burn, 1998).
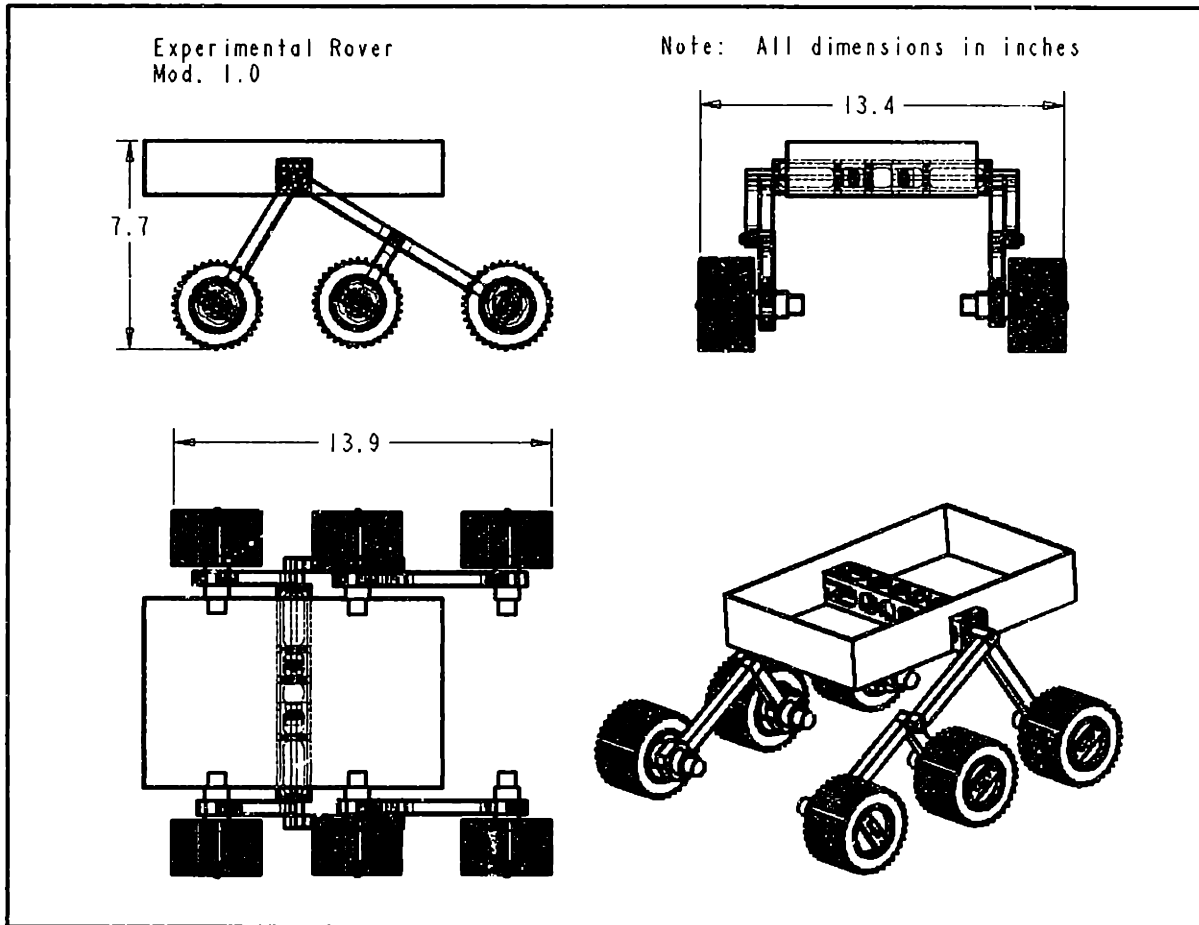
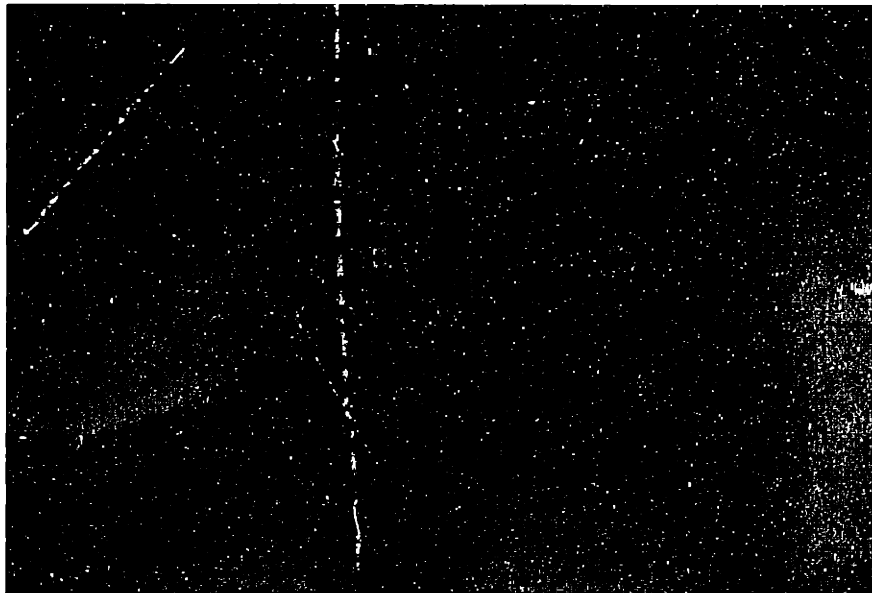Figure 5-1: MIT FSRL Rover Engineering Drawings (Burn, 1998)

Figure 5-2: The MIT/FSRL Rover.

5.2.2. Experimental Environment overview

The rover platform, "Mars", is a 10'x8' area. It has been designed to be a challenging course for the rover. Various slopes of 15, 20 or 30 degrees are accessible to the rover. A ditch, steep in some places and crossable in others, separates the area into two parts, north and south. The north part is defined as the part that includes a 9-inch high hill. It has been designed to be about two thirds of a wheel diameter deep. A 4-inch high plateau is located on the south area. It is challenging to climb as the access slopes are very steep. A picture of the "Mars" platform is shown in Figure 5-3.

Figure 5-3: The "Mars" Platform.

5.2.3. Motors characteristics

he rover wheels are powered by Portescap motors 23 HL 11 216E which are equipped with tachometers. The gear head has a ratio of 501:1 which limits the output angular velocity to 8 rpm and the output torque to 100 oz-in.

In MOD 1.1, the rover motors are powered by voltage to current National Semiconductor LM12CLK amplifiers. They were previously used with a climbing robot called Libra (Sunada, 1994; Bevly, 1997).

Because of the large gear ratio of the motors, friction is an important factor. Thus it is necessary to model the motors. The proposed model is the following :

$$\tau_{out} = r \cdot k_{motor} \cdot i - b_{motor} \cdot \omega_{motor} - \tau_{coulomb} \cdot \text{sgn}(\omega_{motor}) \qquad (5\text{-}1)$$

where τ_{out} is the output torque of the motor, k_{motor} is the motor's torque constant, r is the gear ratio, b_{motor} is the viscous damping constant, $\tau_{coulomb}$ is the coulomb friction torque as seen from the output of the motor, and ω_{motor} is the motor output shaft angular velocity.

Two experiments have been conducted on the motors to determine the values of the unknown constants k_{motor}, b_{motor} and ω_{motor}. First, the static motor torque is measured by attaching to the motor shaft a rod whose mass and center of mass position are known (see Figure 5-4).
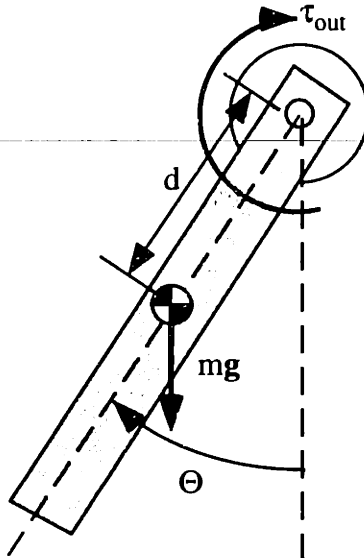

Figure 5-4: Motor Calibration.

The angle Θ measured when the system is at rest leads to the determination of the output torque:

$$\tau_{out} = -m \cdot g \cdot d \cdot \sin(\Theta) \qquad\qquad (5\text{-}2)$$

These experiments lead to the determination of the coulomb friction torque and of the motor torque constant. The constants are (see Appendix D):

Table 5-1: Motor Constants and Coulomb Friction.

k_{1r}=781 oz-in/A	$\tau_{coulomb,\ 1r}$=6.7 oz-in
k_{2r}=932 oz-in/A	$\tau_{coulomb,\ 2r}$=8.5 oz-in
k_{3r}=1022 oz-in/A	$\tau_{coulomb,\ 3r}$=17.2 oz-in
k_{1l}=920 oz-in/A	$\tau_{coulomb,\ 1l}$=4.2 oz-in
k_{2l}=822 oz-in/A	$\tau_{coulomb,\ 2l}$=7.9 oz-in
k_{3l}=1096 oz-in/A	$\tau_{coulomb,\ 3l}$=11 oz-in

where the subscripts r and l refer to the right and left sides of the rover respectively.

A second experiment has been performed on the motors to evaluate their viscous friction component : no load is applied to the motor and a constant current is input to the motor. Therefore, when the motor reaches a steady state, the torque output by the motor is equal to the motor friction. This allows the determination of both the Coulomb and viscous friction constants. The experimental results are shown in Appendix D and are summarized and are summarized in Table 5-2.

Table 5-2: Motor Viscous Friction Constants.

b_{1r} = 3.61 oz-in/rpm	b_{1l} = 1.16 oz-in/V
b_{2r} = 1.41 oz-in/rpm	b_{2l} = 1.26 oz-in/V
b_{3r} = 2.97 oz-in/V	b_{3l} = 1.77 oz-in/V

5.3. Experimental Results

Two kinds of experiments have been performed on the rover. The first category concerns the validation of the model presented in the Chapters 2,3 and 4. The second category is a comparison between PI wheel angular velocity control and fuzzy logic control.

5.3.1. Model Validation

Two sets of experiments have been conducted to validate the model of the rover. First, the statement that the wheel normal forces change as function of the other wheel torques needs to be verified experimentally. This is a central piece of the research and leads to the design of the traction controller. Second, different action plans have been tested and the results predicted by the simulation are compared to the real system.

5.3.1.1. Normal Force changes

The influence of wheel torque on other wheels' normal forces is one of the key elements of the model. The experiment depicted in Figure 5-5 is designed to verify this element. The rover is standing on a platform and a one-axis force sensor measures the force exerted on one wheel in the vertical direction. Torques are applied to every wheel and the effect of these torques on the normal force of the others is measured.
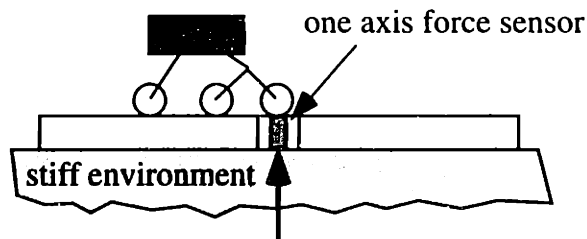

Figure 5-5: Normal Forces Measurement.

The comparisons results are plotted in Figure 5-6. In this graph, the solid lines represent experimental values, and the dashed lines represent simulation results.

Rear Normal Forces Changes	Middle Normal Forces Changes	Front Normal Forces Changes
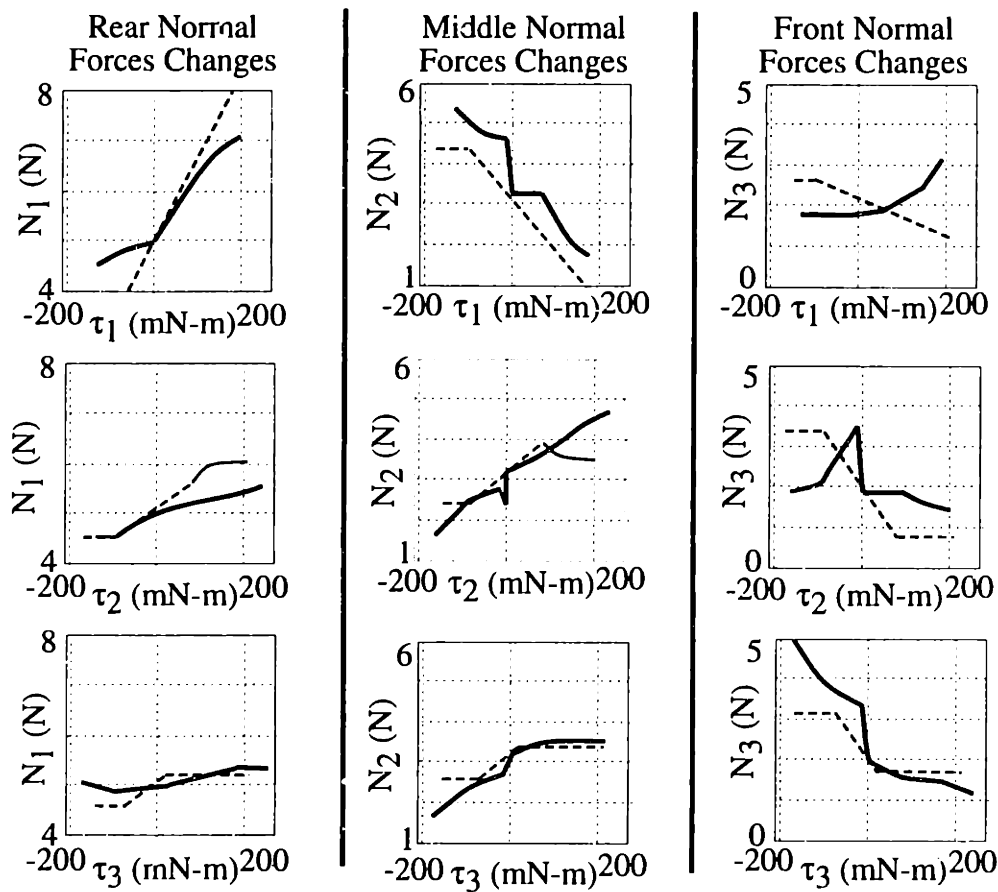
Figure 5-6: Model Validation.

The errors between the model and the actual system are caused by several factors. In the analytical model, when the effect of a wheel torque is considered, the other motors' torques are assumed to be zero. However, the friction in the highly geared motors creates static torque which opposes the commanded torque. The values of these opposing traction forces are unknown, hence errors are induced. Also, even though motor models have been developed, the experimental rover is not equipped with torque sensors so the output torque cannot be known very accurately. The coefficient of friction between the wheels and the ground cannot be determined very accurately either. Hence the simulation might predict

slipping before it actually happens. Finally, unmodeled friction in the rocker-bogie joint can also be shown to create some errors, especially in the front wheel normal force.

Nonetheless, the analytical model predicts the trends seen in the experimental system quite well, which is important for the fuzzy logic controller.

5.3.1.2. Action Plan Validation

The simulation has been used as a tool in action planning. To experimentally verify the correctness of these plans and therefore the rover model, different plans have been tested on the simulation and on the real system. This work has been performed in cooperation with Shane Farritor. The results are fully documented in (Farritor, 1998).

5.3.2. PI/Fuzzy Logic Controllers Comparison

This section compares the performance of two controllers. The most commonly used controller performs PI control on the wheels' angular velocities. Intuitively, this controller should have good traction on even terrain, but some wheels may lose contact or slip if the rover is on a challenging terrain (if the ground angle under each wheel is different, the wheels' relative velocities should be different to remain on the ground). This controller is compared to the fuzzy logic controller described in Section 4.4.

In most cases, these two controllers have similar performances. However, the tasks successfully performed by the PI controller appears to be a subset of the tasks successfully performed by the fuzzy logic controller. Of the many tasks tested, two show a significant difference in behavior.

5.3.2.1. Slope climbing task

In this experiment, the rover must climb a constant slope of 18 degrees. The static coefficient of friction in this task is $\mu = 0.33$, so the rover is on the verge of slipping. The velocity controller climbed the slope 60% of the time. The fuzzy logic controller climbed this slope 85% of time.

The reason for the poorer performance of the PI controller is that the PI velocity control causes each wheel to turn at the desired velocity. The wheels then start to slip and traction is lost because the dynamic coefficient of friction for the ground/tire interface is smaller than the static coefficient of friction. The wheels keep turning at the desired velocity and the vehicle slides down the slope.

On the other hand, the fuzzy logic controller detects the slipping and therefore reduces the torque causing the rover to move slightly forward and then it starts to slide. However, the controller detects this and slows down the wheels. The rover stops sliding and gains sufficient traction to continue forward again. Here, the fuzzy logic controller exploits the change between static and dynamic friction (Van der Burg *et al.*, 1997). Changing the normal forces in this case is also useless because the slope is constant under the wheels.

5.3.2.2. Step and slope climbing

The following task is more comprehensive and challenging. Here, the rover must climb a step, followed by a slope (see Figure 5-7).

In this case, the results are largely in favor of the fuzzy logic controller. This task is completed 63% of the time by the fuzzy logic controller and 27% of the time by the PI velocity controller.

Figure 5-7: A Challenging Task.

In this case, the results are largely in favor of the fuzzy logic controller. This task is completed 63% of the time by the fuzzy logic controller and 27% of the time by the PI velocity controller.
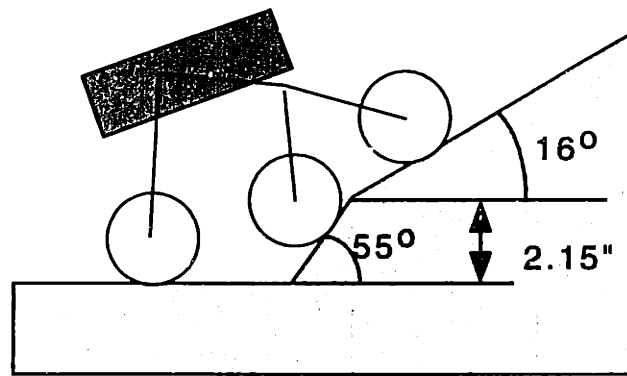
The reason why the PI controller fails so often is as following: when the front two wheels are on the slope and the rear wheel is on the step, most of the weight is transferred to the rear wheel. The front wheel has very little traction, and the torque of the middle wheel tends to pull the front wheel off the ground (see Figure 5-8). The rear wheel does not move while the middle wheel keeps moving at the desired velocity lifting the front wheel. Contact is lost and is not retrieved. The task fails.
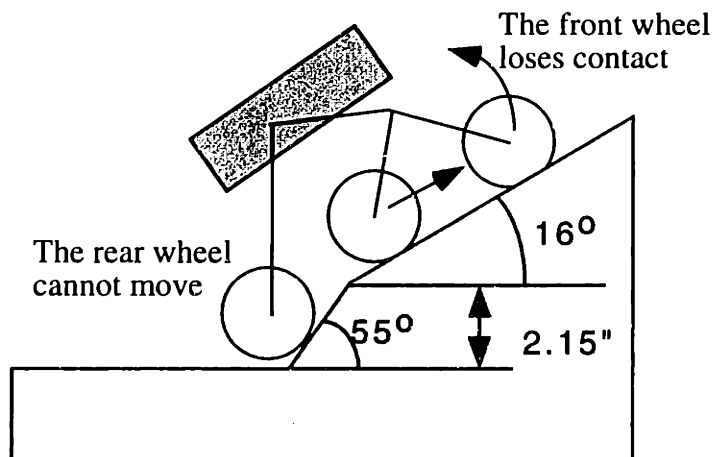

Figure 5-8: PI Controller Failure.

With the fuzzy logic controller, however, the middle wheel is commanded to stop moving. It helps the front wheel to pull the rear wheel. As soon as the rear wheel goes over the step, the task becomes much more manageable.

5.4. Conclusions

This chapter has briefly described the experimental rover that has been built in the Field and Space Robotics Laboratory at MIT. The rover's experimental platform is also outlined. The rover's motors exhibit significant friction, and their model is detailed. Experimental results are presented which verify the rover model presented in Chapters 2 and 3. The fuzzy logic controller is also compared to a PI controller. In some tasks, the fuzzy logic controller proves to perform better than the PI controller, but in most of the cases, the results are quite equivalent.

6. Conclusions and Suggestions for Future Work

6.1. Contributions of this Work

This work has presented the analysis and the simulation of a rocker bogie rover. Such rovers are likely candidates for future Mars exploration missions. They will need to travel relatively long distances and to be partially autonomous. Therefore, it is important to develop a detailed model of such systems.

This analysis considers the full three dimensional rover in its environment. A procedure that solves for the inverse kinematics of the system is developed and presented. This method simplifies the problem and yields accurate results, making it very useful for planning methodology. The quasi-static force analysis of the rover is then provided. The soil/tire interaction is a key element in this analysis as it provides knowledge of the transverse forces. The system is proven to be over-actuated. In other words, the mechanism redundancy induces interactions between the wheels. A method is shown that computes the best wheel torque distribution.

The system over-actuation is exploited in the design of a traction controller. A set of heuristic rules is defined to represent the system mechanics. Based on this set, a fuzzy logic controller is designed to improve traction.

The analysis, the model and the controller are verified on the FSRL/MIT rover. A brief overview of the design of this rover is given and experimental results are presented.

They show that the model represents the real system quite well and that the fuzzy logic controller can improve the traction of the rover.

6.2. Suggestions for Further Work

Improvements can be made to the simulation. For example, the simulation could accommodate different ground/tire interaction models as the implementation of these models and comparison of the results may be useful. Also, the simulation fails when there is no solution to the static balance equations. This does not necessarily mean that the rover will not be able to complete the task: instead, it may slide briefly, or a wheel may lose contact, and be able to recover. An algorithm that could determine when the rover slides, in which direction, and find the next equilibrium point would be a useful enhancement to the simulation.

Further work can be conducted on the rover's traction control. A different approach may be used in the fuzzy logic controller architecture, by considering more complete heuristics that take the ground geometry into account. Sensitivity to ground angles must be studied. At present, the controller does only consider the action of the wheels on one side. It may be possible to consider the influence of the opposing side of the rover in the heuristics. The position of center of mass also proves to be very important and the analysis could be used to determine its optimal location. This location can be changed by altering the manipulator's attitude or actively controlled through an adaptive rover structure.

The laboratory rover itself needs to be improved. Self containment is one of the goals to be achieved. Issues regarding communication with a fixed station will have to be addressed. It would be useful for the rover to be able to determine its position and orientation using visual pattern recognition techniques which could prove to be a very challenging enhancement of the rover.

References

Anton, H., *Calculus with Analytic Geometry - Second Edition*, Anton Textbooks, 1984

Arora,J., *Introduction to Optimal Design*, Mc Graw-Hill Series in Mechanical Engineering, 1989

Beer, F. and Russell Johnston, E., *Mechanics of Materials*, Mc Graw-Hill Series in Mechanical Engineering, 1981

Bekker, M. G., *Introduction to Terrain-Vehicle Systems*, University of Michigan Press, Ann Arbor, Michigan, 1969

Ben Amar, F., Bidaud, P., "Dynamics Analysis of off-road vehicles", *Proceedings of the 4th International Symposium on Experimental Robotics* 4, pages 363-371.

Bevly, D., *Action Module Planning and Cartesian Based Control of an Experimental Climbing Robot*, M.Sc. Thesis, Department of Mechanical Engineering, Massachusetts Institute of technology, Cambridge, MA, 1997

Bickler, B., "A New Family of JPL Planetary Surface Vehicles", *Missions, Technologies, and Design of Planetary Mobile Vehicle*, pages 301-306, Toulouse, France, September 28-30, 1992.

Bonitz, R. G., "Mars Surveyor '98 Lander MVACS Robotic Arm Control System Design Concepts ", *Proceedings of the 1997 IEEE International Conference on Robotics and Automation*, pp. 2465-70, 1997.

Burn, R., *Design of a Mars Exploration Rover*, M.Sc. Thesis, Department of Mechanical Engineering, Massachusetts Institute of technology, Cambridge, MA, 1998

Cassenti, L., *Modeling the Kinematic Behavior of Lightweight Survivable Rovers*, , B.Sc. Thesis, Department of Mechanical Engineering, Massachusetts Institute of Technology, Cambridge, MA, 1997

Chottiner, J. E., *Simulation of a Six-Wheeled Martian Rover Called the Rocker-Bogie*, M.S. Thesis, The Ohio State University, Columbus, Ohio, 1992

Doty, K. L., "A Theory Of Generalized Inverses Applied To Robotics", *International Journal of Robotics Research* Vol 12 n 1 pp 1-19, 1993

Dubowsky, S.*et al.*, "On the Design and Task Planning of Power Efficient Field Robotic Systems", *Proceedings of the 6th ANS Robotic and Remote Systems*, Monterey, CA, 1995.

Farritor, S., Hacot, H., Dubowsky, S., "Physics Based Planning for Planetary Exploration", *Proceedings of the 1998 IEEE International Conference on Robotics and Automation*.

Farritor, S., *On Modular Design and Planning for Field Robotic Systems*, Ph.D. Thesis, Department of Mechanical Engineering, Massachusetts Institute of technology, Cambridge, MA, 1998

Ghasempoor, A. and Sepehri, N., "A Measure Of Machine Stability For Moving Base Manipulators", *IEEE Internetional Conference on Robotics and Automation*, Nagcya, Japan, pp. 2249-2254, May 1995

Hacot, H., *A Guide To The MIT LSR Simulation Software*, June 1998

Hayati, S., et. al., "The Rocky 7 Rover: A Mars Sciencecraft Prototype", *Proceedings of the 1997 IEEE International Conference on Robotics and Automation*, pp. 2458-64, 1997.

Kaliardos, W., *Sensors For Autonomous Navigation And Hazard Avoidance On A Planetary Micro-Rover*, M.Sc. Thesis, Department of Mechanical Engineering, Massachusetts Institute of technology, Cambridge, MA, 1993

Krotkov, E., Hoffman, R., "Terrain Mapping For A Walking Planetary Rover", *IEEE Transactions On Robotics And Automation*, Vol. 10, December 1994

Le, A., Rye, D., Durrant-Whyte, H., "Estimation Of Track-Soil Interactions For Autonomous Tracked Vehicles", *Proceedings of the IEEE International Conference on Robotics and Automation*, pp. 1388-93, Albuquerque, New Mexico 1997

Linderman, R., Eisen, H., "Mobility Analysis, Simulation and Scale Model Testing for the Design of Wheeled Planetary Rovers", *In Missions, Technologies, and Design of Planetary Mobile Vehicle*, pages 531-37, Toulouse, France, September 28-30, 1992

Mars Pathfinder: www.mpf.jpl.nasa.gov

Matthies, L., Balch, T., Wilcox, B., "Fast Optical Hazard Detection for Planetary Rovers using Multiple Spot Laser Triangulation" *IEEE International Conference on Robotics and Automation*, pages 859-66, April, 1997

Messuri, D. A., Klein, C. A., "Automatic Body Regulation For Maintaining Stability Of A Legged Vehicle During Rough Terrain Locomotion" *IEEE International Conference on Robotics and Automation*, pp. 132-141, 1985

Overmars, M., *Forms Library: a Graphical User Interface Toolkit for Silicon Graphics Workstations*, version 2.3, Department of Computer Science, Utrecht University, Netherlands.

Papadopoulos, E. G., Rey, D. A., "A New Measure Of Tipover Stability Margin For Mobile Manipulators", *IEEE International Conference on Robotics and Automation*, pp. 3111-16, April, 1996

Ross, T. J., *Fuzzy Logic With Engineering Applications*, Mac Graw-Hill, 1995

Schenker, P., et. al., "Lightweight Rovers for Mars Science Exploration and Sample Return," *Intelligent Robots and Computer Vision XVI, SPIE Proceedings* 3208, Pittsburg, PA, October, 1997.

Schenker P., et al. (2), "Composite Manipulator Utilizing Rotary Piezoelectric Motors: New Robotic Technologies For Mars In-Situ Planetary Science" *Proceedings of SPIE - The International Society for Optical Engineering Smart Structures and Materials* 1997

Schenker, P. et al (3) "Dexterous Robotic Sampling For Mars In-Situ Science"

Shirley, D. L., and Matijevic, J. R., "Mars rovers : past, present and future" *Proceedings of Princetown Space Studies Institute 20th Anniversary Conference* May, 1997

Sreevinasan, S., Wilcox, B., "Stability and Traction Control of an Actively Actuated Micro-Rover", *Journal of Robotic Systems*-1994, pp. 487-502

Sunada, C., *Coordinated Jacobian Transpose Control and its Application to a Climbing Machine*, M.S. Thesis, Department of Mechanical Engineering, Massachusetts Institute of Technology, September 1994.

Sword, L.F., Harvey, G.D. and Frazier J.A. "Deployable Rigid Wheel", *NASA Tech Briefs*, June 1997

Torres, M. A., *Modeling, Path-Planning and Control of Space Manipulators : The Coupling Map Concept*, Ph.D. Thesis, Department of Mechanical Engineering, Massachusetts Institute of Technology, Cambridge, MA, 1993

Van der Burg, J., Blazevic, P., "Anti-Lock Braking and Traction Control Concept for All-Terrain Robotic Vehicles" *IEEE International Conference on Robotics and Automation*, pages 1400-05, April, 1997

Venkataraman, S. C., Sreenivasan, S. V. and Waldron, K. J., "Active Coordination of Robotic Terrain -Adaptive Wheeled Vehicles for Power Minimization", *Romansy 1997*, pp.223-232.

Weisbin C. R., Lavery D. and Rodriguez G., "Robotics Technology for planetary missions into the 21st century", *Proceedings of the 1997 International. Conference on Mobile Planetary Robots*, Santa Monica, C.

Appendix A : Rover Kinematic Relations.

This Appendix details the expression of some kinematic relations necessary for Chapter 2. Figure A-1 presents the kinematic parameters of the system.
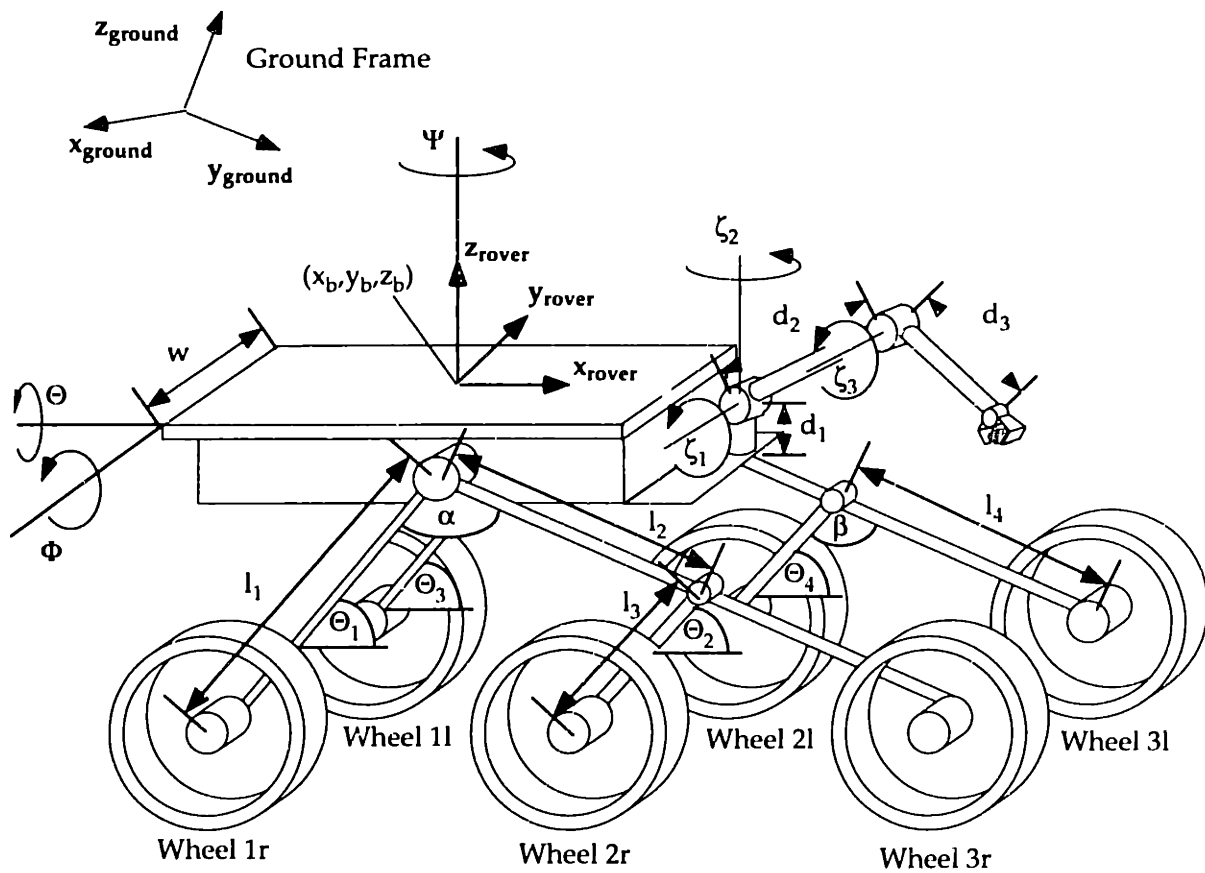

Figure A-1: Planar Force Analysis Presentation.

The inverse kinematics procedure requires the computation of the position of the wheel centers in the ground frame.

The relations between the wheel centers position in R_{ground} (x_{ir}, y_{ir}) and the middle right wheel position are:

$$x_{1r} = x_{2r} + \cos(\Psi) \cdot \left(l_3 \cdot \cos(\Theta_2) + l_2 \cdot \cos(\Theta_1 + \alpha) - l_1 \cdot \cos(\Theta_1)\right)$$
$$- \sin(\Psi) \cdot \sin(\Theta) \cdot \left(l_3 \cdot \sin(\Theta_2) + l_2 \cdot \sin(\Theta_1 + \alpha) - l_1 \cdot \sin(\Theta_1)\right)$$

(A-1)

$$y_{1r} = y_{2r} + \sin(\Psi) \cdot \left(l_3 \cdot \cos(\Theta_2) + l_2 \cdot \cos(\Theta_1 + \alpha) - l_1 \cdot \cos(\Theta_1)\right)$$
$$+ \cos(\Psi) \cdot \sin(\Theta) \cdot \left(l_3 \cdot \sin(\Theta_2) + l_2 \cdot \sin(\Theta_1 + \alpha) - l_1 \cdot \sin(\Theta_1)\right)$$

(A-2)

$$x_{3r} = x_{2r} + \cos(\Psi) \cdot \left(l_3 \cdot \cos(\Theta_2) - l_4 \cdot \cos(\Theta_2 + \beta)\right)$$
$$- \sin(\Psi) \cdot \sin(\Theta) \cdot \left(l_3 \cdot \sin(\Theta_2) + l_4 \cdot \sin(\Theta_2 + \beta)\right)$$

(A-3)

$$y_{3r} = y_{2r} + \sin(\Psi) \cdot \left(l_3 \cdot \cos(\Theta_2) - l_4 \cdot \cos(\Theta_2 + \beta)\right)$$
$$+ \cos(\Psi) \cdot \sin(\Theta) \cdot \left(l_3 \cdot \sin(\Theta_2) + l_4 \cdot \sin(\Theta_2 + \beta)\right)$$

(A-4)

$$x_{1l} = x_{2r} + \cos(\Psi) \cdot \left(l_3 \cdot \cos(\Theta_2) + l_2 \cdot \cos(\Theta_1 + \alpha) - l_1 \cdot \cos(\Theta_3)\right)$$
$$- \sin(\Psi) \cdot \left(\sin(\Theta) \cdot \left(l_3 \cdot \sin(\Theta_2) + l_2 \cdot \sin(\Theta_1 + \alpha) - l_1 \cdot \sin(\Theta_3)\right)\right.$$
$$\left. + \cos(\Theta) \cdot \text{width}\right)$$

(A-5)

$$y_{1l} = y_{2r} + \sin(\Psi) \cdot \left(l_3 \cdot \cos(\Theta_2) + l_2 \cdot \cos(\Theta_1 + \alpha) - l_1 \cdot \cos(\Theta_3)\right)$$
$$+ \cos(\Psi) \cdot \left(\sin(\Theta) \cdot \left(l_3 \cdot \sin(\Theta_2) + l_2 \cdot \sin(\Theta_1 + \alpha) - l_1 \cdot \sin(\Theta_3)\right)\right.$$
$$\left. + \cos(\Theta) \cdot \text{width}\right)$$

(A-6)

$$x_{2l} = x_{2r} + \cos(\Psi) \cdot \left(l_3 \cdot \cos(\Theta_2) + l_2 \cdot \cos(\Theta_1 + \alpha) - l_2 \cdot \cos(\Theta_3 + \alpha)\right.$$
$$\left. - l_3 \cdot \cos(\Theta_4)\right)$$
$$- \sin(\Psi) \cdot \left[\sin(\Theta) \cdot \left(l_3 \cdot \sin(\Theta_2) + l_2 \cdot \sin(\Theta_1 + \alpha)\right.\right.$$
$$\left. - l_3 \cdot \sin(\Theta_4) - l_2 \cdot \sin(\Theta_3 + \alpha)\right)$$
$$\left. + \cos(\Theta) \cdot \text{width}\right]$$

(A-7)

$$y_{2l} = y_{2r} + \sin(\Psi) \cdot \left(l_3 \cdot \cos(\Theta_2) + l_2 \cdot \cos(\Theta_1 + \alpha) - l_2 \cdot \cos(\Theta_3 + \alpha)\right.$$
$$\left. - l_3 \cdot \cos(\Theta_4)\right)$$
$$+ \cos(\Psi) \cdot \left[\sin(\Theta) \cdot \left(l_3 \cdot \sin(\Theta_2) + l_2 \cdot \sin(\Theta_1 + \alpha)\right.\right.$$
$$\left. - l_3 \cdot \sin(\Theta_4) - l_2 \cdot \sin(\Theta_3 + \alpha)\right)$$
$$\left. + \cos(\Theta) \cdot \text{width}\right]$$

(A-8)

$$x_{3l} = x_{2r} + \cos(\Psi) \cdot \left(l_3 \cdot \cos(\Theta_2) + l_2 \cdot \cos(\Theta_1 + \alpha) - l_2 \cdot \cos(\Theta_3 + \alpha)\right.$$
$$\left. + l_4 \cdot \cos(\Theta_4 + \beta)\right)$$
$$- \sin(\Psi) \cdot \left[\sin(\Theta) \cdot \left(l_3 \cdot \sin(\Theta_2) + l_2 \cdot \sin(\Theta_1 + \alpha)\right.\right.$$
$$\left. - l_4 \cdot \sin(\Theta_4 + \beta) - l_2 \cdot \sin(\Theta_3 + \alpha)\right)$$
$$\left. + \cos(\Theta) \cdot \text{width}\right]$$

(A-9)

$$y_{3l} = y_{2r} + \sin(\Psi) \cdot \left(l_3 \cdot \cos(\Theta_2) + l_2 \cdot \cos(\Theta_1 + \alpha) - l_2 \cdot \cos(\Theta_3 + \alpha) \right.$$
$$\left. + l_4 \cdot \cos(\Theta_4 + \beta) \right)$$
$$+ \cos(\Psi) \cdot \left[\sin(\Theta) \cdot \left(l_3 \cdot \sin(\Theta_2) + l_2 \cdot \sin(\Theta_1 + \alpha) \right. \right.$$
$$\left. - l_4 \cdot \sin(\Theta_4 + \beta) - l_2 \cdot \sin(\Theta_3 + \alpha) \right)$$
$$\left. + \cos(\Theta) \cdot \text{width} \right] \qquad \text{(A-10)}$$

Appendix B: Force Analysis

This Appendix details the expression of some parameters used in the Chapter 3 for the planar force analysis. Some properties of these elements are also given.

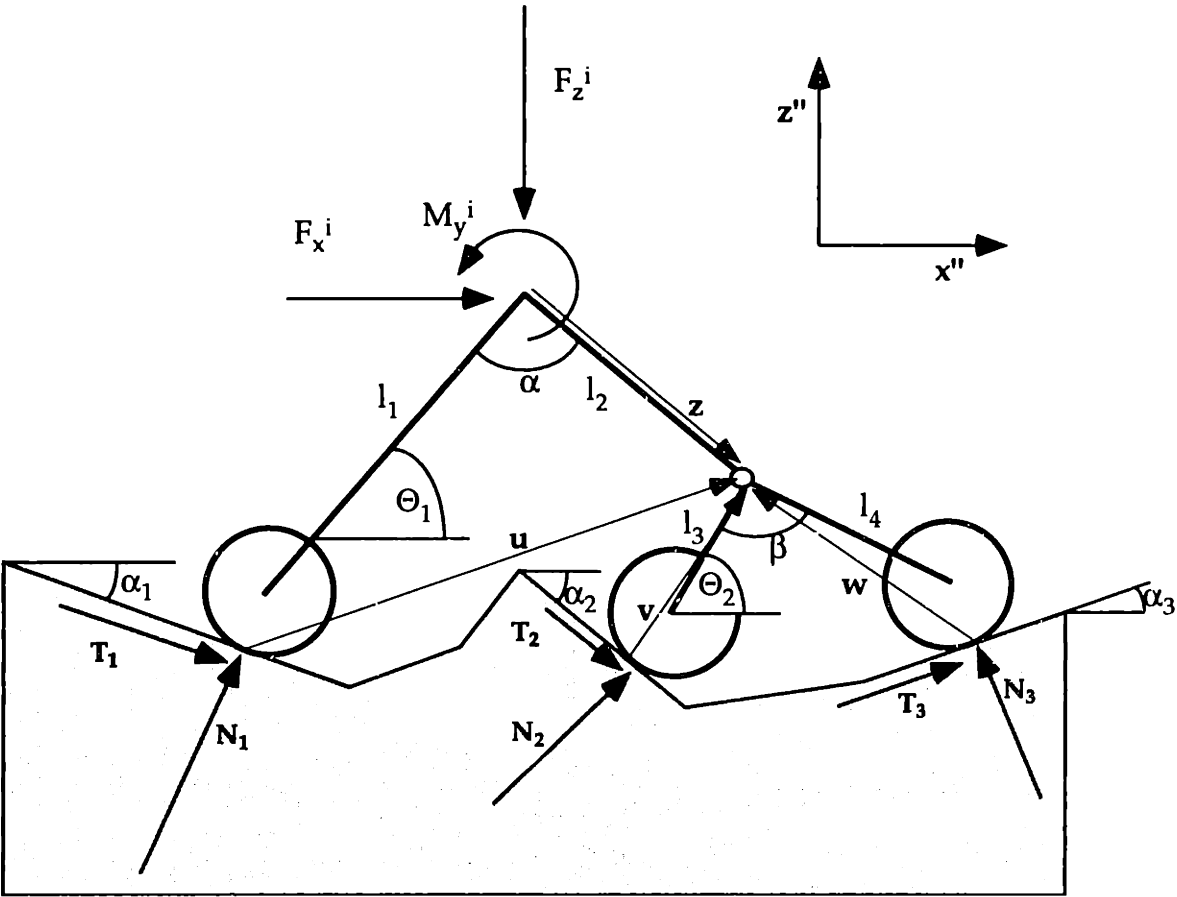Figure B-1 presents the parameters of the system.

Figure B-1: Planar Force Analysis Presentation.

As seen in Chapter 3, the equation of the balance of the system can be in two ways:

$$\mathbf{A} \cdot \begin{bmatrix} T_1 & T_2 & T_3 N_1 & N_2 & N_3 \end{bmatrix}^T = \begin{bmatrix} -F_x^i & F_z^i & -M_y^i - F_x^i \cdot z_y - F_z^i \cdot z_x & 0 \end{bmatrix}^T \qquad \textbf{(B-1)}$$

$$\mathbf{B} \cdot \begin{bmatrix} T_3 & N_1 & N_2 & N_3 \end{bmatrix}^T = \mathbf{C} \cdot T_1 + \mathbf{D} \cdot T_2 + \mathbf{E} \qquad \textbf{(B-2)}$$

Before representing these matrices and vectors, the expressions of $\mathbf{u}$, $\mathbf{v}$, $\mathbf{w}$ and $\mathbf{z}$ must be defined. They are :

$$\mathbf{u} = \begin{bmatrix} u_x \\ u_y \end{bmatrix} = \begin{bmatrix} -rad \cdot \sin(\alpha_1) + l_1 \cdot \cos(\Theta_1) - l_2 \cdot \cos(\Theta_1 + \alpha) \\ rad \cdot \cos(\alpha_1) + l_1 \cdot \sin(\Theta_1) - l_2 \cdot \sin(\Theta_1 + \alpha) \end{bmatrix} \qquad \textbf{(B-3)}$$

$$\mathbf{v} = \begin{bmatrix} v_x \\ v_y \end{bmatrix} = \begin{bmatrix} -rad \cdot \sin(\alpha_2) + l_3 \cdot \cos(\Theta_2) \\ rad \cdot \cos(\alpha_2) + l_3 \cdot \sin(\Theta_2) \end{bmatrix} \qquad \textbf{(B-4)}$$

$$\mathbf{w} = \begin{bmatrix} w_x \\ w_y \end{bmatrix} = \begin{bmatrix} -rad \cdot \sin(\alpha_3) + l_4 \cdot \cos(\Theta_2 + \beta) \\ rad \cdot \cos(\alpha_3) + l_4 \cdot \sin(\Theta_2 + \beta) \end{bmatrix} \qquad \textbf{(B-5)}$$

$$\mathbf{z} = \begin{bmatrix} z_x \\ z_y \end{bmatrix} = \begin{bmatrix} -l_2 \cdot \cos(\Theta_1 + \alpha) \\ -l_2 \cdot \sin(\Theta_1 + \alpha) \end{bmatrix} \qquad \textbf{(B-6)}$$

Using these expressions, $\mathbf{A}$, $\mathbf{B}$, $\mathbf{C}$, $\mathbf{D}$ and $\mathbf{E}$ can be defined. $\mathbf{A} = (A_{ij})$. For compactness, c_i and s_i will refer to $\cos(\alpha_i)$ and $\sin(\alpha_i)$ respectively.

$A_{11} = c_1$

$A_{12} = c_2$

$A_{13} = c_3$

$A_{14} = -s_1$

$A_{15} = -s_2$

$A_{16} = -s_3$

$A_{21} = s_1$

$A_{22} = s_2$

$A_{23} = s_3$

$A_{24} = c_1$

$A_{25} = c_2$

$A_{26} = c_3$

$A_{31} = c_1 \cdot u_y - s_1 \cdot u_x$

$A_{32} = 0$

$A_{33} = 0$

$A_{34} = -s_1 \cdot u_y - c_1 \cdot u_x$

$A_{35} = 0$

$A_{36} = 0$

$A_{41} = 0$

$A_{42} = c_2 \cdot v_y - s_2 \cdot v_x$

$A_{43} = c_3 \cdot w_y - s_3 \cdot w_x$

$A_{44} = 0$

$A_{45} = -c_2 \cdot v_x - s_2 \cdot v_y$

$A_{46} = -c_3 \cdot w_x - s_3 \cdot w_y$

We have : $B_{ij} = A_{i,j+2}$ and $C_i = A_{i,1}$ and $D_i = A_{i,2}$ and $\mathbf{E}$ is the right hand side of equation (B-1).

In Chapter 3, the equations have been solved, assuming that $\mathbf{B}$ is invertible. The determinant of that matrix has been computed analytically. After some simplifications, it is:

$$\det(\mathbf{B}) = (c_1 \cdot u_x + s_1 \cdot u_y) \cdot \left[s_2 \cdot (v_y - w_y) + c_2 \cdot (v_x - w_x) \right] \qquad \text{(B-7)}$$

The system is not invertible when equation (B-8) or equation (B-9) is verified:

$$\tan(\alpha_1) = -\frac{u_x}{u_y} \qquad \text{(B-8)}$$

$$\tan(\alpha_2) = -\frac{v_x - w_x}{v_y - w_y} \qquad \text{(B-9)}$$

The signification of equation (B-8) is represented in Figure B-2.a. Here, the normal force N_1 crosses the rocker bogie joint. Therefore, it has no effect on the balance of the moment of the rocker. This is where under-determination happens. Note that this special case is exactly at the limit where the influence of the rear torque on the rear wheel normal force changes (see Section 4.3.4).

Equation (B-9) is more difficult to interprate. This means that the normal force of wheel 2 (the middle wheel) is passing through the contact point of wheel 3 (the front wheel), see Figure B-2.b. Here again, equation (B-9) means that the normal forces intersect exactly on the stability region defined in section 4.3.3. These locations, where the influence of the traction forces start to reverse, are the only configurations for which the solutions of the system do not exist.
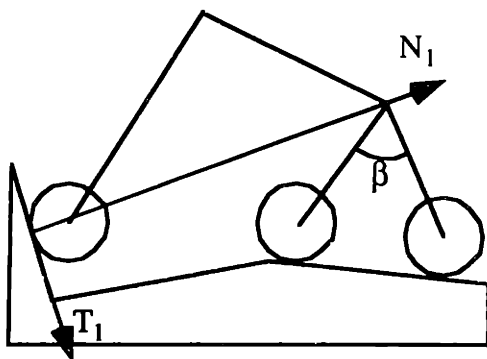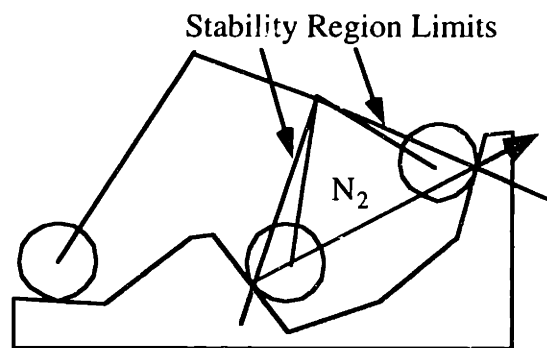

Figure B-2.a

Figure B-2.b

Figure B-2: Non invertibility of B

Appendix C Defuzzification Procedure

This Appendix details the defuzzyfication procedure that computes the output to be sent to the system.

C.1 Problem Statement and General Methods

Chapter 4 outlines how the fuzzy logic controller uses a set of rules to calculate the contribution of each Command Probability Distribution Function (CPDF). The goal is to determine the output from the values of the different CPDFs. The Command fuzzy set is defined as in Figure C-1. Here, V_i refers to the value assigned to the ith CPDF.
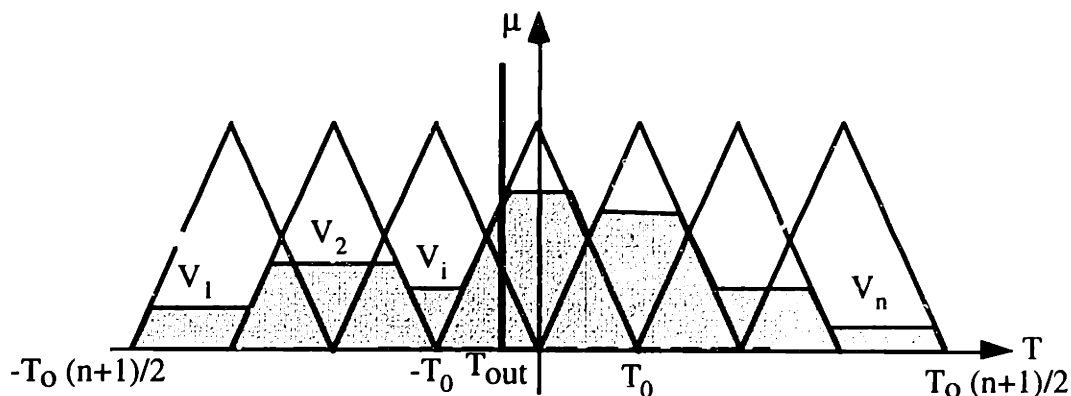
Figure C-1 : The Command Fuzzy Set

Different methods can be used to determine the output (Ross, 1995). The max-membership method takes the output as the position where the maximum of the command fuzzy set is.(see Figure C-2.a). The centroid method (Figure C-2.b) is the method that is used: it computes the "center of mass" of the system. The weighted average method (Figure

C-2.c) calculates the weighted average of the position of all the maxima of the CPDFs. The mean-max method (Figure C-2.d) is used instead of the max-membership method if the maximum is not unique. The method calculates the average of these maxima.
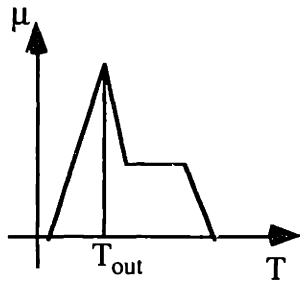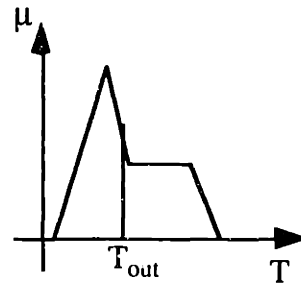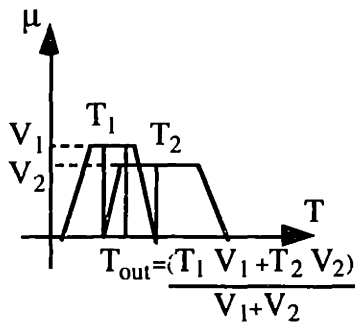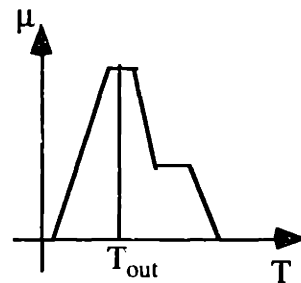

Figure C-2.a.

Figure C-2.b.

Figure C-2.c.

Figure C-2.d.

Figure C-2 : Defuzzification Methods.

In this work, the centroid method has been used.

C.2 Solution

Let the CPDFs distribution be as in Figure C-3. They are triangle functions, whose base's width is $2\ T_0$. Let n be the number of CPDFs. n is obviously an odd number.

The output is given by:

$$T^* = \frac{\int \mu(T) \cdot T \cdot dT}{\int \mu(T) \cdot dT} \qquad \text{(C-1)}$$

The denominator is the area of the command fuzzy set. It can be easily determined by adding the sum of the area of the trapezes formed by each CPDF and by removing their intersections.
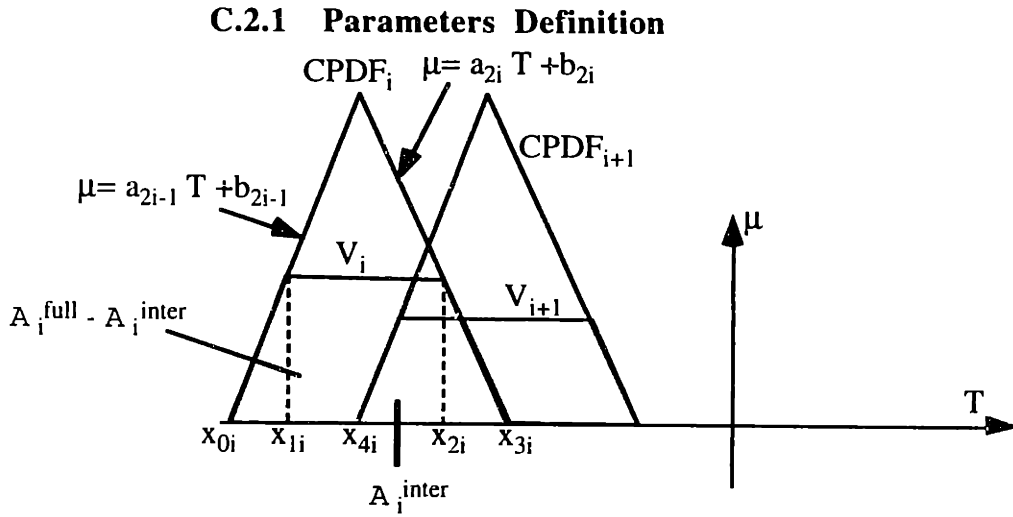
C.2.1 Parameters Definition

Figure C-3 : Parameters Definition.

Let a_i and b_i be the parameters that define respectively the slope and the intersection with the μ axis of the ith line of the system of CPDF (see Figure C-3).

$$a_i = \frac{(-1)^{i+1}}{T_0} \tag{C-2}$$

$$b_{2 \cdot i} = \frac{1 - n + i}{2} \tag{C-3}$$

$$b_{2 \cdot i - 1} = \frac{2 + n - i}{2} \tag{C-4}$$

C.2.2 Full Area Computation

The area of the trapeze contained in the ith triangle, with the vertices x_{0i}, x_{1i}, x_{2i}, x_{3i}, of altitude V_i is given by (C-5) (See Figure C-3). (C-6) gives the weighted area of the same region.

$$A_i^{full} = \frac{x_{3i} - x_{0i} + x_{2i} - x_{1i}}{2} \cdot V_i \tag{C-5}$$

$$V_i^{full} = \frac{a_{2\cdot i-1}}{3}\cdot(x_{1i}^3 - x_{0i}^3) + \frac{b_{2\cdot i-1}}{2}\cdot(x_{1i}^2 - x_{0i}^2) + \frac{V_i}{2}\cdot(x_{2i}^2 - x_{1i}^2)$$
$$+ \frac{a_{2\cdot i}}{3}\cdot(x_{3i}^3 - x_{2i}^3) + \frac{b_{2\cdot i}}{2}\cdot(x_{3i}^2 - x_{2i}^2)$$

(C-6)

where x_{0i}, x_{1i}, x_{2i}, x_{3i} are defined by :

$$x_{0i} = \frac{-b_{2\cdot i-1}}{a_{2\cdot i-1}}$$

(C-7)

$$x_{1i} = \frac{V_i - b_{2\cdot i-1}}{a_{2\cdot i-1}}$$

(C-8)

$$x_{2i} = \frac{V_i - b_{2\cdot i}}{a_{2\cdot i}}$$

(C-9)

$$x_{3i} = \frac{-b_{2\cdot i}}{a_{2\cdot i}}$$

(C-10)

C.2.3. Intersection Computations

Four distinct cases have to be studied to determine what is the extra surface or weighted area to be removed (see Figure C-4).

• Case 1: $V_i > V_{i+1}$ and $V_{i+1} < 0.5$ (see Figure C-4.a.): then A_i^{inter} and V_i^{inter}, respectively the extra area and weighted area are:

$$A_i^{inter} = \frac{x_{3i} - x_{4i} + x_{6i} - x_{5i}}{2}\cdot V_{i+1}$$

(C-11)

$$V_i^{inter} = \frac{a_{2\cdot i+1}}{3}\cdot(x_{5i}^3 - x_{4i}^3) + \frac{b_{2\cdot i+1}}{2}\cdot(x_{5i}^2 - x_{4i}^2) + \frac{V_{i+1}}{2}\cdot(x_{6i}^2 - x_{5i}^2)$$
$$+ \frac{a_{2\cdot i}}{3}\cdot(x_{3i}^3 - x_{6i}^3) + \frac{b_{2\cdot i}}{2}\cdot(x_{3i}^2 - x_{6i}^2)$$

(C-12)

where x_{4i}, x_{5i} and x_{6i} are (see Figure C-4.a)) :

$$x_{4i} = \frac{-b_{2\cdot i+1}}{a_{2\cdot i+1}}$$

(C-13)

$$x_{5i} = \frac{V_{i+1} - b_{2 \cdot i+1}}{a_{2 \cdot i+1}}$$

<div align="right">(C-14)</div>

$$x_{6i} = \frac{V_{i+1} - b_{2 \cdot i}}{a_{2 \cdot i}}$$
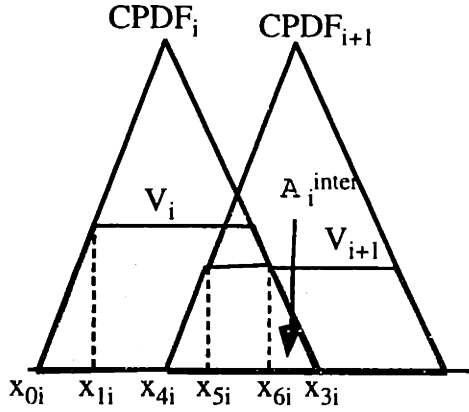
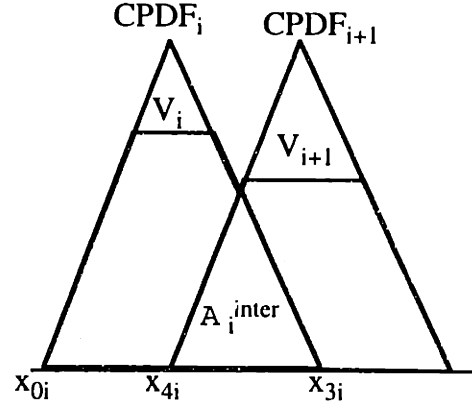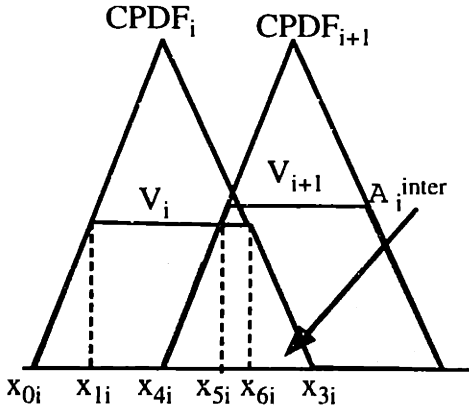<div align="right">(C-15)</div>
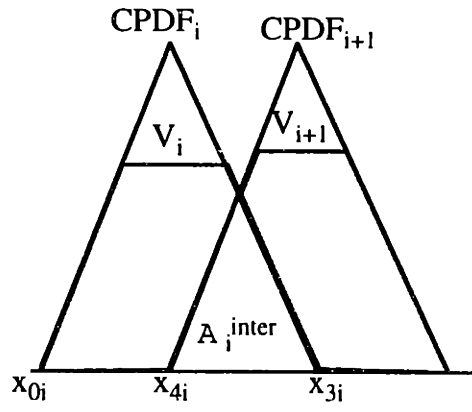

Figure C-4.a.

Figure C-4.b

Figure C-4.c.

Figure C-4.d.

Figure C-4 : Intersection areas Calculation.

• _Case 2_: $V_i > V_{i+1}$ and $V_{i+1} > 0.5$ (see Figure C-4.b.): then A_i^{inter} and V_i^{inter}, respectively the extra area and weighted area are:

$$A_i^{inter} = \frac{x_{3i} - x_{4i}}{4}$$

<div align="right">(C-16)</div>

$$V_i^{inter} = \frac{a_{2 \cdot i+1}}{3} \cdot (x_{5i}^3 - x_{4i}^3) + \frac{b_{2 \cdot i+1}}{2} \cdot (x_{5i}^2 - x_{4i}^2)$$
$$+ \frac{a_{2 \cdot i}}{3} \cdot (x_{3i}^3 - x_{5i}^3) + \frac{b_{2 \cdot i}}{2} \cdot (x_{3i}^2 - x_{5i}^2)$$

<div align="right">(C-17)</div>

where x_{4i} is given by (C-13) and x_{5i} is (see Figure C-4.b)) :

$$x_{5i} = \frac{x_{3i} + x_{4i}}{2} \qquad \text{(C-18)}$$

• Case 3: $V_i < V_{i+1}$ and $V_i < 0.5$ (see Figure C-4.c): then A_i^{inter} and V_i^{inter}, respectively the extra area and weighted area are:

$$A_i^{inter} = \frac{x_{3i} - x_{4i} + x_{6i} - x_{5i}}{2} \cdot V_i \qquad \text{(C-19)}$$

$$V_i^{inter} = \frac{a_{2i+1}}{3} \cdot (x_{5i}^3 - x_{4i}^3) + \frac{b_{2i+1}}{2} \cdot (x_{5i}^2 - x_{4i}^2) + \frac{V_i}{2} \cdot (x_{6i}^2 - x_{5i}^2) \qquad \text{(C-20)}$$
$$+ \frac{a_{2i}}{3} \cdot (x_{3i}^3 - x_{6i}^3) + \frac{b_{2i}}{2} \cdot (x_{3i}^2 - x_{6i}^2)$$

where x_{4i} is given by (C-13) and x_{5i} and x_{6i} are (see Figure C-4.c)) :

$$x_{5i} = \frac{V_i - b_{2i+1}}{a_{2i+1}} \qquad \text{(C-21)}$$

$$x_{6i} = \frac{V_i - b_{2i}}{a_{2i}} \qquad \text{(C-23)}$$

• Case 4: $V_i < V_{i+1}$ and $V_i > 0.5$ (see Figure C-4.d), then the results are exactly the same than for case 2.

The output of the defuzzification can then be easily determined :

$$T_{out} = \frac{\sum\limits_{i=1}^{n-1} (V_i^{full} - V_i^{inter}) + V_n^{full}}{\sum\limits_{i=1}^{n-1} (A_i^{full} - A_i^{inter}) + A_n^{full}} \qquad \text{(C-24)}$$

Appendix D : Experimental Rover.

This appendix presents the FSRL/MIT experimental Mars Rover. Different design stages of the system are briefly presented, and the budget of the project is included. Mod 1.1 is there after studied in closer details. Results of the motor calibration experiments detailed in Chapter 5 are presented. They infer the characteristics of the motors.

D.1 Project Description.

The FSRL/MIT rover project started in May 1997. Design studies have been performed on the rover. Several stages of the design evolution have been planned. MOD1 (see Figure D-1) is a mechanical evaluation of the design. No controller is implemented on the rover. MOD 1.1 includes sensors (see Figure D-2): an accelerometer, four potentiometers placed on the rocker-bogie joints and on the rocker-body joints enable the knowledge of the posture of the rover. Feedback from the motors is in the form of analog signals from tachometer units on each motor. Angular velocity is then directly measured. This rover is controlled with a PC. Voltage to current amplifiers are used, thus enabling the direct control of the wheel torques. The experiments depicted in this research are conducted on this rover.

Future MODs include the attachment of a manipulator on the body and its control (MOD 3) (see Figure D-3). Self containment is the ultimate projected goal, that will require the use of PC/104 technology (see Figure D-4).
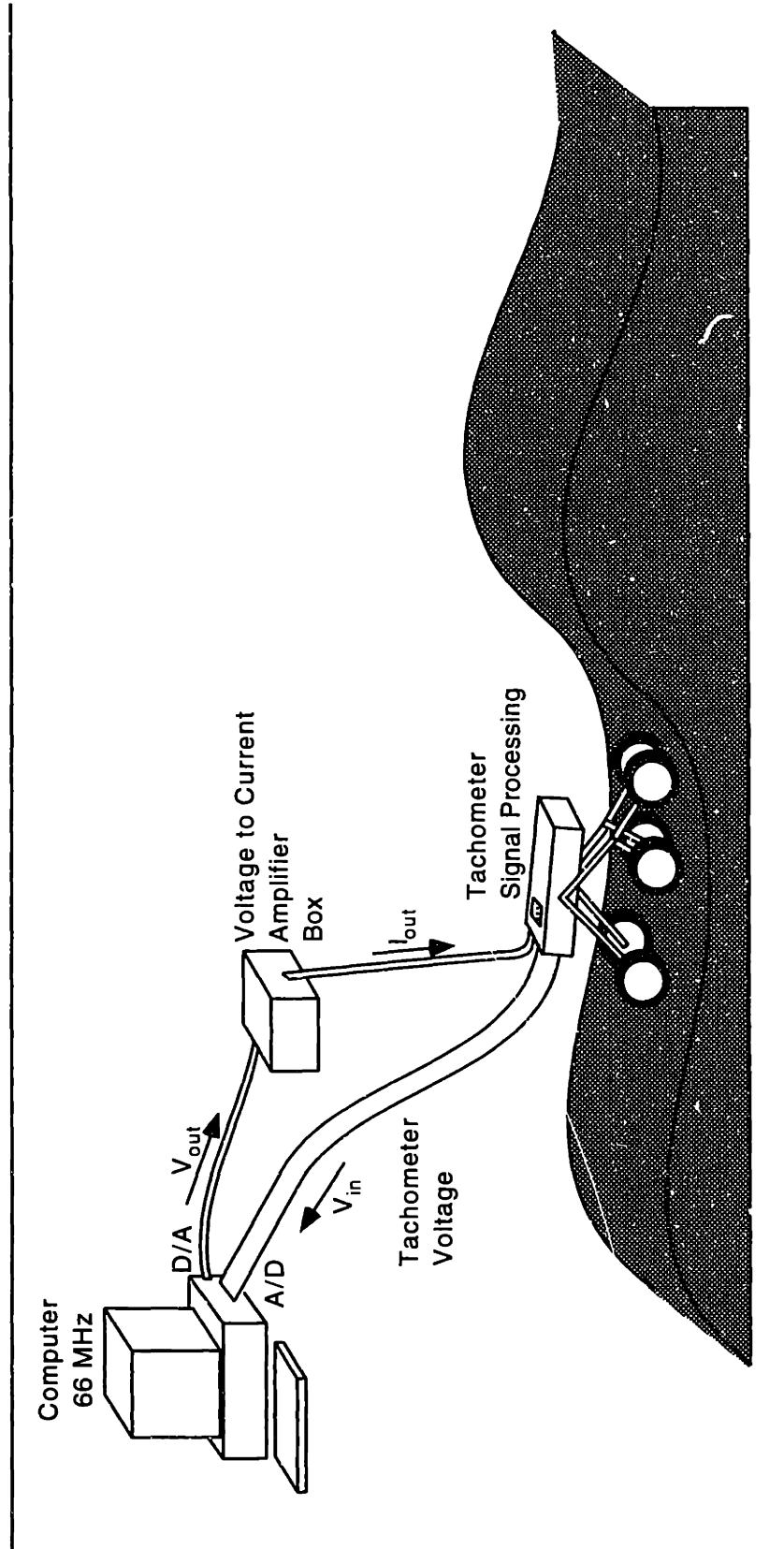
Figure D-1: MOD 1 Rover

MOD 1.1

Model Verification

Sensor feedback for position and attitude of the Rover

$$I_{out} = \begin{bmatrix} I_{motor1} \\ \vdots \\ I_{motor6} \end{bmatrix}$$

$$V_{in} = \begin{bmatrix} \omega_{mot1} \\ \vdots \\ \omega_{mot6} \\ \Theta_{rocker} \\ \vdots \\ pitch \\ roll \end{bmatrix}$$

Computer 66 MHz

Voltage to Current Amplifier Box

D/A V_{out}

A/D V_{in}

I_{out}

Power source regulation for sensors

External power source

Y

X

Accelerometer

Potentiometers

Camera   Laser

Ground Scanning System (used separately)
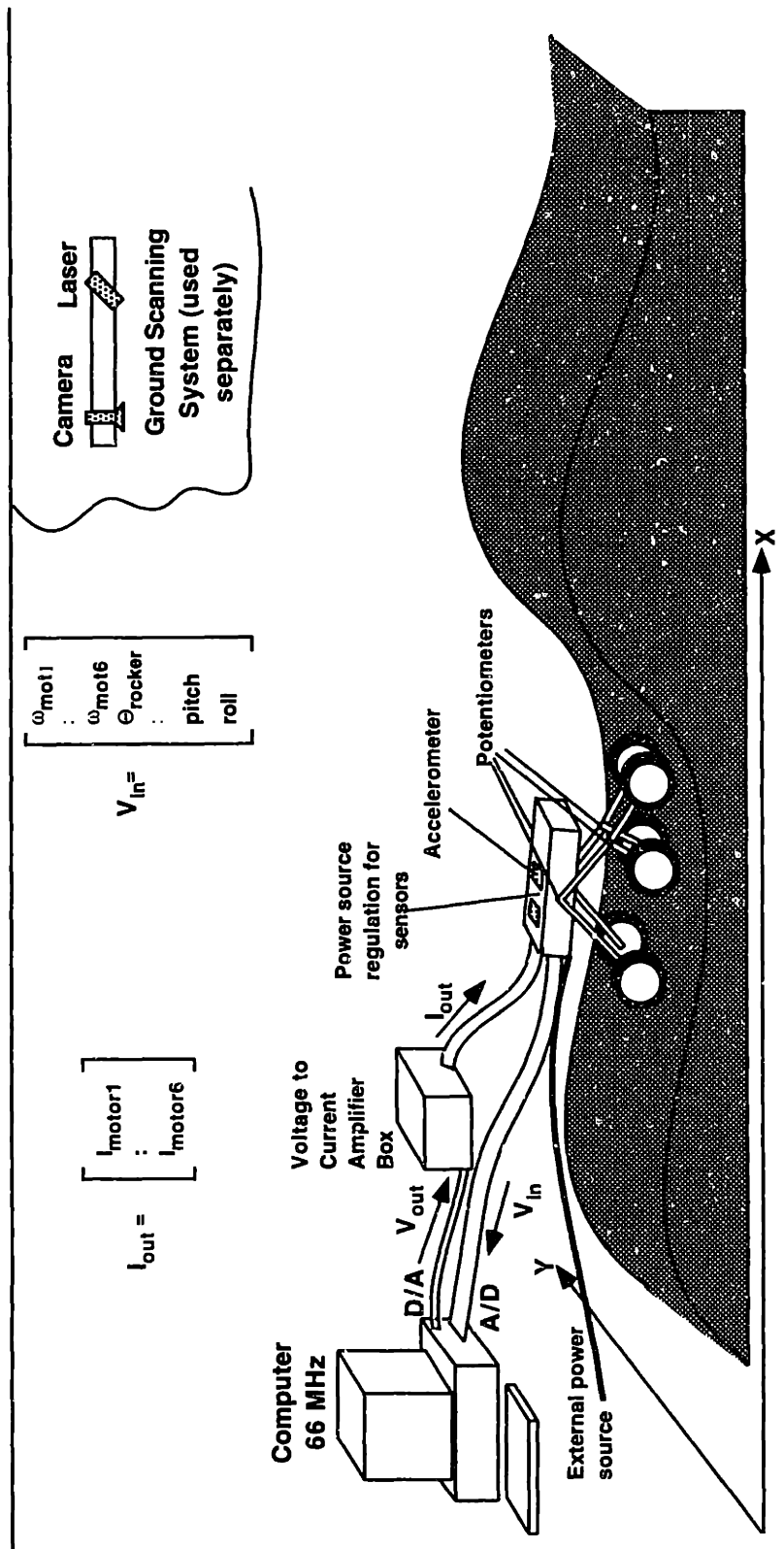
Figure D-2: MOD 1.1 Rover

MOD 2
Manipulator Control
Tethered electronics

$$I_{out} = \begin{bmatrix} I_{motor1} \\ . \\ I_{motor9} \end{bmatrix} \qquad V_{in} = \begin{bmatrix} \omega_{mot1} \\ .. \\ \omega_{mot6} \\ \Theta_{rocker} \\ .. \\ \Theta_{arm3} \\ pitch \\ roll \end{bmatrix}$$

Computer
66 MHz

D/A V_{out}

A/D V_{in}

12 on-board
Power Amplifiers

x

Y
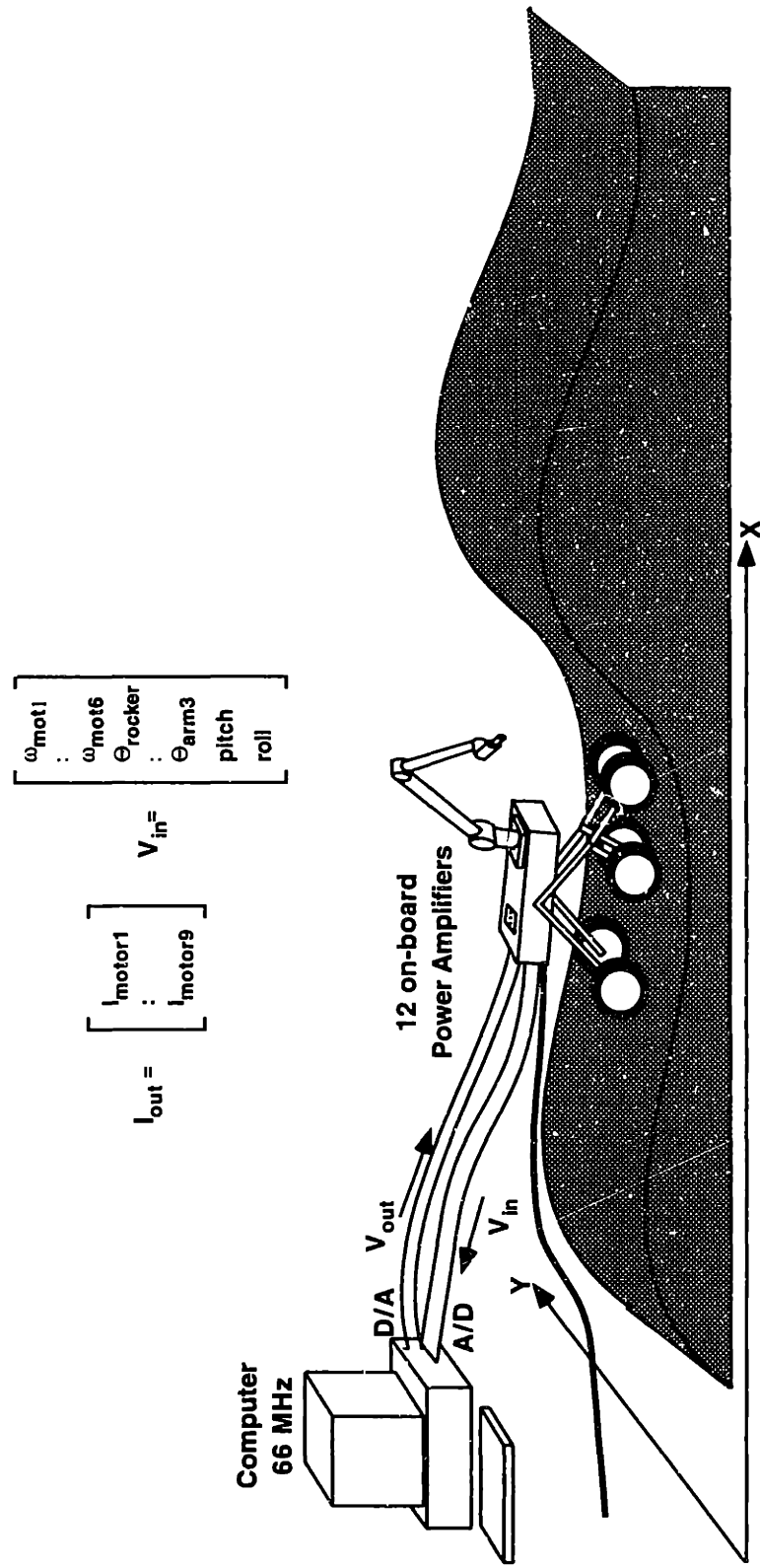
Figure D-3: Mod 2 Rover

MOD 3

Self-Contained Rover

Attitude sensors:
Accelerometer
4 Potentiometers

Manipulator sensors:
Force-Torque sensor
Cameras
Motor Encoders

PC/104 boards :
D/A
A/D
Frame Grabber
Encoder

Wheel Feedback:
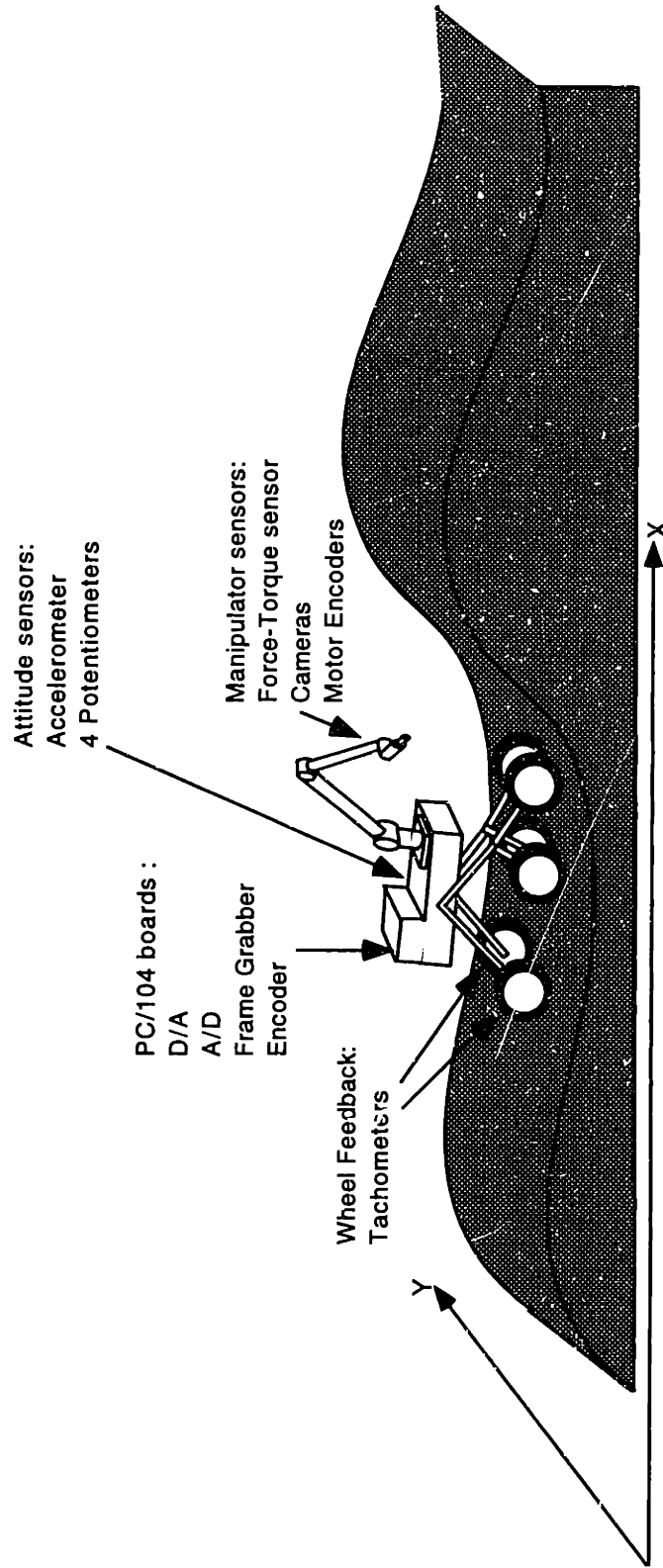Tachometers

X

Y

Figure D-4: MOD 3 Rover

D.2 MOD 1.1 Calibration

Chapter 5 has presented experiments that were performed for motor calibration. The model of the motors is represented by:

$$\tau_{out} = r \cdot k_{motor} \cdot i - b_{motor} \cdot \omega_{motor} - \tau_{coulomb} \cdot \text{sgn}(\omega_{motor}) \qquad \textbf{(D-1)}$$

The first set of experiments is static. In other words, a constant current is sent to the motor and the torque can be measured (see Figure 5-3). When the system is in equilibrium, equation (5-2) can be applied:

$$\tau_{out} = r \cdot k_{motor} \cdot i - \tau_{coulomb} \qquad \textbf{(D-2)}$$

This section presents the results of these experiments. Figure D-5 presents the results obtained in the first experiment described in Section 5.2.3, for the motor static torques. The solid and thick lines represent the experimental measurements. From these, the best linear approximation is deduced (represented here by a dashed line). The slope of this linear approximation is $r\,k_{motor}$. Since r is known, k_{motor} can be deduced. The difference between the ideal motor characteristic and the actual characteristic is the Coulomb friction. The results of these experiments are given in Chapter 5.
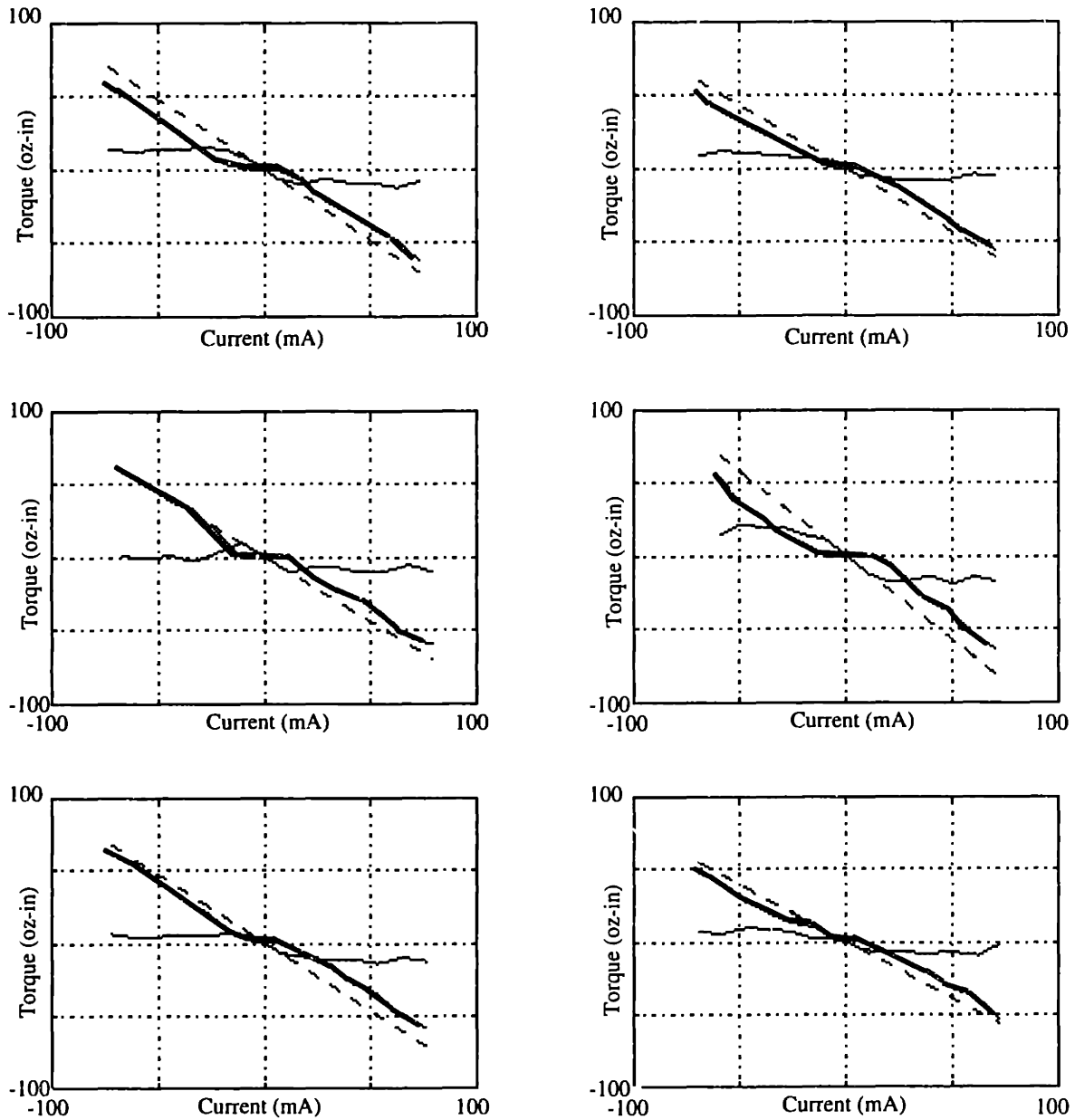
Figure D-5: Rover Motor Static Experiments

The second set of experiments is aimed at determining the viscous friction parameter b_{motor}. Here, no load is applied to the motor and a constant current is sent. Therefore, equation (5-3) applies when the motor reaches a stedy state.

$$r \cdot k_{motor} \cdot i = b_{motor} \cdot \omega_{motor} + \tau_{coulomb} \cdot \text{sgn}(\omega_{motor})$$ \hfill **(D-3)**

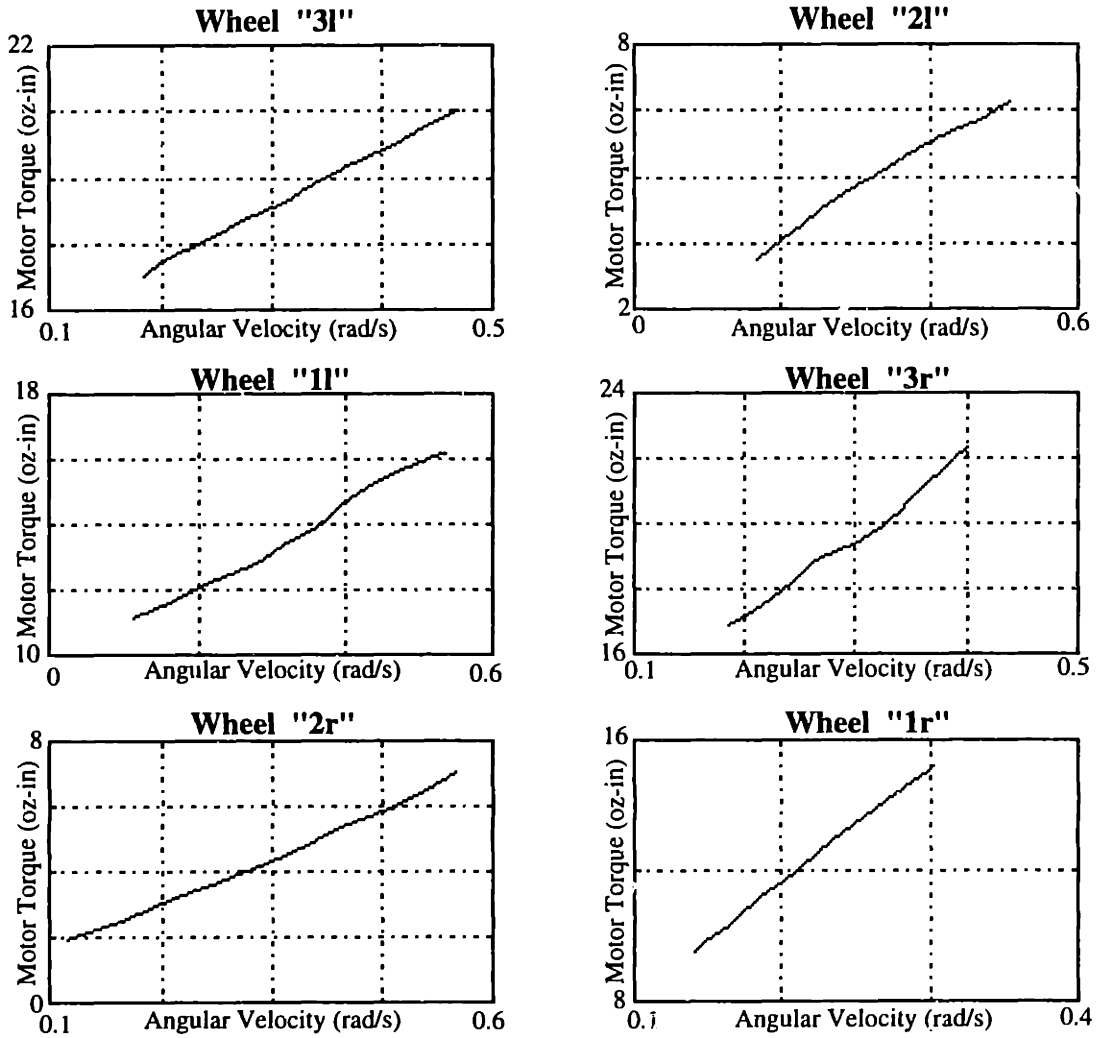The experimental results are shown in Figure D-6, and the experimental measurements are detailed in Section 5.2.3.

Figure D-6: Rover Viscous Parameters Determination.